To the Graduate Council:

I am submitting herewith a dissertation written by Ryan Scott Brame entitled "Bayesian Methods for Internal and External Radiation Dosimetry." I have examined the final paper copy of this dissertation for form and content and recommend that it be accepted in partial fulfillment of the requirements for the degree of Doctor of Philosophy, with a major in Nuclear Engineering.

Dr. Peter G. Groer, Major Professor

We have read this dissertation
and recommend its acceptance:

Dr. Frank M. Guess

Dr. Laurence F. Miller

Dr. Lawrence W. Townsend

Accepted for the Council:

Vice Provost and Dean of
Graduate Studies

BAYESIAN METHODS FOR INTERNAL AND EXTERNAL RADIATION DOSIMETRY

A Dissertation

Presented for the

Doctor of Philosophy

Degree

The University of Tennessee Knoxville

Ryan Brame

May 2002

DEDICATION

For PaPa and NeNe

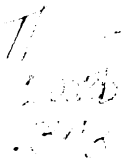

ACKNOWLEDGEMENTS

I am deeply indebted to Dr. Peter G. Groer, my major professor, for his patient tutelage during the course of this research. I also thank Dr. Lawrence Townsend, Dr. Laurence Miller, and Dr. Frank Guess for serving on my graduation committee. More generally, I wish to express my sincere appreciation for every member of the faculty and staff of the Nuclear Engineering Department. All have contributed in no small way to making my time at the University of Tennessee a pleasure.

I am forever grateful to the family and friends who have supported me in innumerable ways over the years. I especially thank my wonderful wife Courtney for her encouragement and love.

ABSTRACT

Bayesian statistical methods are applied to several problems in internal and external radiation dosimetry. In each case, Bayesian methods produce results that are clear, coherent (i.e.-following the rules of probability calculus), and free of "ad-hockery" often associated with alternative frequentist statistical methods.

Research in the area of internal radiation dosimetry focuses on compartmental modeling of ^{45}Ca biokinetics. Several approaches are taken to predict compartmental activity at fixed times. One approach is numerical calculation of the expected value and variance of compartmental activity using quasi-Monte Carlo integration. This approach considers the uncertainty of parameter estimates in the calculation, an improvement on the usual practice of estimating compartmental activity with point estimates of transfer coefficients. The second approach focuses on the calculation of posterior probability distributions for the compartmental activities. Predictive densities for observations of compartmental activity and posterior distributions for expected values of compartmental activity are calculated for a 2-compartment caternary model with simulated data and for the ^{45}Ca model. The predictive density for an observation is shown to be computable in all cases, but less desirable than the posterior distribution of the expected value due to greater uncertainty. The more desirable posterior distribution for the expected value of compartmental activity cannot be calculated except for extremely simple cases. Instead, these posterior distributions for the expected value can be approximated using point estimates of the expectation and variance and an assumption of normality. The final

topic considered in the area of internal radiation dosimetry is compartmental modeling with missing observations. The general approach of Box et al. (1970) for multiresponse nonlinear fitting with missing observations is made specific to compartmental modeling. The method is demonstrated using the ^{45}Ca biokinetic data by omitting one and two observations. In both cases, posterior distributions are derived for transfer coefficients as well as for the missing observations.

Research in the area of external radiation dosimetry focuses on dose estimation with chromosome aberrations. The topics considered include: chromosome dosimetry for a single radiation type, for doses received during a criticality accident, with uncertain calibration doses, and with overdispersed calibration data. The work of Groer et al. (1987) for chromosome dosimetry following exposure to a single radiation type is extended to several new calibration data sets. The results reinforce the practicality and usefulness of the calibrative density as a tool for chromosome dosimetry. A new method is developed and demonstrated for chromosome dosimetry following criticality accidents that permits estimation of the total dose as well as the individual dose contributions from fission-spectrum neutrons and gamma rays with an imprecise neutron to gamma dose ratio. This new approach is an improvement over the frequentist methods currently used for estimating the dose received from a criticality excursion, which rely on an assumption of precisely-known neutron to gamma dose ratios. Another novel method is developed for chromosome dosimetry with uncertain calibration doses. It is clear that all doses in calibration data sets are estimates, and as such they are subject to uncertainty. This method produces dose estimates that consider the inherent uncertainty of the calibration

doses. The last topic considered is model selection/identification. The concerns are the assumption of Poisson statistics for high linear energy transfer radiations, and the assumption of a linear dose response for low doses of neutrons. Bayes Factors and Partial Bayes Factors are used to compare the probabilities of the competing models. The results show that the Polya model is preferred over the Poisson model for chromosome dosimetry with high linear energy transfer radiations, and that an assumption of linear dose response is appropriate for the induction of dicentric chromosome aberrations by low doses of neutrons.

TABLE OF CONTENTS

LIST OF FIGURES

CHAPTER 1: INTRODUCTION

1.1 Background

One fundamental problem faced in all statistical research is how to infer future behavior from prior knowledge and/or data. The scientific approach to inference, commonly known as statistics, began in the early to mid-eighteenth century (O'Hagan 1994). Presently, two major statistical schools have emerged and coexist: the classical, or frequentist school and the Bayesian. Several authors including Lindley (1971, 1983), Jeffreys (1998), Howson et al. (1995), and Savage (1972) make convincing arguments for the Bayesian approach. They show a Bayesian approach yields results that are clear, coherent, and free of "adhockery" (Good 1959; De Finetti 1974) often found in classical inference.

The clarity of results is due to the "language" of Bayesian statistics, namely probability calculus. Uncertainty is described by probability; no other quantity is needed (Lindley 1983). Coherence is ensured by strict adherence to the rules of probability calculus. The axiomatic foundation of probability calculus consists of three fundamental rules: convexity, meaning that all probabilities must lie between 0 and 1, with $0 \equiv$ impossibility and $1 \equiv$ certainty, and the laws of addition and multiplication. All other rules, including the Bayes Rule, can be derived from these three (Howson et al. 1995).

It is obvious from the ubiquity of classical methods that there is more to the story. The popularity of classical methods is due partially to the difficulty presented by many of the calculations required in a Bayesian approach. The price of clarity and coherence is the considerable computational effort necessary for multidimensional numerical integration of complicated functions. Historically, such calculations have been virtually impossible, necessitating the use of approximations that, while ingenious in nature, were necessarily of unproven accuracy. However, the rapid rise in the availability of computational resources is easing this burden, sparking a revival of Bayesian methods.

1.2 Purpose and Scope

The general purpose of this research is to explore the application of Bayesian methods for internal and external radiation dosimetry.

1.2.1 External Radiation Dosimetry

The goal of external radiation dosimetry is the accurate estimation or prediction of the radiation doses received by persons exposed to an external source. Typical sources of information used in dose estimation include, for example, personal dosimeter readings and the results of dose reconstruction calculations. Another well-established technique is chromosome dosimetry, which uses knowledge of the dose response of chromosome aberrations to make dose estimates. Radiation dosimetry with chromosome aberrations has the advantage that the dose to cells of an exposed individual can be directly estimated

from the response of the individual's cells to radiation and does not have to be inferred by extrapolation from the response of an external dosimeter. Calibration data are used to establish the correlation between the number of chromosome aberrations per cell and radiation doses (Inoue 1995*a*, *b*; Lloyd et al. 1979). Following work by Groer et al. (1987, 1998), a Bayesian approach is used to generate dose estimates for high and low doses of neutrons as wells as for x-rays. The so-called calibrative density (Aitchison et al. 1975) of the unknown dose to an individual is derived for controlled calibration experiments. This density describes the remaining uncertainty of the final dose estimate after considering all available information.

A closely related topic is estimating the dose received during a criticality accident. The situation is more complex than that considered above, since the dose received during such an accident is due to a combination of fission spectrum neutrons and gamma rays. A new approach to this problem is developed and applied to experimental data of Voisin et al. (1997).

An issue that has received little attention in the literature on chromosome dosimetry is how to account for the inherent uncertainty associated with the doses in calibration data. The adjective "inherent" is used in recognition of the fact that the calibration doses are not directly observed, but instead are estimates based on information such as source strength, geometry, etc. As such, the estimates are subject to error. A novel hierarchical model approach is used to examine the relationship between calibration dose and the

number of chromosome aberrations per cell when both are subject to error. The method is applied to three different dose response models.

The final topic considered in the area of external dosimetry is model selection/identification. The concerns are the assumption of Poisson statistics for high linear energy transfer (LET) radiations, and the assumption of linear dose response for low doses of neutrons. Bayes Factors and Partial Bayes Factors are used, respectively, to compare the probabilities of the competing models.

1.2.2 Internal Radiation Dosimetry

The goal of internal radiation dosimetry is to accurately estimate the dose delivered by emitters located inside the body. It is therefore necessary to construct compartmental models of the biokinetic behavior of internal emitters. Generally speaking, compartmental modeling refers to any method that seeks to describe a system or process through a series of interconnected compartments (Godfrey 1983; Jacquez 1972; Anderson 1983). It is a diverse area of research with applications in a variety of fields including chemical engineering, nuclear medicine, health physics, and pharmacology (Gavalas 1968; Welch et al. 1972; Welling 1986). The specific new areas of focus in this dissertation include Bayesian methods for prediction of compartmental activities and the impact of missing data on parameter and dose estimates.

The first issue considered is a continuation of work by Lo (2000) on the 2-compartment model describing the exchange of ^{45}Ca between plasma and the bone surface of beagles. Previously, point estimates of the transfer coefficients were used to estimate compartmental activities at fixed times. While computationally easier, the use of point estimates is undesirable, as knowledge of the uncertainty associated with the estimated model parameters is not considered. In recognition of this fact, multidimensional quasi-Monte Carlo numerical integration (Wolfram 1996) is used to calculate the expected value and standard deviation of compartmental activities for fixed times.

The next issue addressed is compartmental modeling with missing data. There are many reasons why observations might be missed in biokinetic experiments; a Bayesian method for dealing with this situation is described and demonstrated using the ^{45}Ca biokinetic data of Rowland (1966). The method is a specific form of the more general approach of Box et al. (1970) for estimation of missing values in multiresponse nonlinear modeling. Posterior distributions are derived for transfer coefficients and missed observations for the cases of 1 and 2 missing observations.

The final topic considered in the area of internal radiation dosimetry is prediction of compartmental activity at fixed times. Consistent with the Bayesian notion that the probability distribution is the best descriptor of an unknown quantity, two different approaches are considered. The first method is a reinterpretation of the method used for compartmental modeling with missing data, and yields predictive distributions for observed values of compartmental activity. The second method is a transformation of

variables that produces the posterior density for the expected value of the compartmental activity. Two different compartmental models are used: a 2-compartment caternary model with simulated data and the 2-compartment model for ^{45}Ca biokinetics with the Rowland data (1966). Predictive densities for observations of compartmental activity and posterior distributions for the expected value of the compartmental activity are derived for each model.

The remainder of this dissertation is laid out as follows. Chapters 2-5 contain the external dosimetry research, and Chapters 6 and 7 deal with the internal dosimetry portion. Chapter 8 contains concluding remarks and recommendations for future work. References and an Appendix containing computer programs conclude the dissertation.

CHAPTER 2: THE CALIBRATIVE DENSITY FOR CHROMOSOME DOSIMETRY

2.1 Introduction

The objective of this portion of the research is to use information on chromosome aberrations for dose estimation. Chromosome damage and repair following exposure to radiation are well studied and documented (Bender et al. 1988). One dosimetrically useful product of radiation damage is the dicentric chromosome aberration, a response variable of choice for biological dosimetry due to the relative ease with which it is scored and its low background rate (Moquet et al. 2000). Knowledge of the dose-response for dicentric aberrations is gleaned from controlled calibration experiments. Speaking in general terms, a controlled calibration experiment consists of the following steps: exposing a sample of blood to known doses of radiation, d_i (rad), scoring the number of dicentrics, y_i, observed in a sample of n_i peripheral lymphocytes, and then repeating the first two steps for i=(1, 2,..., k) predetermined dose levels. The parameters of the model assumed to describe the underlying statistical relationship between y, n, and d are then estimated conditional on the calibration data $D_c = \{d_i, y_i, n_i\}$. The usual assumption is that y is Poisson distributed with a mean that is either a linear or linear-quadratic function of d (e.g.- $y_i \sim \text{Po}[n_i\theta d_i]$ or $y_i \sim \text{Po}[n_i(\alpha+\theta d_i+\gamma d_i^2)]$).Three different calibration data sets will be analyzed below, including high and low neutron doses and x-ray doses (Lloyd et al. 1979; Inoue 1995*a*, *b*).

2.2 High Doses of Neutrons

The first data set contains the results of exposing lymphocytes to 0.7 MeV fission neutrons from the British Experimental Pile Zero reactor (BEPO). This data set is referred to as the BEPO data set and given by the vectors (Lloyd et al. 1979):

$$\mathbf{d}=\{50, 75, 100, 150, 200, 250, 300\}$$

$$\mathbf{n}=\{269, 78, 115, 90, 84, 59, 37\}$$

$$\mathbf{y}=\{109, 47, 94, 114, 138, 125, 97\}$$

The notation for these vectors follows the naming convention for the subscripted variables used in Section 2.1. The induced aberration rates are high enough that the background rate can be neglected. The number of dicentric chromosome aberrations y observed in a sample of n lymphocytes is assumed to be Poisson distributed with mean $n\beta d$. The posterior distribution of the slope parameter β in proportional ($\propto$) form with a constant improper prior for β is given as

$$p(\beta|D_c) \propto \prod_{i=1}^{7} (\beta d_i)^{y_i} \exp\{-n_i \beta d_i\} \qquad \textbf{(2.1)}$$

where D_c is the calibration data. The marginal density of β is shown in Figure 2.1. For dose estimation the calibrative density, discussed by Aitchison et al. (1975), is used. This density characterizes the uncertainty of the dose estimate conditional on all available data

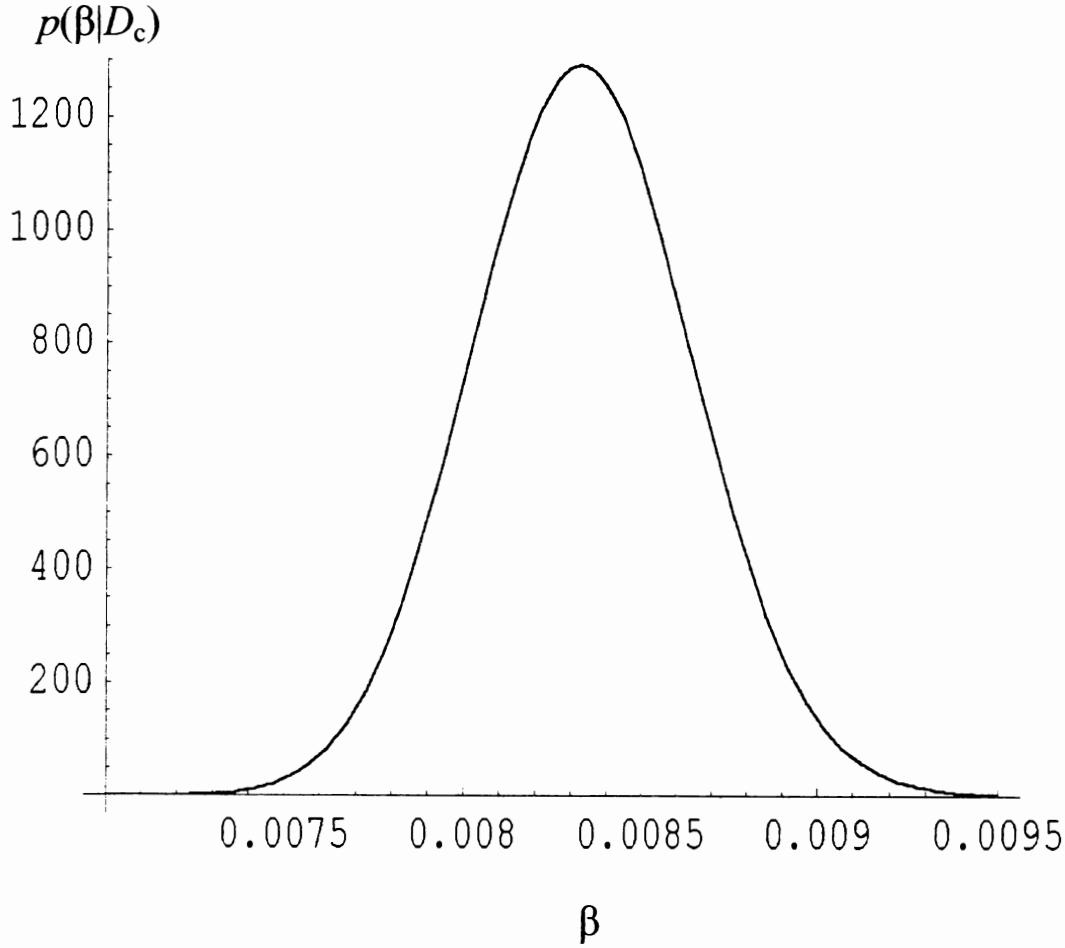

Figure 2.1: Marginal posterior density of β for the BEPO data set

D_A, which consist of the calibration data D_c and the number of dicentrics, y_f, observed in a sample of n_f lymphocytes taken from a hypothetical individual exposed to unknown dose d_f. The calibrative density for the case of exposure to high doses of neutrons and a controlled calibration experiment is given by

$$p(d_f|D_A) \propto p(d_f)\int_B (n_f\beta d_f)^{y_f} \exp\{-n_f\beta d_f)p(\beta|D_c)d\beta \qquad \textbf{(2.2)}$$

$p(d_f)$ is the prior density of the unknown dose d_f, $p(\beta|\ D_c)$ is the posterior density of the slope parameter, and the remaining terms inside the integrand comprise the likelihood of a "future" observation based on the Poisson assumption. Collectively, the integral over the posterior density of the parameter and the likelihood of a future observation form the predictive density. For the BEPO data, dose estimates were made assuming $y_f = 120$ and $n_f = 55$. To demonstrate the manner in which ancillary information may be incorporated into the analysis, a gamma prior with mean of 260 and variance of 100 was assumed for $p(d_f)$, representing a prior estimate of the dose based on TLD readings or maybe dose reconstruction calculations. The calibrative densities calculated with and without $p(d_f)$ are shown in Figure 2.2.

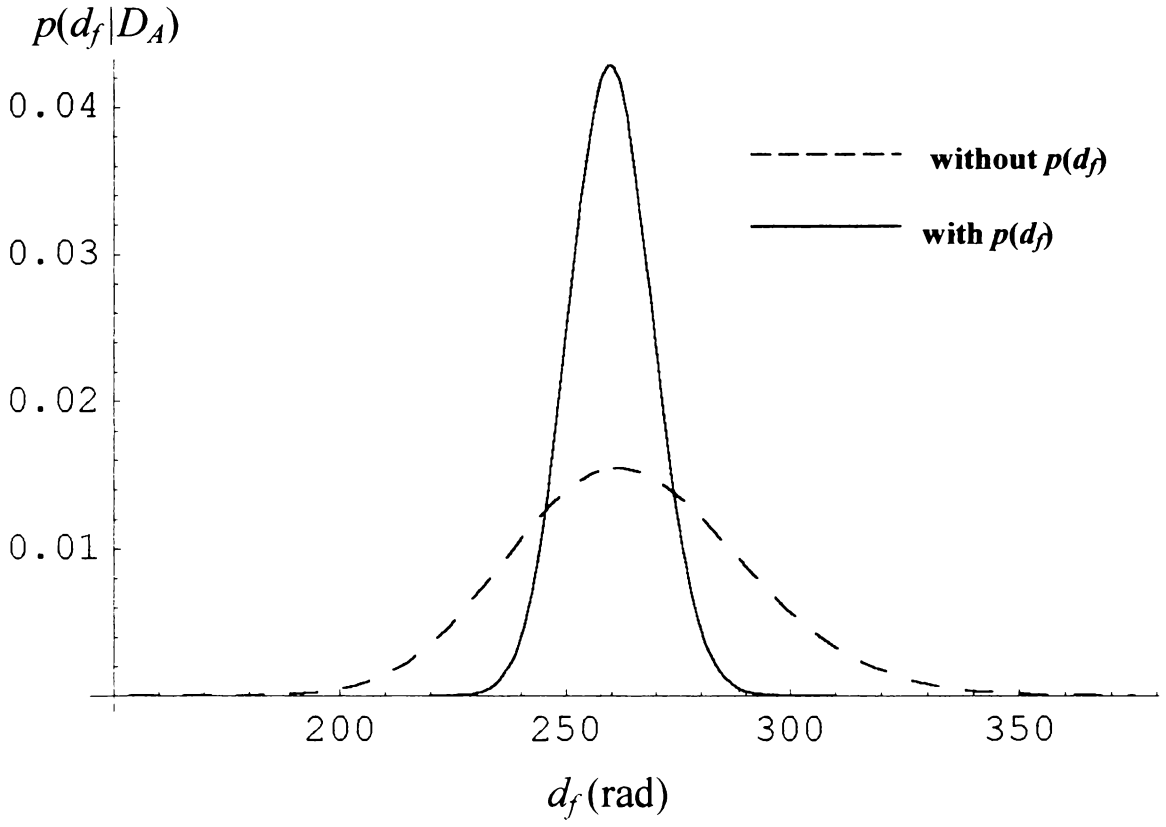

Figure 2.2: Calibrative densities for the BEPO data set with $y_f = 120$ and $n_f = 55$, calculated with and without $p(d_f)$

2.3 Low Doses of Neutrons

The second calibration data set is from Inoue (1995*a*) for exposure to low doses of neutrons from a ^{252}Cf neutron source. Below this data set is referred to as the ^{252}Cf data and given by the following vectors:

$$\mathbf{d}=\{0.0, 0.2, 0.5, 0.75, 1.0, 2.0\}$$

$$\mathbf{n}=\{16000, 10000, 9300, 4660, 2477, 708\}$$

$$\mathbf{y}=\{10, 35, 70, 47, 39, 24\}$$

Unlike the BEPO data set, the doses in the ^{252}Cf data set and the corresponding aberration rates are low enough so that the contribution from background must be considered. It is therefore assumed that the number of dicentric chromosome aberrations y observed in a sample of n lymphocytes is Poisson distributed with mean $n(\alpha+\beta d)$, where α is the background rate. If constant improper priors are assumed for α and β, the joint posterior density for the parameters in proportional form is given by:

$$p(\alpha,\beta|D_c) \propto \prod_{i=1}^{6} (\alpha+\beta d_i)^{y_i} \exp\{-n_i(\alpha+\beta d_i)\} \qquad \textbf{(2.3)}$$

Marginal densities may be obtained from the joint density by numerical integration over the other parameter. Figures 2.3 and 2.4 show the marginal densities of α and β, respectively.

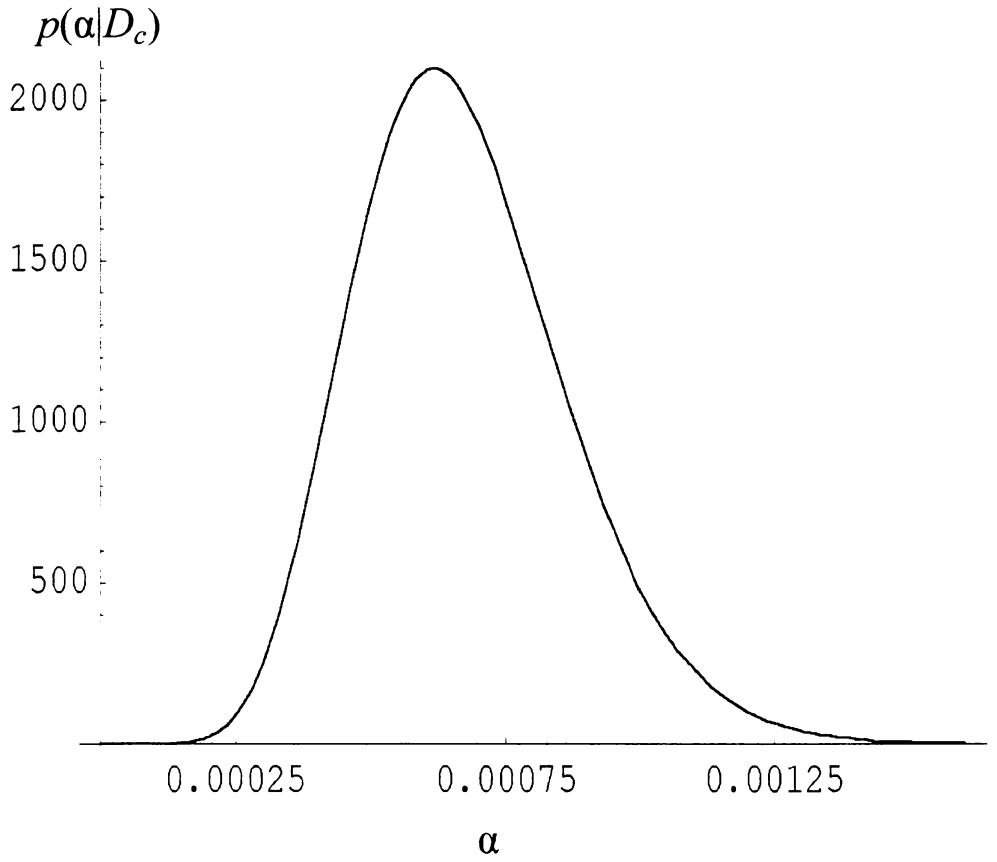

Figure 2.3: Marginal posterior density of α for the ^{252}Cf data set

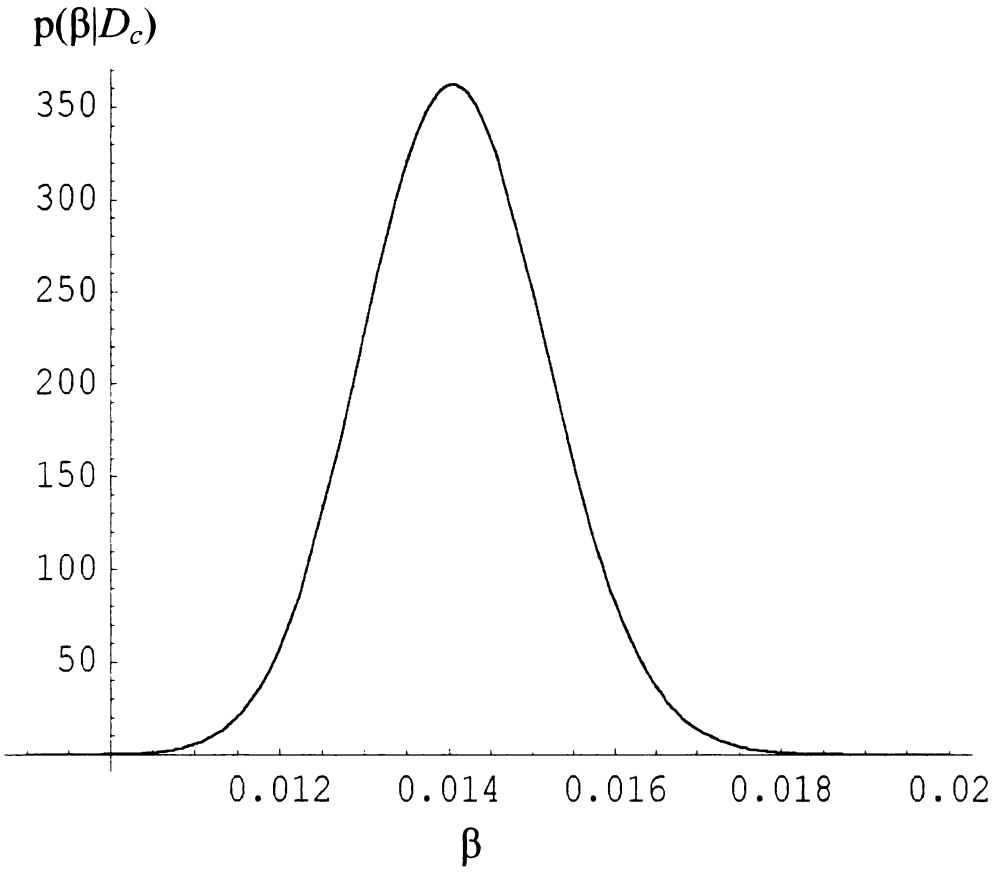

Figure 2.4: Marginal posterior density of β for the ^{252}Cf data set

The calibrative density is again used to estimate the unknown dose d_f, resulting in y_f dicentric chromosome aberrations in a sample of n_f lymphocytes. For the ^{252}Cf data the calibrative density is given as

$$p(d_f|D_A) \propto p(d_f) \int_B \int_A n_f^{y_f} (\alpha + \beta d_f)^{y_f} \exp\{-n_f(\alpha + \beta d_f)\} p(\alpha, \beta|D_c) d\alpha d\beta \qquad \textbf{(2.3)}$$

$p(d_f)$ is the prior density of the unknown dose d_f, $p(\alpha, \beta| D_c)$ is the joint posterior density of the parameters, and the remaining terms inside the integrand represent the likelihood of a "future" observation. Dose estimates were made assuming $y_f = 25$ and $n_f = 5000$ and a constant prior for d_f. The calibrative density is shown in Figure 2.5.

2.4 X-ray Doses

The third calibration data set is from Inoue (1995*b*) for exposure to x-rays. This data set is referred to below as the X-ray data set and is given by the following vectors:

d={0.0, 0.05, 0.1, 0.2, 0.3, 0.4, 0.5, 1.0, 1.5, 2.0}

n={16000, 6000, 6000, 5000, 3500, 3000, 1674, 1179, 1284, 1325}

y={10, 21, 24, 36, 53, 53, 34, 88, 174, 220}

It is assumed that the number of dicentric chromosome aberrations y observed in a sample of n lymphocytes is Poisson distributed with mean $n(\alpha+\beta d+\gamma d^2)$. Assuming

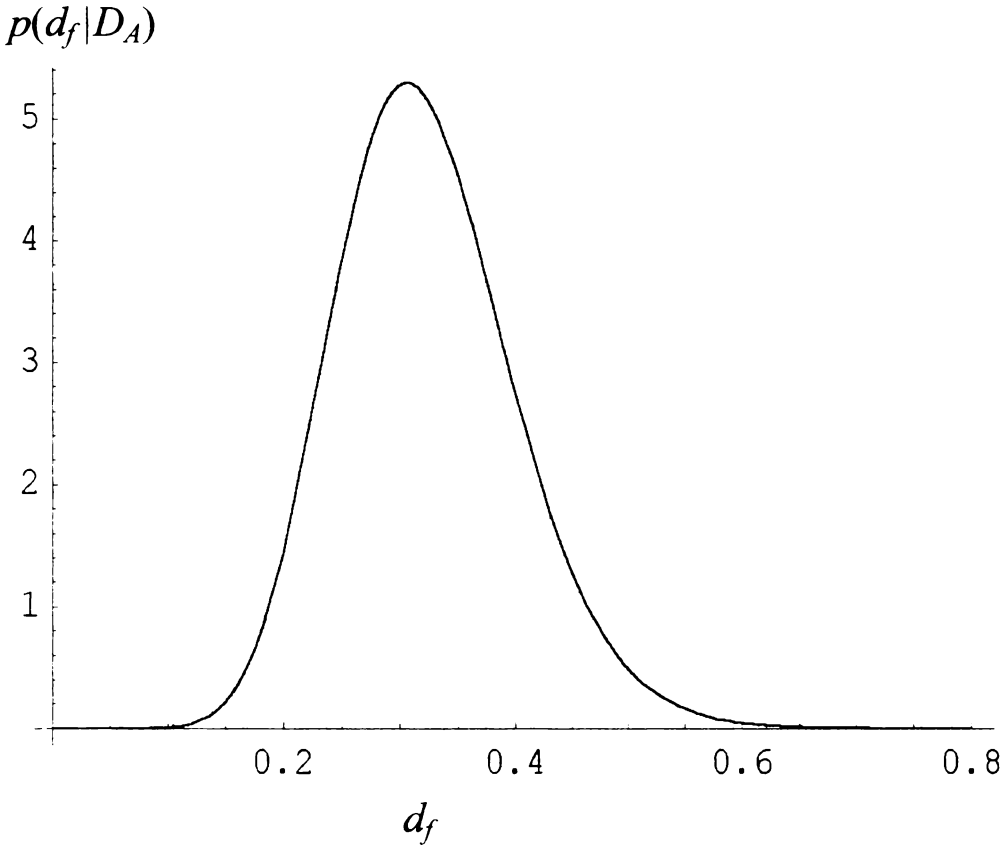

Figure 2.5: Calibrative density for the ^{252}Cf data set with $y_f = 25$ and $n_f = 5000$

constant improper priors for α, β, and γ, the joint posterior density for the parameters in proportional form is given by:

$$p(\alpha,\beta,\gamma|D_c) \propto \prod_{i=1}^{10} (\alpha+\beta d_i+\gamma d_i^{\,2})^{y_i} \exp\{-n_i(\alpha+\beta d_i+\gamma d_i^{\,2})\} \qquad \textbf{(2.4)}$$

Marginal densities may be obtained from the joint density by numerical integration over the other parameters. Figures 2.6, 2.7, and 2.8 show the marginal densities of α, β, and γ respectively.

The calibrative density is given by Equation 2.5:

$$p(d_f|D_A) \propto p(d_f) \int_{\Gamma} \int_{B} \int_{A} n_f^{\,y_f} (\alpha+\beta d_f+\gamma d_f^{\,2})^{y_f} \exp\{-n_f(\alpha+\beta d_f+\gamma d_f^{\,2})\} p(\alpha,\beta,\gamma|D_c) d\alpha d\beta d\gamma$$

Dose estimates were made assuming $y_f = 30$, $n_f = 1500$, and a constant prior for d_f. The calibrative density is shown in Figure 2.9.

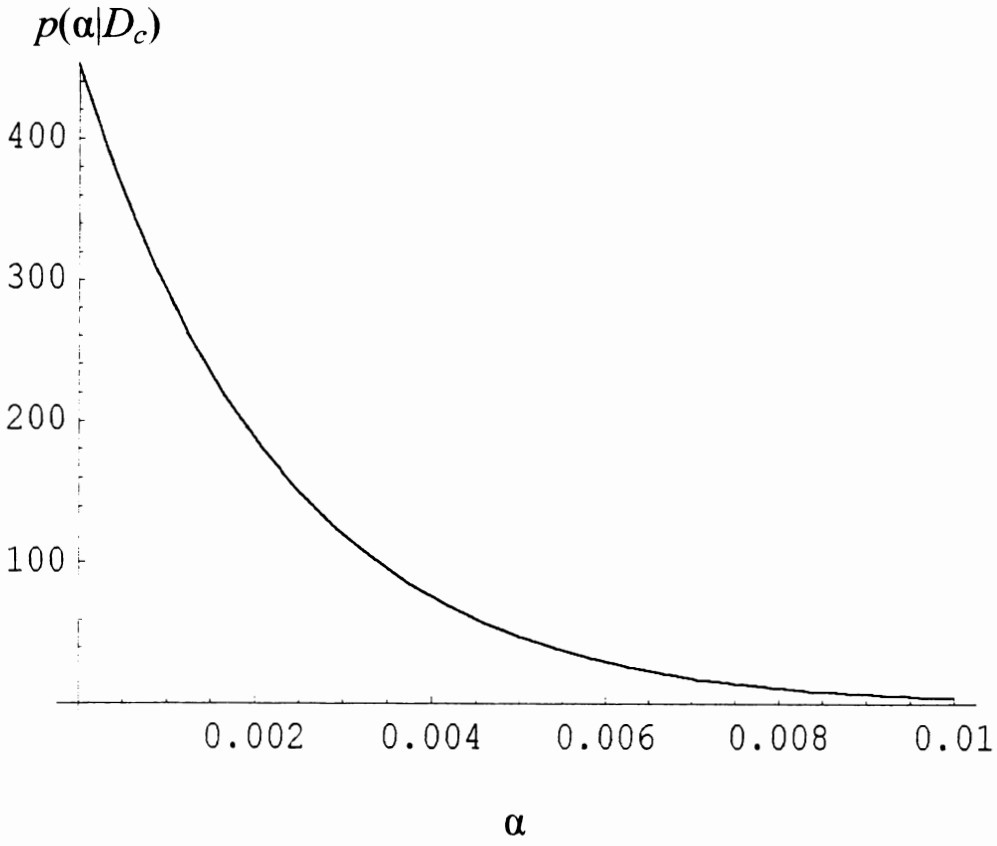

Figure 2.6: Marginal posterior density of α for the X-ray data set

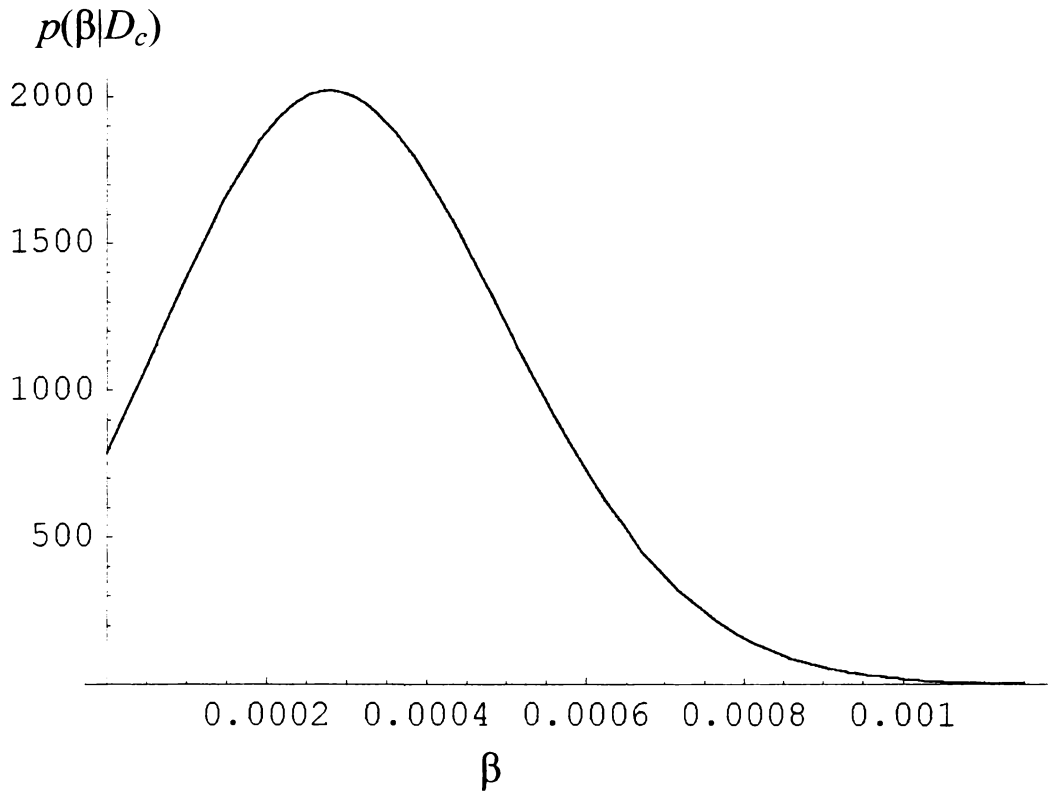

Figure 2.7: Marginal posterior density of β for the X-ray data set

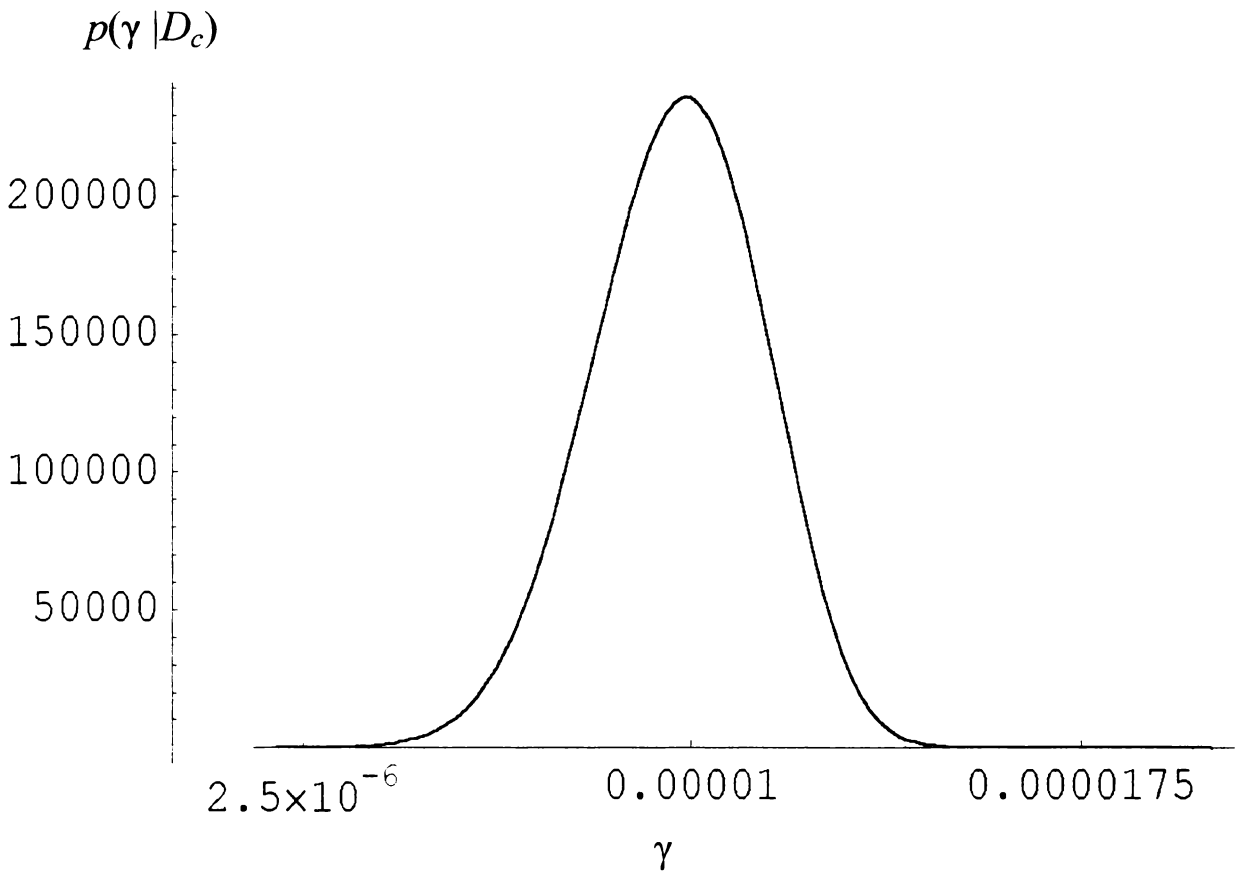

Figure 2.8: Marginal posterior density of γ for the X-ray data set

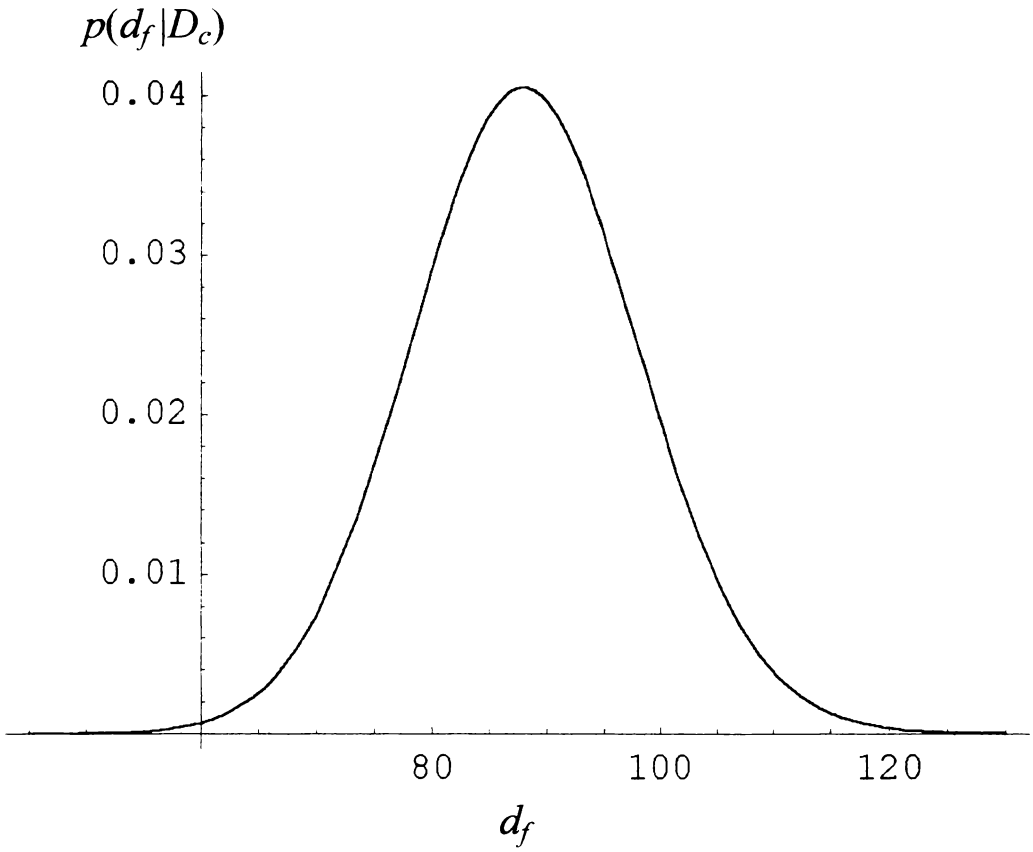

Figure 2.9: Calibrative density for the X-ray data set with $y_f = 30$ and $n_f = 1500$

2.5 Discussion

Aside from the inherent benefits of coherence and clarity discussed in Chapter 1, the Bayesian approach to chromosome dosimetry demonstrated above has the particular advantage over the routine frequentist approaches that diverse sources of information can be incorporated into the analysis through prior distributions for the parameters and/or the unknown dose. This is particularly attractive in an area, such as this, where an extensive body of pertinent information is available for use.

CHAPTER 3: CHROMOSOME DOSIMETRY FOLLOWING A CRITICALITY ACCIDENT

3.1 Introduction

The objective of this chapter is to present an approach to dose estimation with chromosome aberrations following a criticality event. In Chapter 2, a method was demonstrated for dose estimation with dicentric chromosome aberrations assuming the dose was deposited by a single radiation type. The situation considered here is more complex because the total dose received by an individual during a criticality accident will be from a combination of fission spectrum neutrons and gamma rays. Aside from estimating the total dose (T) received, it is also desirable to discriminate between the neutron and gamma ray contributions to T, denoted N and G respectively. As there is no discernible difference between aberrations induced by gamma rays and those induced by neutrons, ancillary information must be provided regarding the contributions of each radiation type to T. In practice this information is expressed in the form of a neutron/gamma dose ratio, denoted ρ below, and comes from readings of physical dosimeters worn by the exposed personnel or from accident dose reconstruction calculations. Voisin et al. (1997) used frequentist techniques to estimate T, N, and G under the assumption that ρ is precisely known. The Bayesian method developed here allows dose estimation with uncertain ρ.

3.2 Method and Data

Experimental results found in Voisin et al. (1997) will be used below, including an estimated neutron/gamma dose ratio of $\rho = 4.76$ and post-accident sample results of $y_f =$ 100 dicentrics scored in $m_f = 34$ lymphocytes. For more experimental results and a detailed discussion of experiments readers are referred to this article.

It is assumed that the number of dicentric chromosome aberrations, y_i, observed in a sample of m_i lymphocytes following exposure to high doses of neutrons is Poisson distributed with a mean that is linear in neutron dose n_i (i.e.- $y_i \sim \text{Po}[m_i \alpha n_i]$). For gamma rays the assumption is that $y_i \sim \text{Po}[m_i (\beta g_i + \gamma g_i^2)]$ where g_i is the gamma dose. Note that the background rate is again assumed to be negligible. The model parameters, denoted collectively by $\underline{\pi} = \{\alpha, \beta, \gamma\}$, are usually estimated with data from controlled calibration experiments. Because the response of dicentrics to radiation is dependent on the dose rate, the parameter estimates used for dose estimation following a criticality accident must be based on data from calibration experiments conducted with similar dose rates. In this analysis, no such calibration data were available. Instead, point estimates of $\hat{\alpha}=0.835$, $\hat{\beta}=0.0142$, and $\hat{\gamma}=0.0759$ (Voisin et al. 1997) were used. The point estimates, denoted by $\underline{\hat{\tau}} = \{\hat{\alpha}, \hat{\beta}, \hat{\gamma}\}$, were used to formulate prior distributions for the parameters, $p(\alpha)$, $p(\beta)$, and $p(\gamma)$ respectively. Gamma distributions were assumed for the priors, each parameterized so that $E(\pi_i) = \lambda_i / \varphi_i = \hat{\tau}_i$ and $\text{Var}(\pi_i) = \lambda_i / \varphi_i^2$ for i=(1,2,3). As no

confidence limits for the $\hat{\tau}_i$ were provided in Voisin et al. (1997), the values assumed for the variances are arbitrary, but sufficient for the purpose of demonstrating the approach.

For dose estimation the calibrative density was again employed. This density characterizes the uncertainty about T_f, N_f, or G_f conditional on all available data D_A. In this analysis, remembering that no detailed calibration data were available, D_A consists of the point estimates and standard deviations for the parameters α, β, γ, ρ, and the observation of y_f=100 dicentrics in m_f=34 lymphocytes. Based on the assumption that the number of dicentrics, y_f, observed in a post-exposure sample of m_f lymphocytes is Poisson distributed with a mean of $m_f(\alpha\, n_f + \beta\, g_f + \gamma\, g_f^2)$, the calibrative density of the unknown dose t_f is given by

$$p(t_f|D_A) \propto \int_P \int_\Gamma \int_B \int_A L(\alpha,\beta,\gamma,\rho|m_f, y_f, t_f)\, p(\alpha)p(\beta)p(\gamma)p(t_f)\, p(\rho)\, d\alpha\, d\beta\, d\gamma\, d\rho \qquad \textbf{(3.1)}$$

$p(\alpha)$, $p(\beta)$, and $p(\gamma)$ are the gamma priors discussed above, $p(t_f)$ is the prior density of the unknown total dose, and $p(\rho)$ is the prior density for the neutron/gamma dose ratio. The remaining term inside the integrand, $L(\alpha,\beta,\gamma,\rho|m_f, y_f, t_f)$, is the likelihood of a future observation. If ρ is expressed in terms of the fractional contribution of gamma rays to the total dose, $\theta = 1 / (\rho + 1)$, the likelihood term can be written as

$$L(\alpha,\beta,\gamma,\theta|m_f, y_f, t_f) \propto (\alpha(1-\theta)t_f + \beta\theta t_f + \gamma(\theta t_f)^2)^{y_f} \exp\{-m_f(\alpha(1-\theta)t_f + \beta\theta t_f + \gamma(\theta t_f)^2)\} \qquad \textbf{(3.2)}$$

Following analytical integration over α, β, and γ and assuming that $p(t_f)$ is proportional to a constant, the calibrative density is given by

$$p(t_f|D_A) \propto \int_{\Theta}\left[\sum_{j=0}^{y_f}\binom{y_f}{j}(1-\theta)^{y_f-j}A(\theta)\left(\sum_{k=0}^{j}\binom{j}{k}\theta^{j+k}t_f^{y_f+k}B(\theta)C(\theta)\right)p(\theta)\right]d\theta \qquad \textbf{(3.3)}$$

where

$$A(\theta) = \frac{\Gamma(y_f+\lambda_\alpha-j)}{(m_f(t_f-t_f\theta)+\phi_\alpha)^{y_f+\lambda_\alpha-j}}$$

$$B(\theta) = \frac{\Gamma(j+\lambda_\beta-k)}{(m_f\theta t_f+\phi_\beta)^{j+\lambda_\beta-k}}$$

$$C(\theta) = \frac{\Gamma(k+\lambda_\gamma)}{(m_f(\theta t_f)^2+\phi_\gamma)^{k+\lambda_\gamma}}$$

Calibrative densities for the neutron dose and gamma dose can be obtained from Equation 3.3 by transformation of variables. The calibrative density for the unknown gamma contribution, g_f, to the total dose is derived as follows:

$$p(g_f|D_A) \propto p(t_f(g_f)|D_A)\left|\frac{dt_f(g_f)}{dg_f}\right|$$

$$\propto \int_{\Theta} p(t_f(g_f),\theta|D_A)\left|\frac{dt_f(g_f)}{dg_f}\right|p(\theta)d\theta$$

3.3 Results

The gamma priors used for $p(\alpha)$, $p(\beta)$, and $p(\gamma)$ are shown in Figures 3.1, 3.2, and 3.3, respectively.

Two analyses were conducted. In the first, the neutron/gamma dose ratio was assumed precise. In the second, an uncertain ratio was considered by specifying a prior for θ. The prior of θ was obtained in two steps. First, a normal prior with mean of 4.76 and a standard deviation of 0.5 was assumed for the neutron/gamma dose ratio. $p(\theta)$ was then obtained with a variable transformation:

$$p(\theta) = p(\rho(\theta))\left|\frac{d\rho(\theta)}{d\theta}\right|$$

Figure 3.4 shows the result.

Figures 3.5, 3.6, and 3.7 show comparisons of the estimates of t_f, n_f, and g_f for the two analyses. The results show that in this case an uncertain neutron/gamma dose ratio leads to greater uncertainty in the estimates of g_f while having no discernible impact on estimates of t_f and n_f.

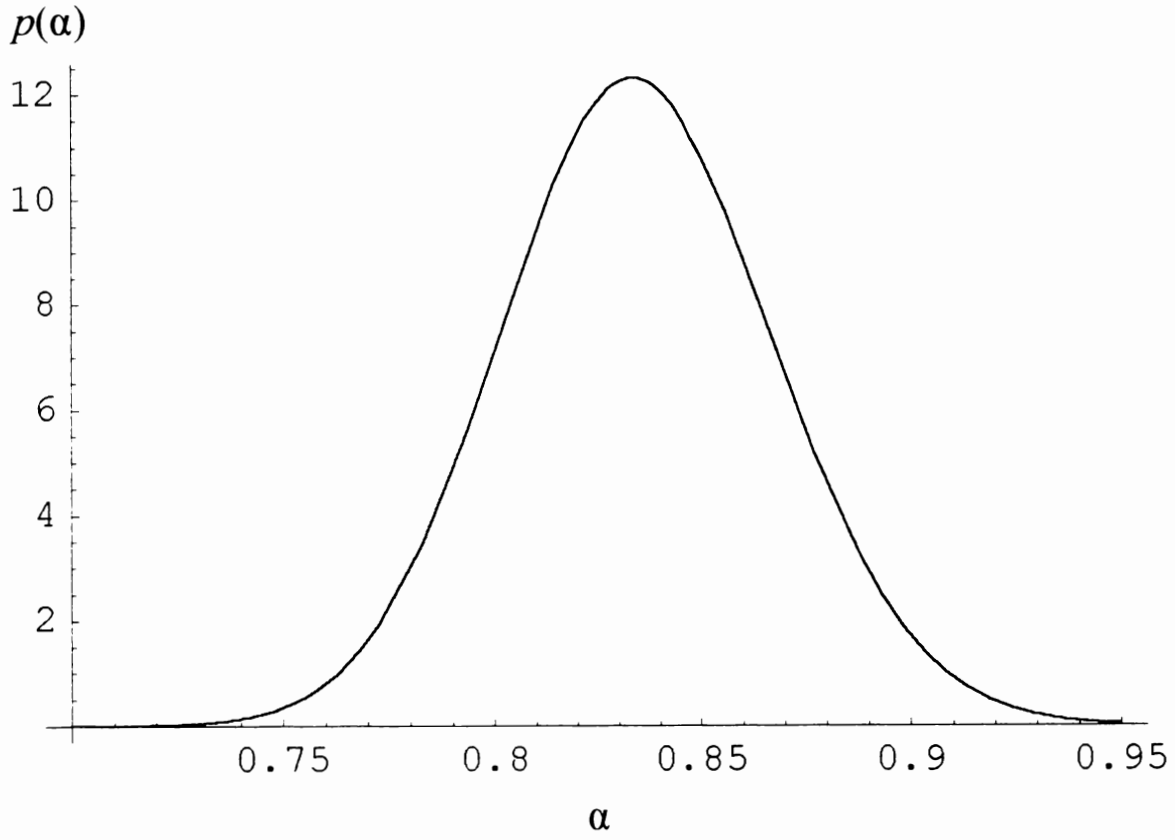

Figure 3.1: Gamma prior for α based on point estimates from Voisin et al. (1997)

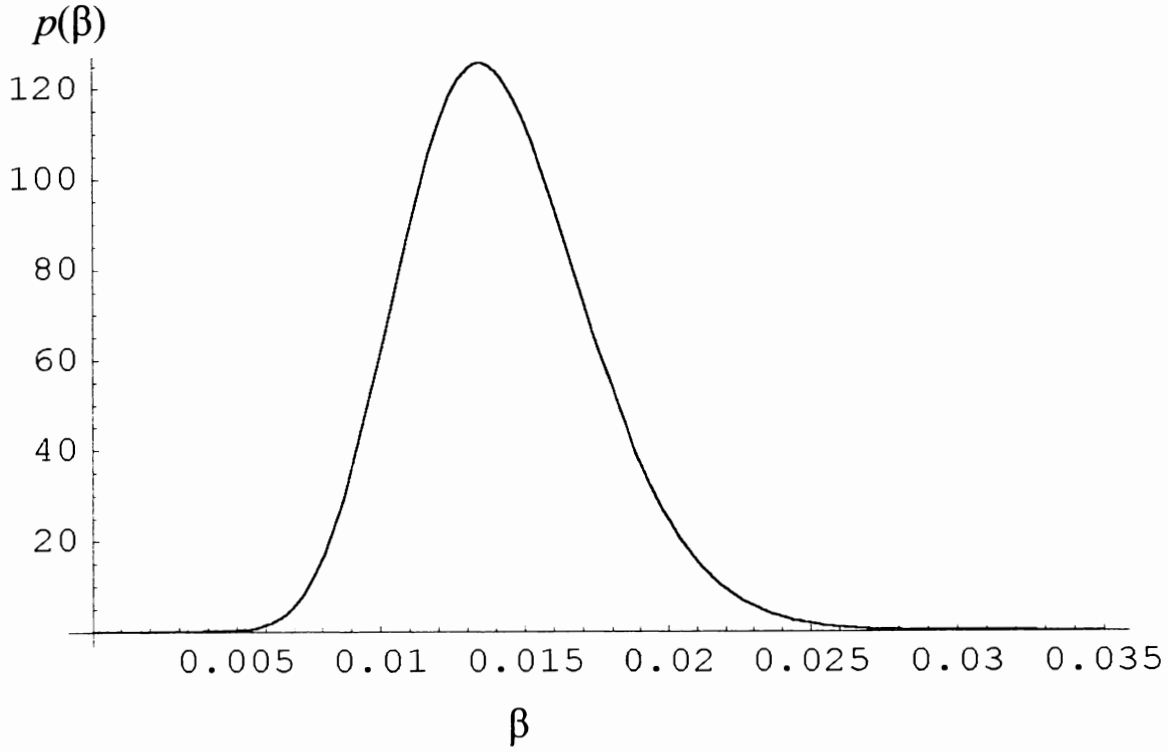

Figure 3.2: Gamma prior for β based on point estimates from Voisin et al. (1997)

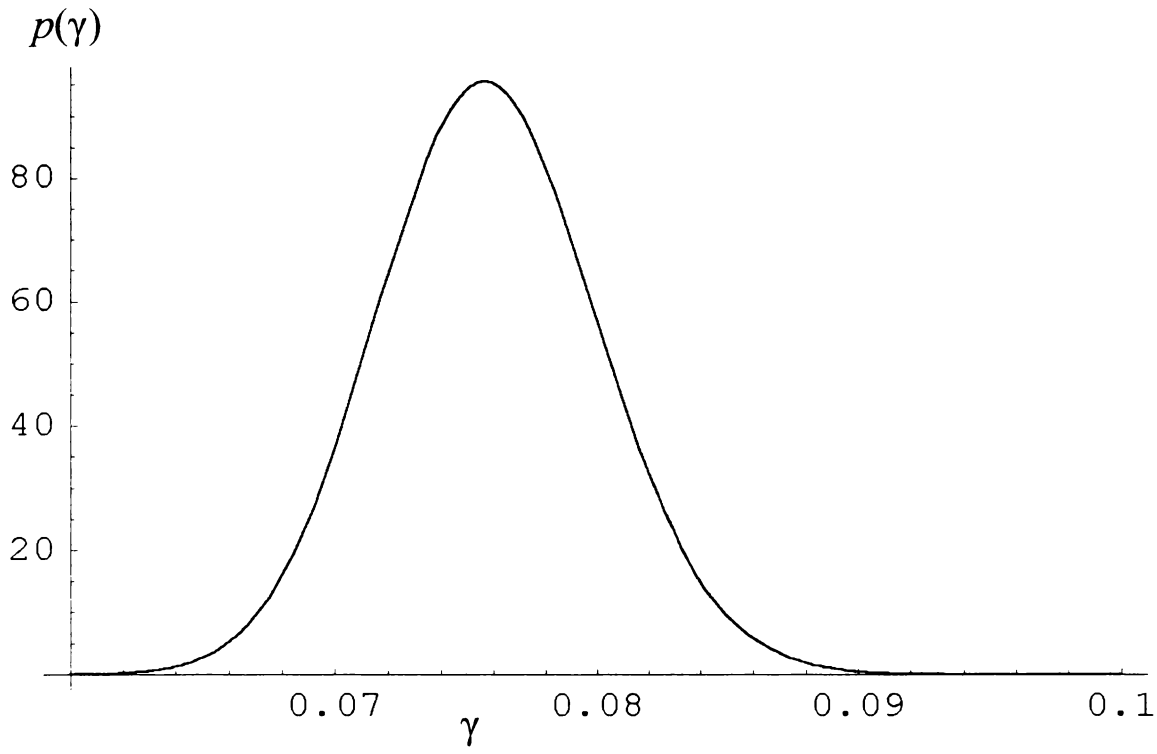

Figure 3.3 Gamma prior for γ based on point estimates from Voisin et al. (1997)

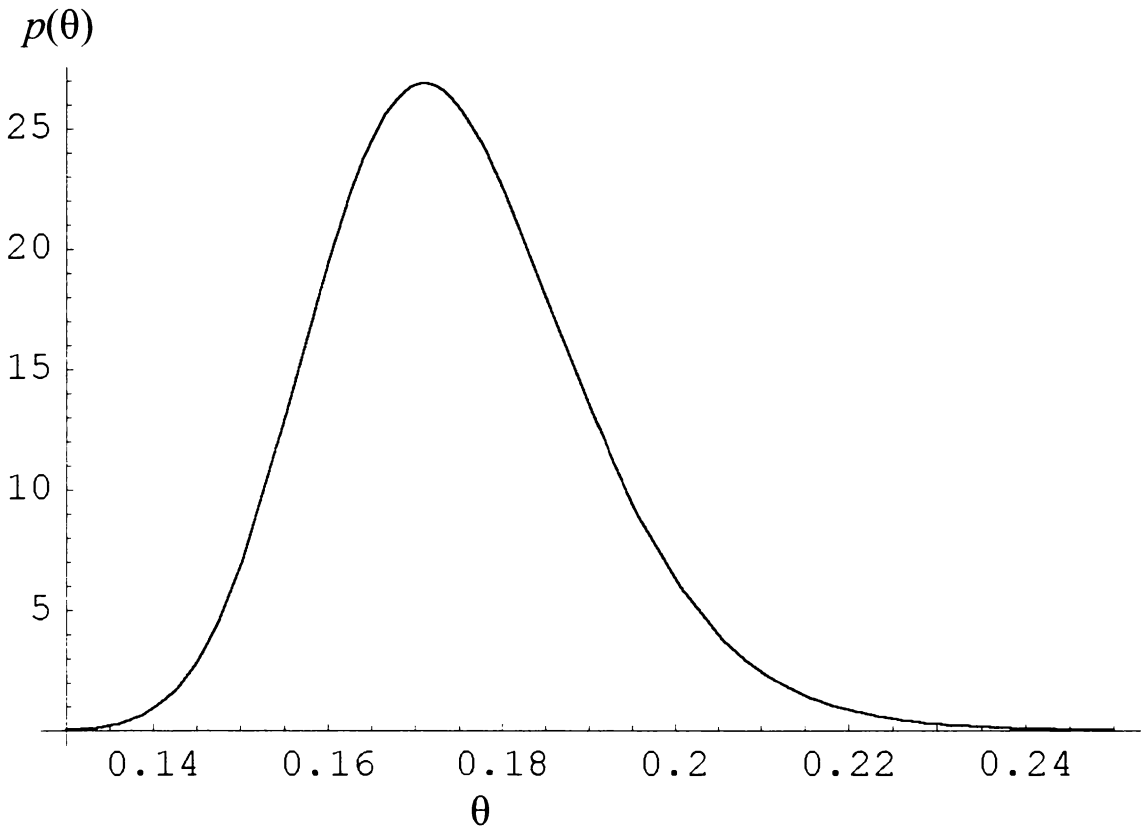

Figure 3.4: Prior density for θ based on experimental results from Voisin et al. (1997)

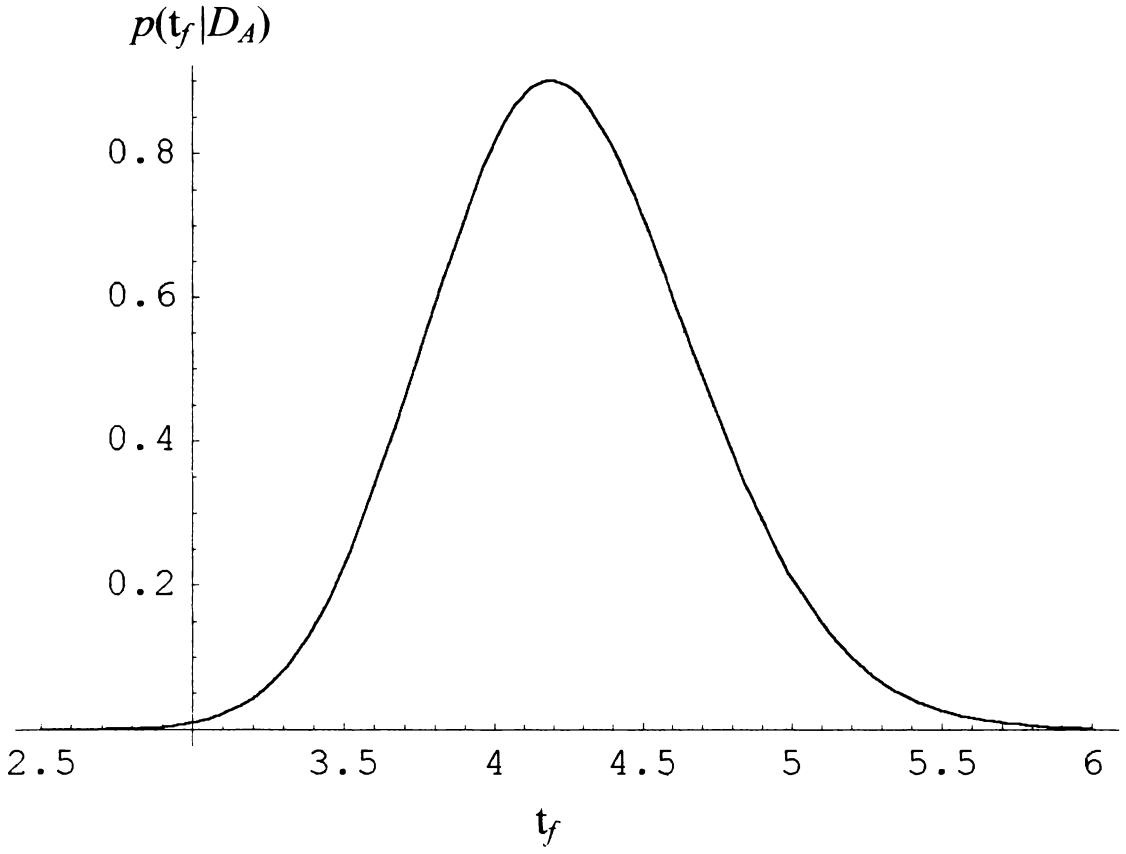

Figure 3.5: Calibrative density for the total dose t_f with $y_f = 100$ and $n_f = 34$

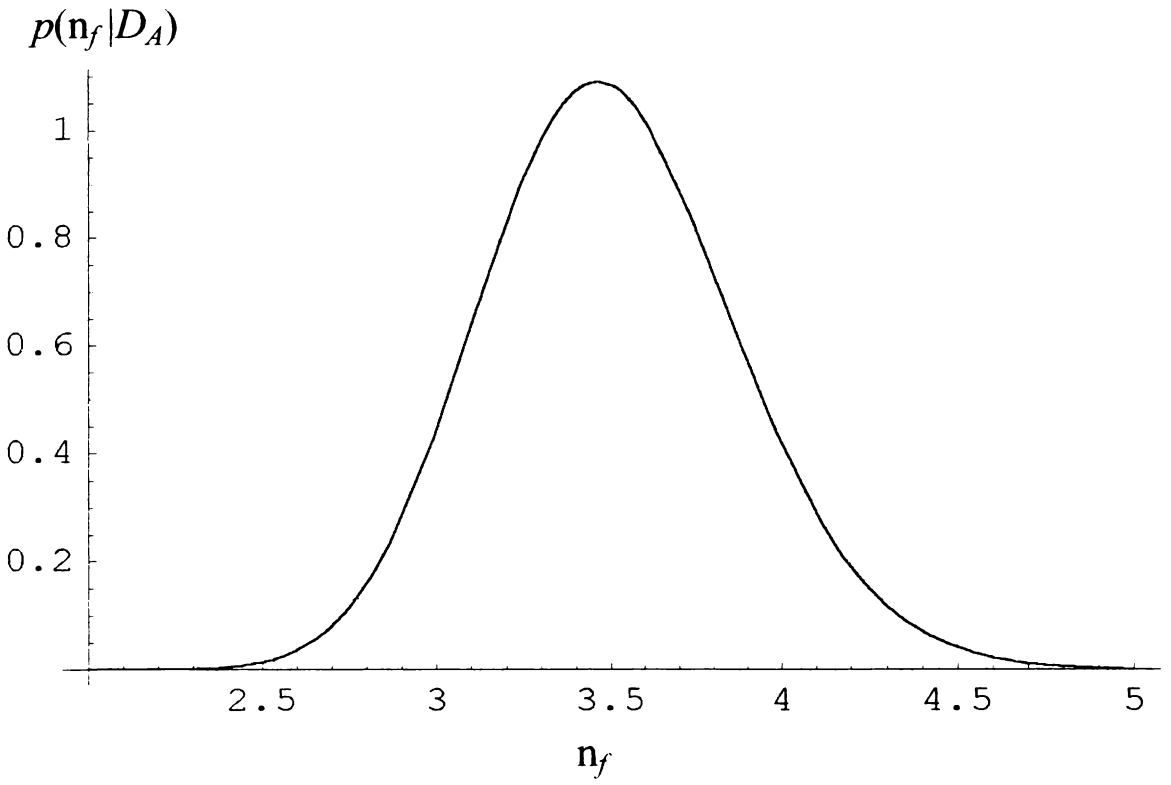

Figure 3.6: Calibrative density for the neutron dose n_f with $y_f = 100$ and $n_f = 34$

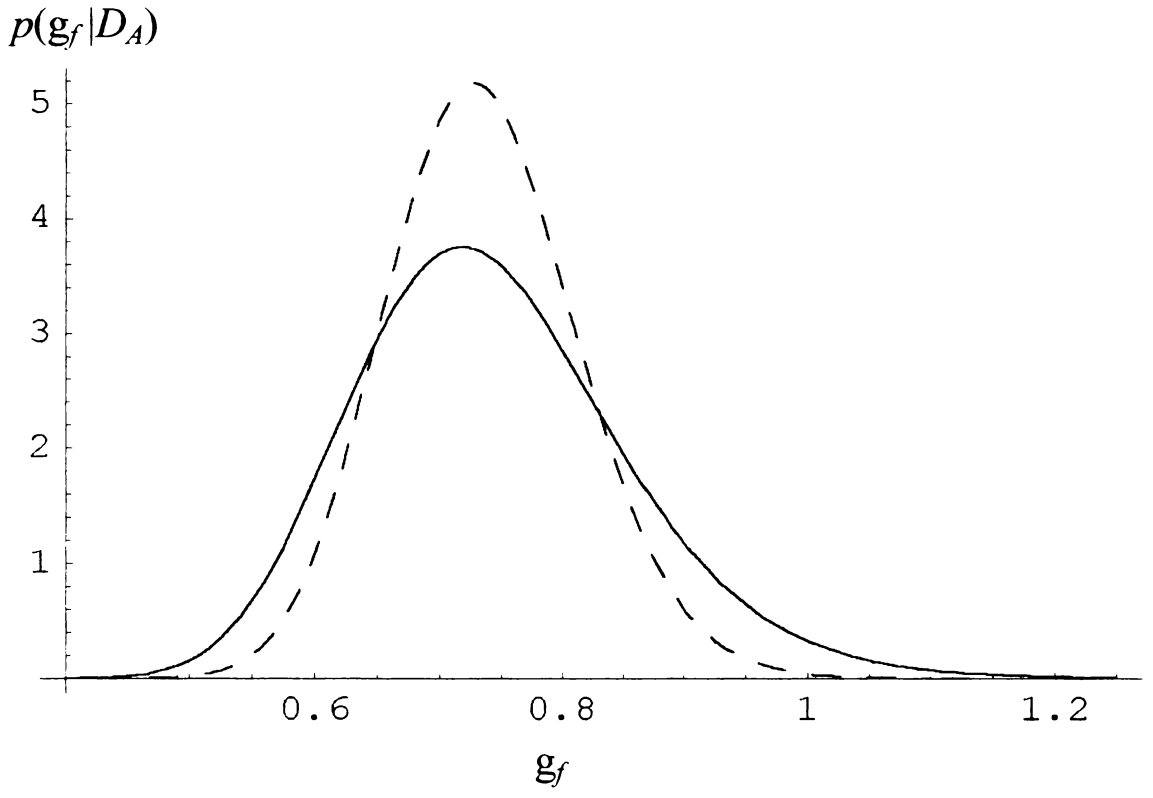

Figure 3.7: Calibrative density for the gamma dose g_f with $y_f = 100$ and $n_f = 34$

3.4 Discussion

It is extremely unlikely that the true value of the neutron/gamma dose ratio would be known precisely following a criticality accident. The Bayesian approach presented above provides a means for estimating the influence of the uncertainty of this ratio on estimates of the total dose as well as the neutron and gamma components. This fact, combined with the ability to incorporate ancillary information and to quantify the uncertainty of dose estimates probabilistically shows that this approach is an improvement over the methods currently used to estimate doses after a criticality accident.

CHAPTER 4: CHROMOSOME DOSIMETRY WITH UNCERTAIN CALIBRATION DOSES

4.1 Introduction

In Chapters 2 and 3, Poisson models were used to analyze radiation-induced dicentrics in lymphocytes with the assumption of precise doses in the calibration experiment. In this chapter, the influence of uncertain calibration doses on the calibrative density is investigated. In Section 4.2, the method is developed for the simplest dose response model: linear dependence on dose with negligible background. In Section 4.3, the method is demonstrated for three different calibration data sets: high doses of neutrons, low doses of neutrons, and X-ray exposures. The resulting parameter and dose estimates are compared to those obtained with an assumption of precise calibration doses. Finally, a discussion in Section 4.4 concludes the chapter.

4.2 Method

This portion of the research benefited from the work of Lindley et al. (1966, 1967) on functional relationships. Although their error-in-variables models were not employed, much of their original argument and notation was used. The development begins with a discussion and reinterpretation of calibration experiments.

As noted earlier, a calibration experiment consists of the following steps: exposing a sample of blood to a dose of radiation, ξ_i, scoring the number of dicentrics, y_i, observed in a sample of n_i lymphocytes (or genome equivalents (GE), depending on the staining technique), and then repeating the first two steps for i=(1, 2,..., k) dose levels. Clearly, the ξ_i are not directly observable, instead they are estimated based on information such as source strength, geometry, etc. In precise dose analyses these estimates of the true doses ξ_i, denoted t_i, are assumed to be equal to the true doses. Below, hierarchical models are used to account for the uncertainty about ξ_i.

The simplest example of a relationship between the number of aberrations, η, the number of lymphocytes scored, n, and dose ξ (rads) is given generically by

$$\eta = n\,\theta\,\xi \qquad \textbf{(4.1)}$$

The development is limited to this simplest model to minimize the complexity of the notation and expressions. It is assumed that y_i is an observation of η_i, Poisson distributed with mean $\eta_i = n_i\,\theta\,\xi_i$. The true doses, ξ_i, are treated as parameters having priors, denoted $p(\xi_i)$, with $E(\xi_i)= t_i$ and $Var(\xi_i) = \tau_i^2$. Uncertainty with regards to the discrepancy between a particular ξ_i and its estimate t_i can be accounted for by numerical integration over τ_i, referred to as a hyperparameter, where the range of integration reflects beliefs about the smallest and largest credible discrepancies.

The parameter θ is usually referred to as "structural" since it appears in the likelihood of all the observations, and the ξ_i, and τ_i are labeled "incidental" as they are associated with a particular $\{y_i\}$ only. The incidental parameter vectors will be denoted by $\boldsymbol{\xi} = \{\xi_1, \xi_2, \ldots, \xi_k\}$ and $\boldsymbol{\tau} = \{\tau_1, \tau_2, \ldots, \tau_k\}$. Similarly, the notation $\mathbf{t} = \{t_1, t_2, \ldots, t_k\}$ and $\mathbf{n} = \{n_1, n_2, \ldots, n_k\}$ is used for the estimated doses and lymphocytes scored. The following assumptions are made:

(1) $$p(\theta,\boldsymbol{\tau}) = p(\theta)p(\boldsymbol{\tau}) \propto \text{constant}$$

(2) the ξ_i, given $\mathbf{t}$ and $\boldsymbol{\tau}$, are independent:

$$p(\boldsymbol{\xi}|\mathbf{t},\boldsymbol{\tau}) = \prod_{i=1}^{k} p(\xi_i|\mathbf{t},\boldsymbol{\tau})$$

(3) for a given t_i and τ_i, ξ_i is independent of all t_j and τ_j with $j \neq i$

$$p(\xi_i|\mathbf{t},\boldsymbol{\tau}) = p(\xi_i|t_i,\tau_i)$$

(4) the y_i, given $\boldsymbol{\xi}$, θ, and $\mathbf{n}$, are independent:

$$p(\mathbf{y}|\boldsymbol{\xi},\theta,\mathbf{n}) = \prod_{i=1}^{k} p(y_i|\boldsymbol{\xi},\theta,\mathbf{n})$$

(5) for a given ξ_i, θ, and n_i, y_i is independent of all ξ_j and n_j with j $\neq$ i

$$p(y_i|\boldsymbol{\xi},\theta,\mathbf{n}) = p(y_i|\xi_i,\theta,n_i)$$

For the analyses to follow in Section 4.3, the $p(\xi_i)$ were assumed to have gamma distributions parameterized such that $E(\xi_i) = t_i = \lambda_i / \rho_i$ and $Var(\xi_i) = \tau_i^2 = \lambda_i/\rho_i^2$. Gamma

distributions were used for computational convenience. They permit analytical elimination of the ξ_i, and are flexible enough to permit expression of a wide variety of prior opinions. Numerical values for λ_i and ρ_i were calculated by solving $E(\xi_i)= t_i = \lambda_i/\rho_i$ and $Var(\xi_i) = (\sigma_i/3)^2 = \lambda_i/(\rho_i)^2$, for λ_i and ρ_i, where $t_i \pm \sigma_i$ corresponds to an approximate 99% probability interval for ξ_i. Using these distributional assumptions and (1)-(5) from above, the posterior distribution of θ can be constructed and the incidental ξ's eliminated as follows

$$p(\theta|\mathbf{y},\mathbf{n},\mathbf{t},\boldsymbol{\lambda},\boldsymbol{\rho}) \propto \int_{\Xi} p(\mathbf{y},\boldsymbol{\xi}|\theta,\boldsymbol{\lambda},\boldsymbol{\rho},\mathbf{n},\mathbf{t})d\boldsymbol{\xi} \qquad \text{(by assumption (1))}$$

$$\propto \int_{\Xi} p(\mathbf{y}|\boldsymbol{\xi},\theta,\mathbf{n})p(\boldsymbol{\xi}|\mathbf{t},\boldsymbol{\lambda},\boldsymbol{\rho})\mathrm{d}\boldsymbol{\xi}$$

$$\propto \int_{\Xi}\prod_{i=1}^{k} p(y_i|\boldsymbol{\xi},\theta,\mathbf{n})p(\xi_i|\mathbf{t},\boldsymbol{\lambda},\boldsymbol{\rho})\mathrm{d}\boldsymbol{\xi} \qquad \text{(by assumptions (2) and (4))}$$

$$\propto \prod_{i=1}^{k}\int_{0}^{\infty}(\theta\xi_i)^{y_i}\exp\{-n_i\theta\xi_i\}\xi_i^{\lambda_i-1}\exp\{-\rho_i\xi_i\}d\xi_i) \qquad \text{(by assumptions (3) and (5))}$$

$$\propto \prod_{i=1}^{k}(\theta^{y_i}\int_{0}^{\infty}\xi_i^{y_i+\lambda_i-1}\exp\{-\xi_i(n_i\theta+\rho_i)\}d\xi_i)$$

$$\propto \prod_{i=1}^{k}\frac{\theta^{y_i}\Gamma(y_i+\lambda_i)}{(n_i\theta+\rho_i)^{y_i+\lambda_i}} \qquad \textbf{(4.2)}$$

For dose estimation the calibrative density was again used. This density characterizes here the uncertainty about Ξ_f conditional on all available data D_A, which consist of the calibration data D_c and the number of dicentrics, y_f, observed in a sample of n_f

lymphocytes, or GE, taken from a hypothetical individual exposed to an unknown dose Ξ_f. The calibrative density for a controlled calibration experiment is given by:

$$p(\xi_f|D_A) \propto p(\xi_f)\int_{\Theta} p(y_f|n_f,\xi_f,\theta)p(\theta|\mathbf{y},\mathbf{n},\mathbf{t},\boldsymbol{\lambda},\boldsymbol{\rho})d\theta \qquad \textbf{(4.3)}$$

$p(\xi_f)$ is the prior density for Ξ_f, $D_A=D_c+\{y_f|\, n_f\}$, $p(y_f \mid n_f, t_f, \theta)$ is the Poisson likelihood for a future observation, and $p(\theta|\mathbf{y},\mathbf{n},\mathbf{t},\boldsymbol{\lambda},\boldsymbol{\rho})$ is the posterior density of the parameter from Equation 4.2.

4.3. Examples

4.3.1 High Neutron Dose Data

The first calibration data set analyzed, denoted D_B, is from Lloyd et al. (1979) for exposure to 0.7 MeV fission neutrons from the British Experimental Pile Zero reactor (BEPO). The data consist of calculated dose values, t_i (rad), the number of lymphocytes scored, n_i, and the number of dicentric chromosome aberrations observed, y_i. D_B is given by the vectors

$$\mathbf{t}=\{50, 75, 100, 150, 200, 250\ 300\}$$

$$\mathbf{n}=\{269, 78, 115, 90, 84, 59, 37\}$$

$$\mathbf{y}=\{109, 47, 94, 114, 138, 125, 97\}$$

The distributional assumptions made were: $y_i \sim \text{Po}[n_i \beta \xi_i]$ and $p(\xi_i) \sim \text{Ga}[\lambda_i, \rho_i]$. The λ_i and ρ_i were calculated by assuming approximate 99% probability intervals for the doses of 50 ± 30, 75 ± 40, 100 ± 52.5, 150 ± 67.5, 200 ± 75, 250 ±75, and 300 ± 67.5 (rads). Note that these probability intervals are only used for demonstration and do not necessarily reflect the dose uncertainty in the original published experiments. The resulting values are given by the vectors

$$\boldsymbol{\lambda} = \{25, 28.70, 32.65, 44.44, 64, 100, 177.77\}$$

$$\boldsymbol{\rho} = \{0.5, 0.38, 0.33, 0.30, 0.32, 0.4, 0.6\}$$

Figure 4.1 shows the $p(\xi_i)$.

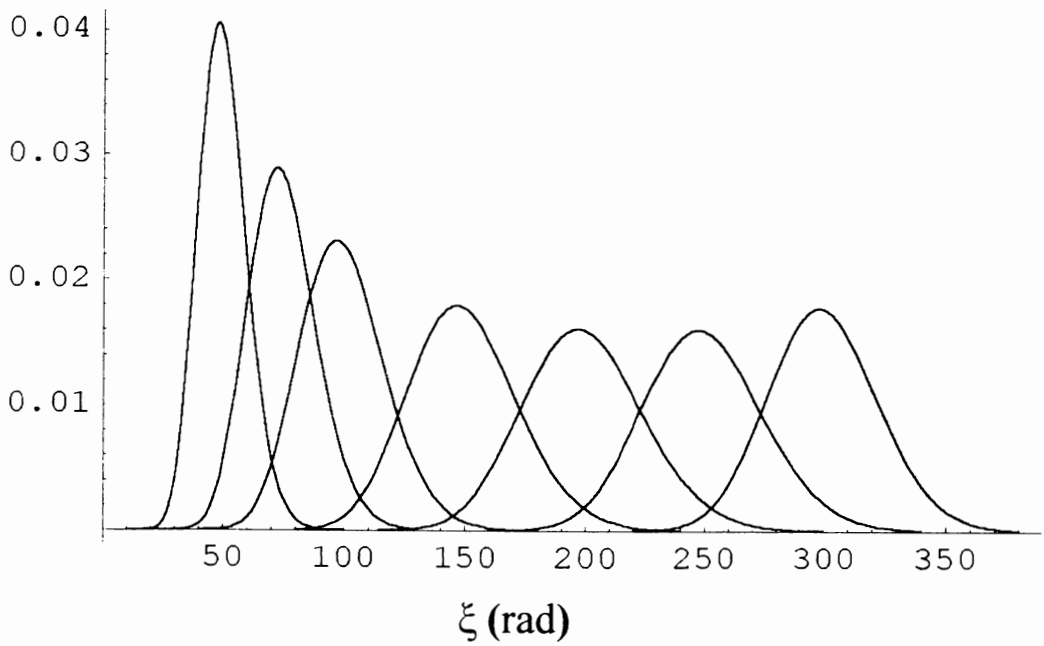

Figure 4.1: Gamma priors for the true doses (BEPO data)

The posterior density for the slope parameter β in proportional form was derived as follows

$$p(\beta|\boldsymbol{\lambda},\boldsymbol{\rho},D_B) \propto \int_{\Xi}\prod_{i=1}^{6}(\beta\xi_i)^{y_i}\exp\{-n_i\beta\xi_i\}\xi_i^{\lambda_i-1}\exp\{-\rho_i\xi_i\}d\boldsymbol{\xi}$$

$$\propto \prod_{i=1}^{6}(\beta^{y_i}\int_{0}^{\infty}\xi_i^{y_i+\lambda_i-1}\exp\{-\xi_i(n_i\beta+\rho_i)\}d\xi_i)$$

$$\propto \prod_{i=1}^{6}\frac{\beta^{y_i}\Gamma(y_i+\lambda_i)}{(n_i\beta+\rho_i)^{y_i+\lambda_i}} \qquad \textbf{(4.4)}$$

Figure 4.2 shows a comparison of the marginal densities for β for precise and uncertain doses.

In the dose estimation example it was assumed that y_f= 64 dicentrics were observed in n_f =104 scored lymphocytes of the accident victim. The calibrative density is given by

$$p(\xi_f|D_A) \propto p(\xi_f)\int_{B}(\beta\xi_f)^{y_f}\exp\{-n_f\beta\xi_f\}p(\beta|\boldsymbol{\lambda},\boldsymbol{\rho},D_B)d\beta \qquad \textbf{(4.5)}$$

D_A=D_B+{y_f| n_f}, $p(\xi_f)$ is assumed constant, and $p(\beta|\boldsymbol{\lambda},\boldsymbol{\rho},D_B)$ is from Equation 4.4.

Figure 4.3 compares the calibrative densities for precise and uncertain calibration doses. The influence of calibration dose uncertainty on ξ_f was small in this case.

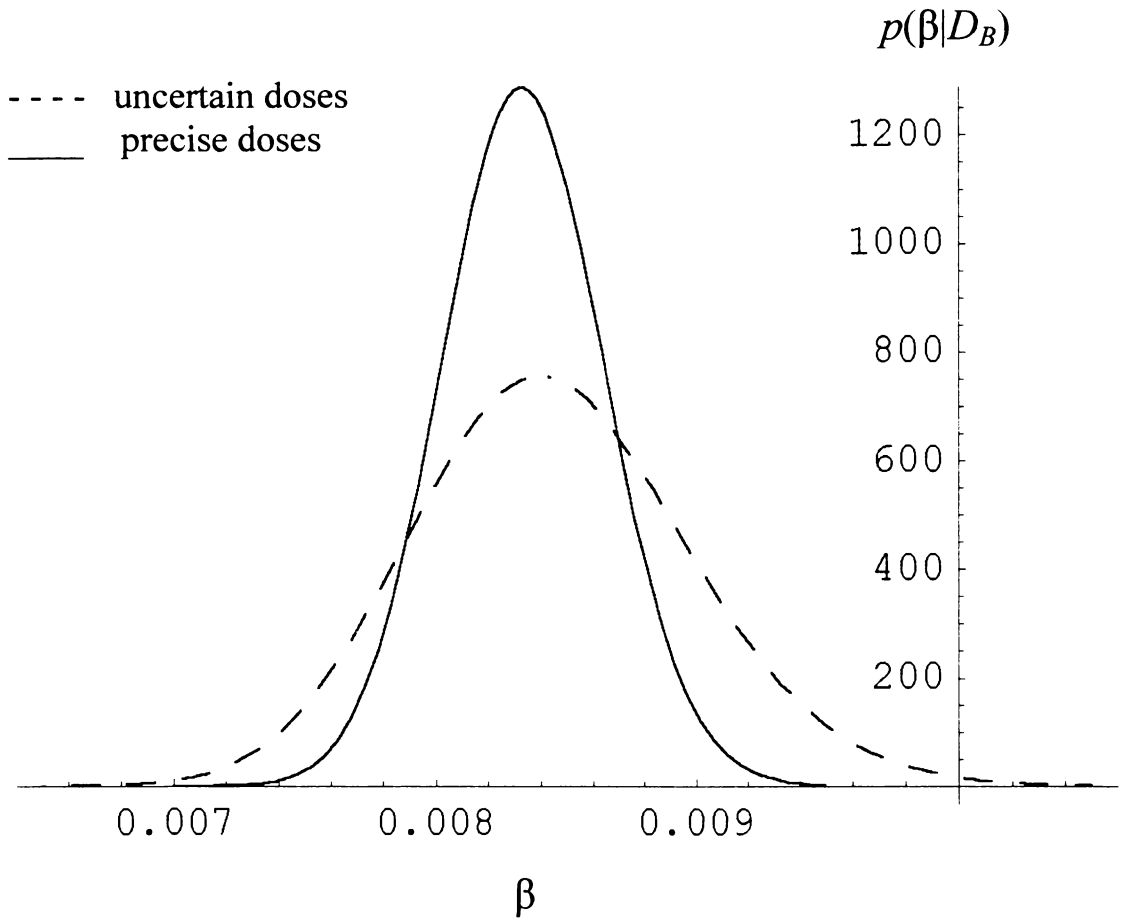

Figure 4.2: Marginal Densities of β for the BEPO data

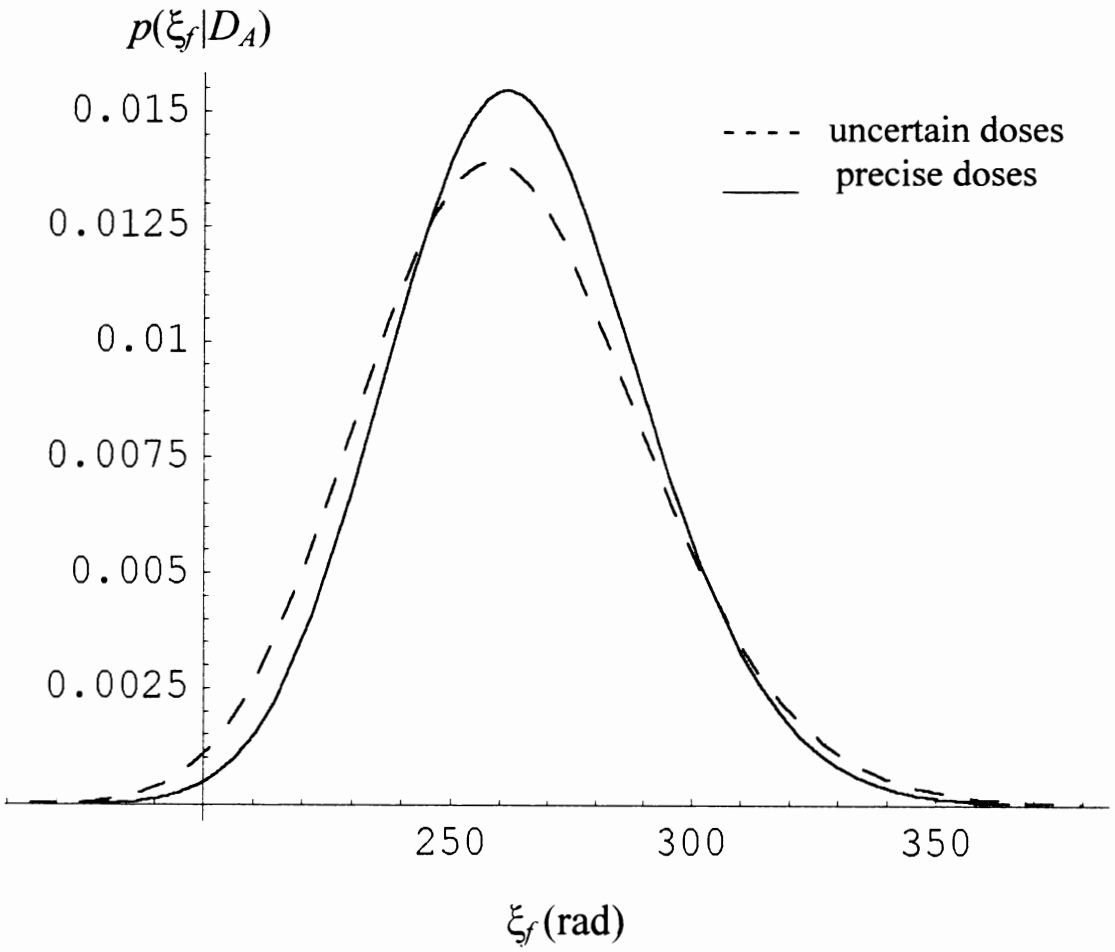

Figure 4.3: Calibrative densities for the BEPO data set with $y_f = 64$ and $n_f = 104$

4.3.2 Low Neutron Dose Data

The second calibration data set analyzed, denoted D_I, was from Inoue (1995*a*) for exposure to low doses of neutrons from a ^{252}Cf neutron source. The vectors comprising D_I have descriptions analogous to those previously given for the high neutron dose data. D_I is given by the vectors

$$\mathbf{t}=\{0.0, 0.2, 0.5, 0.75, 1.0, 2.0\}$$

$$\mathbf{n}=\{16000, 10000, 9300, 4660, 2477, 708\}$$

$$\mathbf{y}=\{10, 35, 70, 47, 39, 24\}$$

The distributional assumptions made were that $y_i \sim \text{Po}[n_i(\alpha+\beta\xi_i)]$ and $p(\xi_i)\sim\text{Ga}[\lambda_i, \rho_i]$. The λ_i and ρ_i were calculated by assuming approximate 99% probability intervals for the doses of 0.2 ± 0.2, 0.5 ± 0.45, 0.75 ± 0.6, 1.0 ± 0.7, and 2.0 ± 1.0 (rads). Note that the zero dose level was assumed precise. The results are given by the vectors

$$\boldsymbol{\lambda}=\{0, 9.0, 11.11, 14.06, 18.37, 36.0\}$$

$$\boldsymbol{\rho}=\{0, 45.0, 22.22, 18.75, 18.37, 18.0\}$$

The first element in both vectors is a dummy entry that accounts for the assumption of a precise zero dose level. The $p(\xi_i)$ are shown in Figure 4.4:

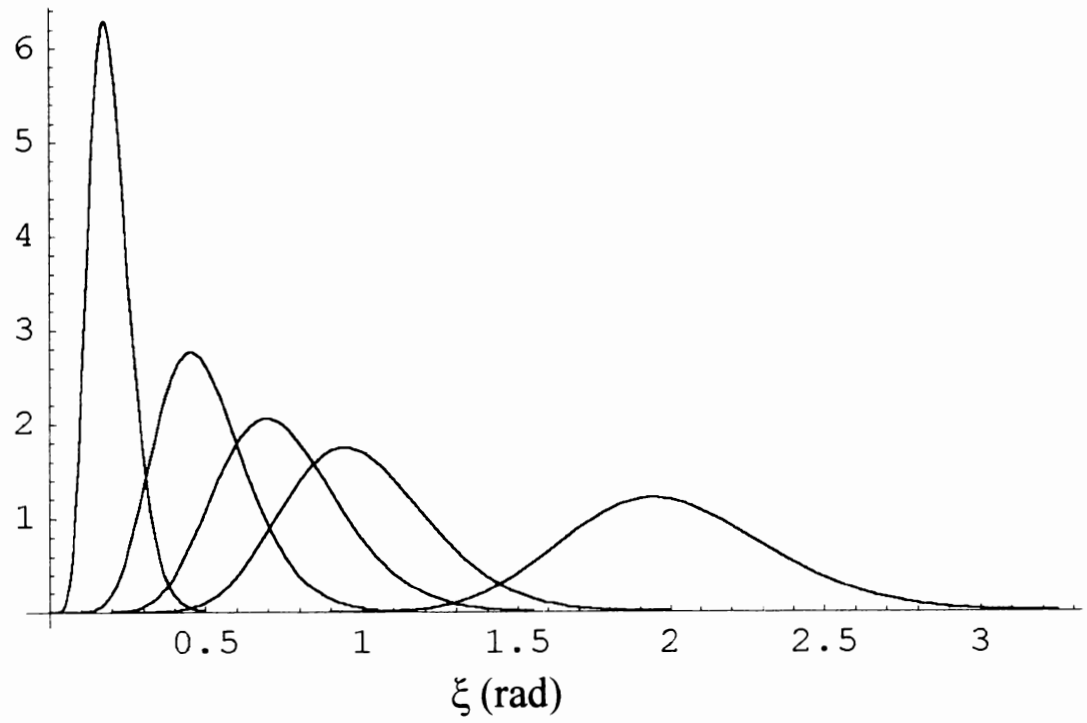

Figure 4.4: Gamma priors for the true doses (^{252}Cf data)

The joint posterior density for the parameters α and β in proportional form was derived as follows

$$p(\alpha,\beta|\boldsymbol{\lambda},\boldsymbol{\rho},D_I) \propto \alpha^{y_1}\exp\{-n_1\alpha\}\int_{\Xi}\prod_{i=2}^{6}(\alpha+\beta\xi_i)^{y_i}\exp\{-n_i(\alpha+\beta\xi_i)\}\xi_i^{\lambda_i-1}\exp\{-\rho_i\xi_i\}d\boldsymbol{\xi}$$

$$\propto \alpha^{y_1}\exp\{-n_1\alpha\}\int_{\Xi}\prod_{i=2}^{6}\left(\sum_{j=0}^{y_i}\binom{y_i}{j}\alpha^{y_i-j}\beta^{j}\xi_i^{j+\lambda_i-1}\exp\{-n_i\alpha-\xi_i(n_i\beta+\rho_i)\}\right)d\boldsymbol{\xi}$$

$$\propto \alpha^{y_1}\exp\{-n_1\alpha\}\prod_{i=2}^{6}\left(\sum_{j=0}^{y_i}\binom{y_i}{j}\alpha^{y_i-j}\exp\{-n_i\alpha\}\beta^{j}\int_0^{\infty}\xi_i^{j+\lambda_i-1}\exp\{-\xi_i(n_i\beta+\rho_i)\}d\xi_i\right)$$

$$\propto \alpha^{y_1}\exp\{-n_1\alpha\}\prod_{i=2}^{6}\left(\sum_{j=0}^{y_i}\binom{y_i}{j}\alpha^{y_i-j}\exp\{-n_i\alpha\}\beta^{j}\frac{\Gamma(\lambda_i+j)}{(n_i\beta+\rho_i)^{\lambda_i+j}}\right) \qquad \textbf{(4.6)}$$

Analytic forms of the marginal densities for α or β were obtained by integrating over the other parameter. The marginal densities in proportional form are given by

$$p(\alpha|\boldsymbol{\lambda},\boldsymbol{\rho},D_I) \propto \prod_{i=2}^{6}\left(\sum_{j=0}^{y_i}\binom{y_i}{j}\alpha^{y_i+y_1-j}\exp\{-\alpha(n_i+n_1)\}\Gamma(\lambda_i+j)\int_0^{\infty}\frac{\beta^j}{(n_i\beta+\rho_i)^{\lambda_i+j}}d\beta\right)$$

$$\propto \prod_{i=2}^{6}\left(\sum_{j=0}^{y_i}\binom{y_i}{j}\alpha^{y_i+y_1-j}\exp\{-\alpha(n_i+n_1)\}\frac{(\rho_i)^{1-j}}{n_i^{j+1}}\Gamma(1+j)\Gamma(\lambda_i-1)\right) \quad \textbf{(4.7)}$$

$$p(\beta|\boldsymbol{\lambda},\boldsymbol{\rho},D_I) \propto \prod_{i=2}^{6}\left(\sum_{j=0}^{y_i}\binom{y_i}{j}\beta^j\frac{\Gamma(\lambda_i+j)}{(n_i\beta+\rho_i)^{\lambda_i+j}}\int_0^{\infty}\alpha^{y_i+y_1-j}\exp\{-\alpha(n_i+n_1)\}d\alpha\right)$$

$$\propto \prod_{i=2}^{6}\left(\sum_{j=0}^{y_i}\binom{y_i}{j}\beta^j\frac{\Gamma(\lambda_i+j)}{(n_i\beta+\rho_i)^{\lambda_i+j}}\frac{\Gamma(y_i+y_1-j+1)}{(n_i+n_1)^{y_i+y_1-j+1}}\right) \quad \textbf{(4.8)}$$

Figures 4.5 and 4.6 show the marginal densities for precise and uncertain doses. There was a slight difference in the posterior densities of α, and a more pronounced difference in the posterior densities of β.

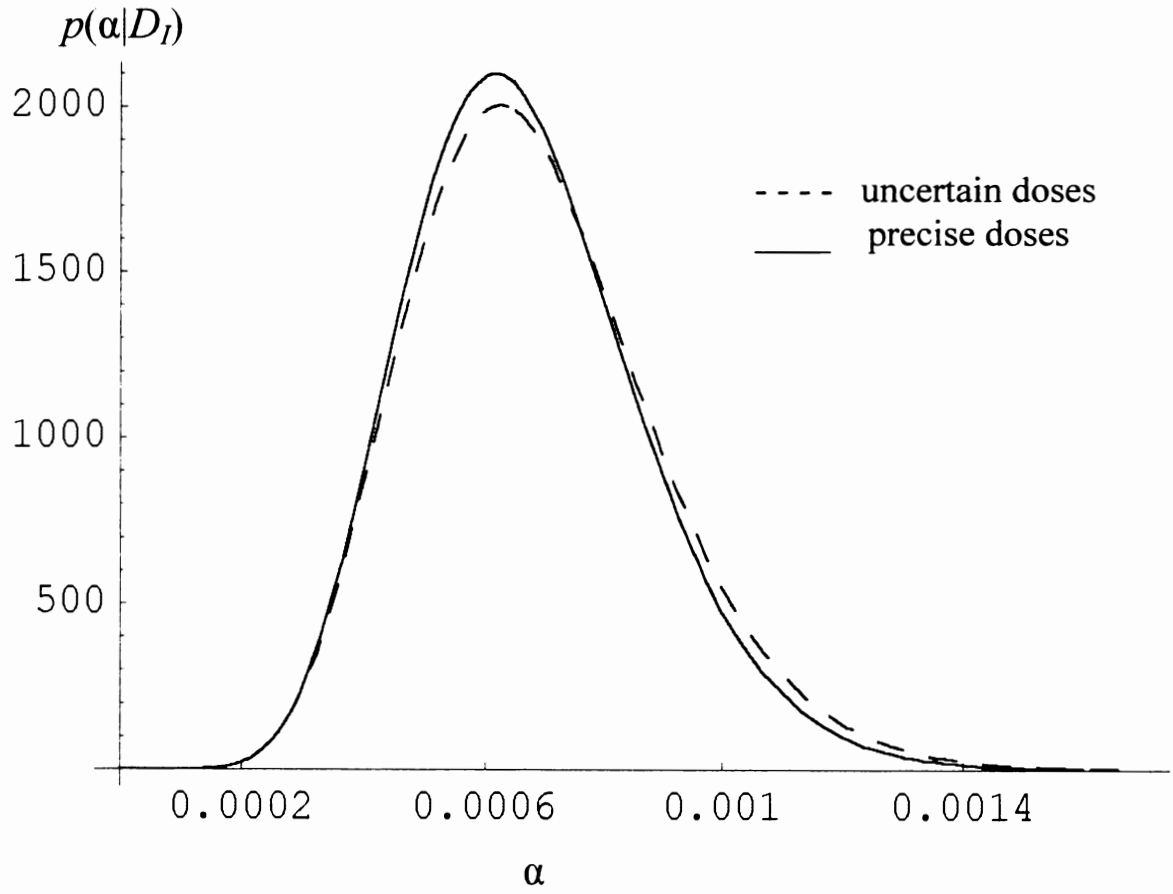

Figure 4.5: Marginal densities of α for the ^{252}Cf data set

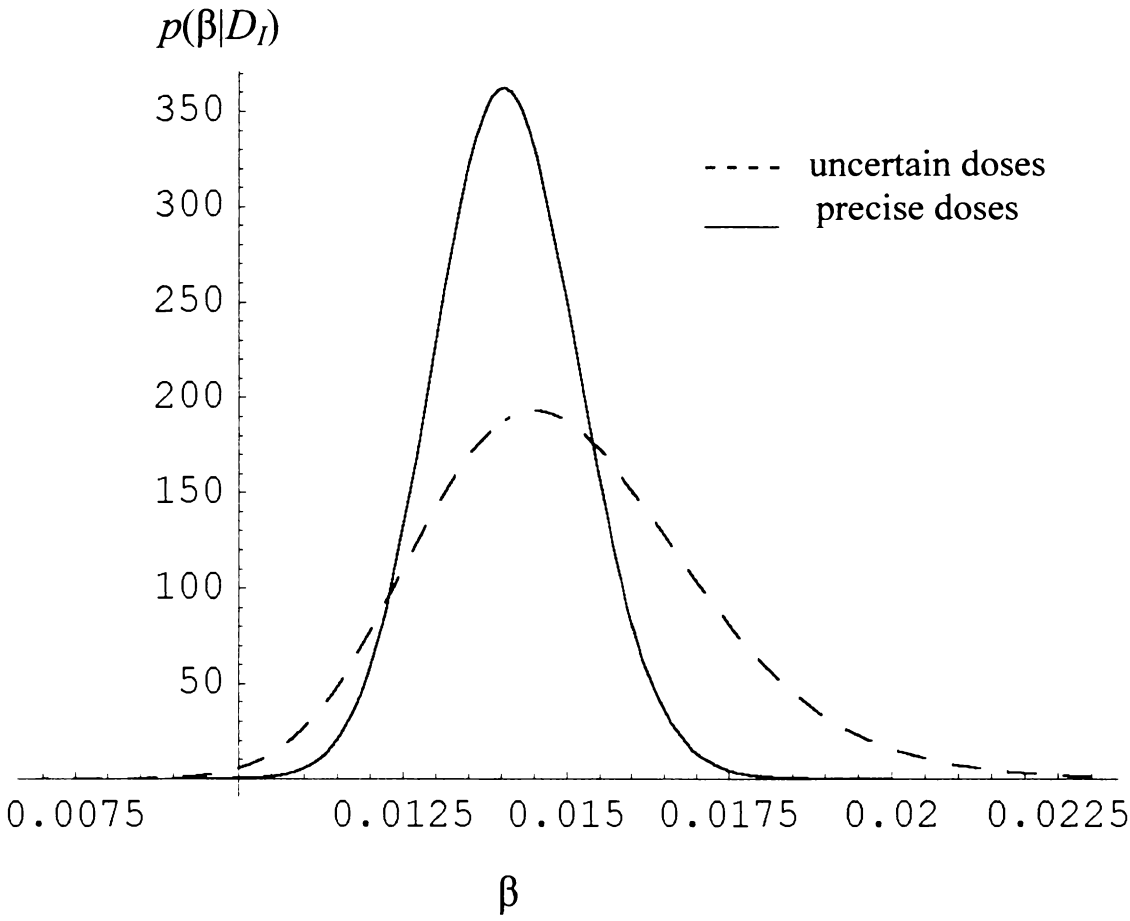

Figure 4.6: Marginal densities of β for the ^{252}Cf data set

For the dose estimation example it was assumed that y_f= 25 dicentrics were observed in n_f=5000 lymphocytes of the accident victim. The calibrative density is given by

$$p(\xi_f|D_A) \propto p(\xi_f) \int_B \int_A (\alpha+\beta\xi_f)^{y_f} \exp\{-n_f(\alpha+\beta\xi_f)\} p(\alpha,\beta|\boldsymbol{\lambda},\boldsymbol{\rho},D_I) d\alpha d\beta \quad \textbf{(9)}$$

D_A=D_I+{y_f| n_f}, $p(\xi_f)$ is assumed constant, and $p(\alpha,\beta|\boldsymbol{\lambda},\boldsymbol{\rho},D_I)$ is from Equation 4.6. Figure 4.6 compares the calibrative densities for precise and uncertain doses. The influence of dose uncertainty on ξ_f was again found to be small.

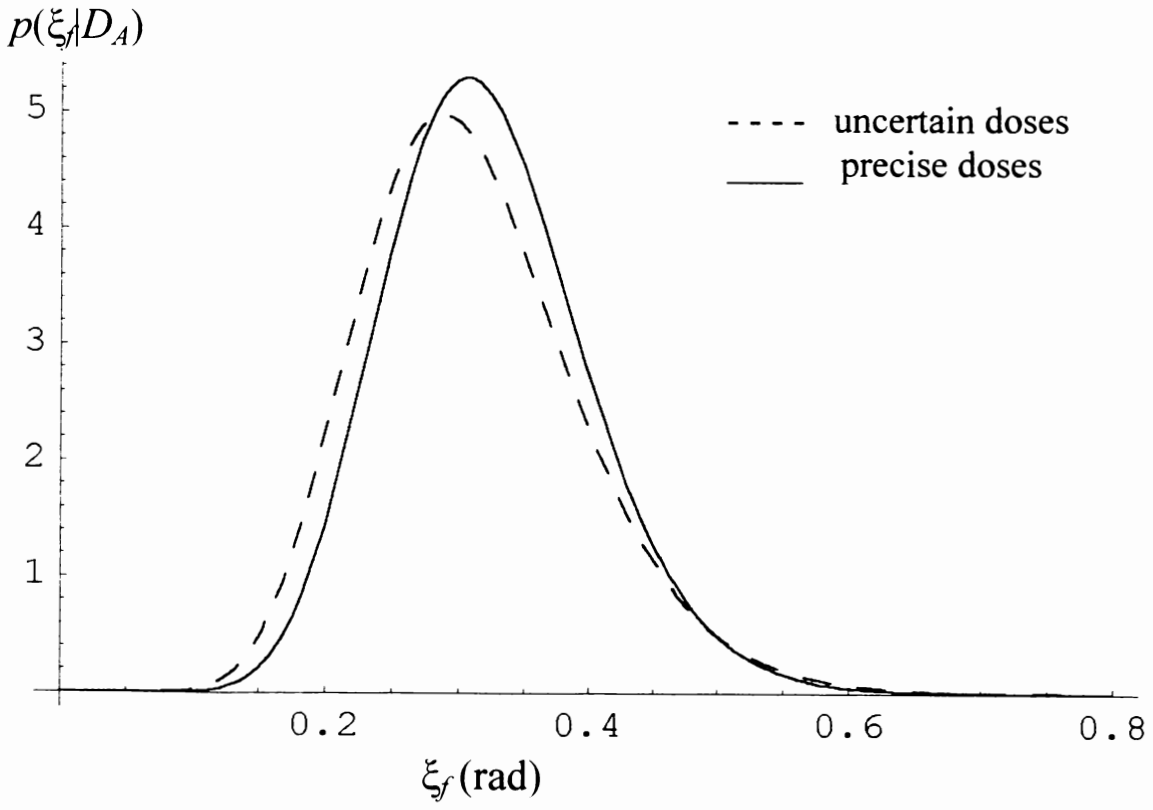

Figure 4.7: Calibrative densities for the ^{252}Cf data with y_f = 25 and n_f = 5000

4.3.3 X-ray Calibration Data

The final calibration data set analyzed, denoted D_F, was from Bothwell et al (2000) for exposure to X-rays generated by a Seiffert therapeutic X ray machine. The vectors comprising the data set are analogous to the vectors given for the two previous data sets except that the n_i represent the number of GE rather than the number of lymphocytes since fluorescent in situ hybridization (FISH) was used. D_F is given by the following vectors

$$\mathbf{t}=\{0.0, 33.5, 65.8, 98.8, 196.1\}$$

$$\mathbf{n}=\{424, 409, 328, 341, 239\}$$

$$\mathbf{y}=\{0, 9, 21, 44, 105\}$$

The distributional assumptions made were that $y_i \sim \text{Po}[n_i(\alpha+\beta\xi_i+\gamma\xi_i^2)]$ and $p(\xi_i)\sim\text{Ga}[\lambda_i, \rho_i]$. The λ_i and ρ_i were calculated by assuming approximate 99% probability intervals for the doses of 33.5 ±33.5, 65.8 ± 59.22, 98.8 ± 79.04, and 196.1 ± 117.6 (rads). The results are given by the vectors

$$\boldsymbol{\lambda} = \{0, 9.0, 11.11, 14.06, 25.0\}$$

$$\boldsymbol{\rho} = \{0, 0.27, 0.17, 0.14, 0.13\}$$

Note that the zero dose level was again assumed precise and that a dummy entry was inserted into the first position of both vectors. The $p(\xi_i)$ are shown in Figure 4.8.

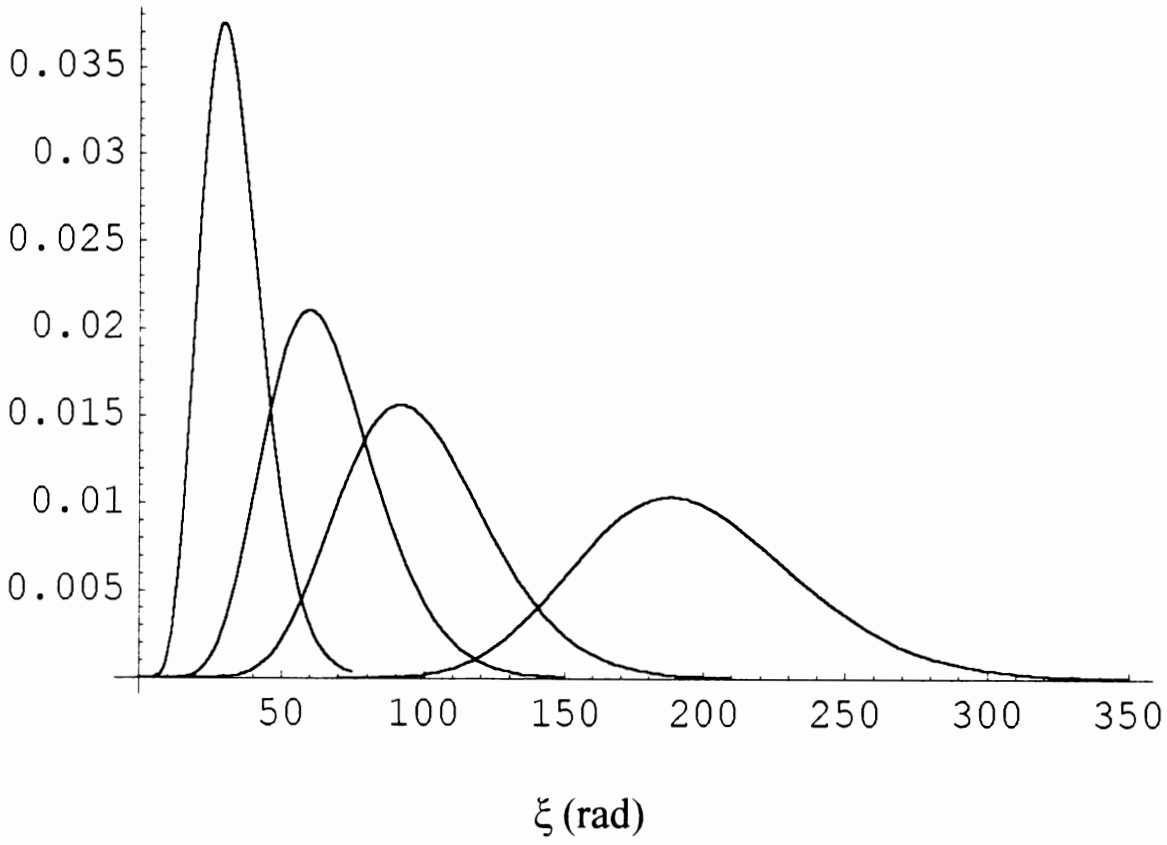

Figure 4.8: Gamma priors for the true doses (FISH data)

The incidental ξ_i were eliminated and the joint posterior density of the parameters derived as follows:

$$p(\alpha,\beta,\gamma|\boldsymbol{\lambda},\boldsymbol{\rho},D_F) \propto \int_{\Xi} \alpha^{y_1} e^{-n_1\alpha} \prod_{i=2}^{5} p(y_i|\boldsymbol{\xi},\alpha,\beta,\gamma,n_i)p(\boldsymbol{\xi}|\mathbf{t},\boldsymbol{\lambda},\boldsymbol{\rho})d\boldsymbol{\xi} \qquad \textbf{(4.10)}$$

$$\propto \alpha^{y_1} e^{-n_1\alpha} \int_{\Xi} \prod_{i=2}^{5} (\alpha+\beta\xi_i+\gamma\xi_i^2)^{y_i} \exp\{-n_i(\alpha+\beta\xi_i+\gamma\xi_i^2)-\rho_i\xi_i\}\xi_i^{\lambda_i-1} d\boldsymbol{\xi}$$

$$\propto \int_{\Xi} \prod_{i=2}^{5} \left(\sum_{j=0}^{y_i} \binom{y_i}{j} \alpha^{y_i+y_1-j} \exp\{-\alpha(n_i+n_1)\} \left(\sum_{m=0}^{j} \binom{j}{m} \beta^{j-m}\gamma^m \xi_i^{j+m+\lambda_i-1} \right) \exp\{-\xi_i^2 n_i\gamma - \xi_i(n_i\beta+\rho_i)\} \right)$$

$$\propto \prod_{i=2}^{5} \left(\sum_{j=0}^{y_i} \binom{y_i}{j} \alpha^{y_i+y_1-j} \exp\{-\alpha(n_i+n_1)\} \left(\sum_{m=0}^{j} \binom{j}{m} \beta^{j-m}\gamma^m \int_0^{\infty} \xi_i^{j+m+\lambda_i-1} \exp\{-\xi_i^2 n_i\gamma - \xi_i(n_i\beta+\rho_i)\} d\xi_i \right) \right)$$

$$\propto \prod_{i=2}^{5} \left(\sum_{j=0}^{y_i} \binom{y_i}{j} \alpha^{y_i+y_1-j} \exp\{-\alpha(n_i+n_1)\} \left(\sum_{m=0}^{j} \binom{j}{m} \beta^{j-m}\gamma^m \times A(\beta,\gamma) \right) \right) \qquad \textbf{(4.11)}$$

where

$$A(\beta,\gamma) = \frac{1}{2}(n_i\gamma)^{\frac{-(j+m+\lambda_i+1)}{2}} \left(\sqrt{n_i\gamma}\,\Gamma\left(\frac{j+m+\lambda_i}{2}\right)\Phi\left(\frac{j+m+\lambda_i}{2},\frac{1}{2},\frac{(n_i\beta+\rho_i)^2}{4n_i\gamma}\right) - (n_i\beta+\rho_i)\Gamma\left(\frac{j+m+\lambda_i+1}{2}\right)\Phi\left(\frac{j+m+\lambda_i+1}{2},\frac{3}{2},\frac{(n_i\beta+\rho_i)^2}{4n_i\gamma}\right) \right)$$

Φ(a,b,c) represents the confluent hypergeometric function.

The joint posterior density of β and γ was obtained by analytical integration over α:

$$p(\beta,\gamma|\boldsymbol{\lambda},\boldsymbol{\rho},D_F)\propto\prod_{i=2}^{5}\left(\sum_{j=0}^{y_i}\binom{y_i}{j}\frac{\Gamma(y_i+y_1-j+1)}{(n_i+n_1)^{y_i+y_1-j+1}}\left(\sum_{m=0}^{j}\binom{j}{m}\beta^{j-m}\gamma^m\times A(\beta,\gamma)\right)\right) \quad \textbf{(4.12)}$$

The complexity of Equations 4.11 and 4.12 forced the use of quasi-Monte Carlo numerical integration (Wolfram, 1996) of Equation 10 over Ξ and the appropriate structural parameters instead of using Equations 4.11 and 4.12 directly to obtain marginal densities for α, β, and γ. Figures 4.9, 4.10, and 4.11 compare the marginal densities for precise and uncertain doses.

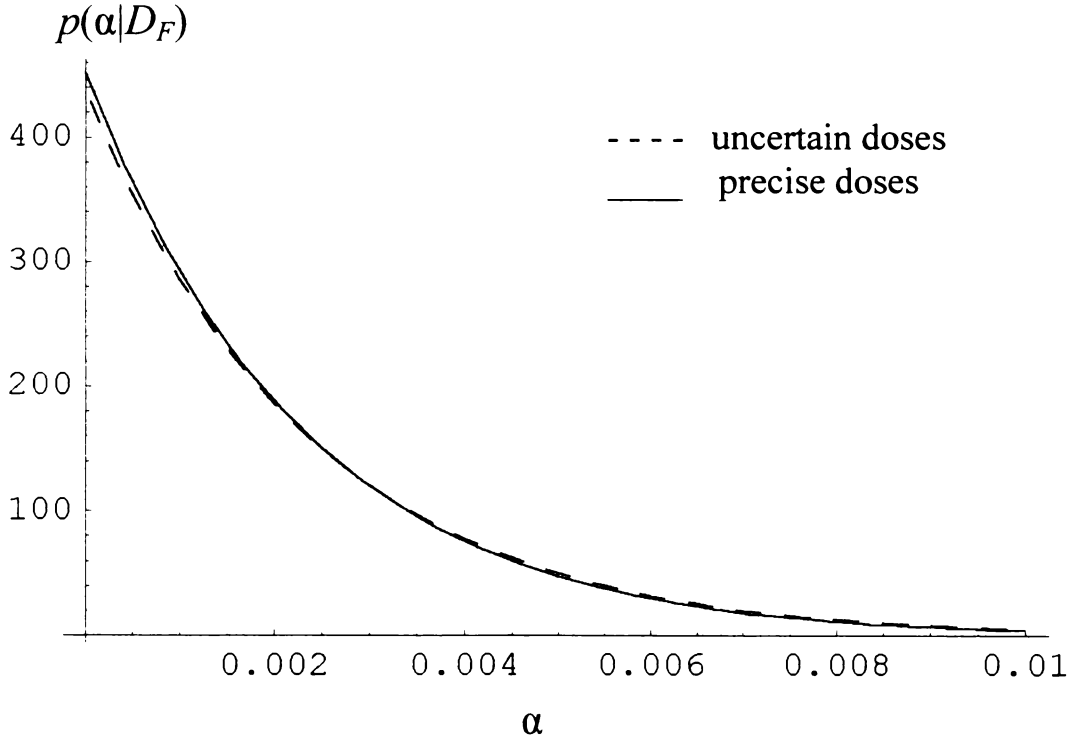

Figure 4.9: Marginal densities of α for the FISH data

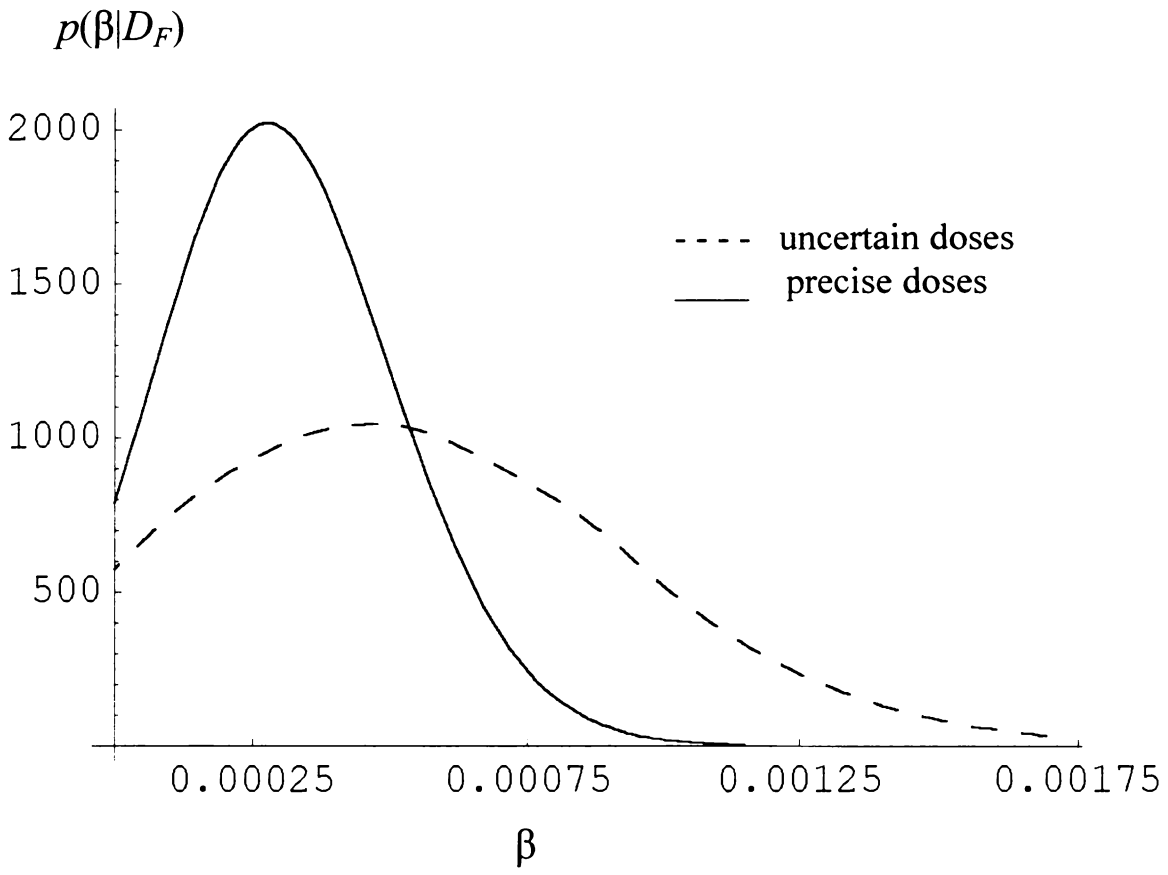

Figure 4.10: Marginal densities of β for the FISH data

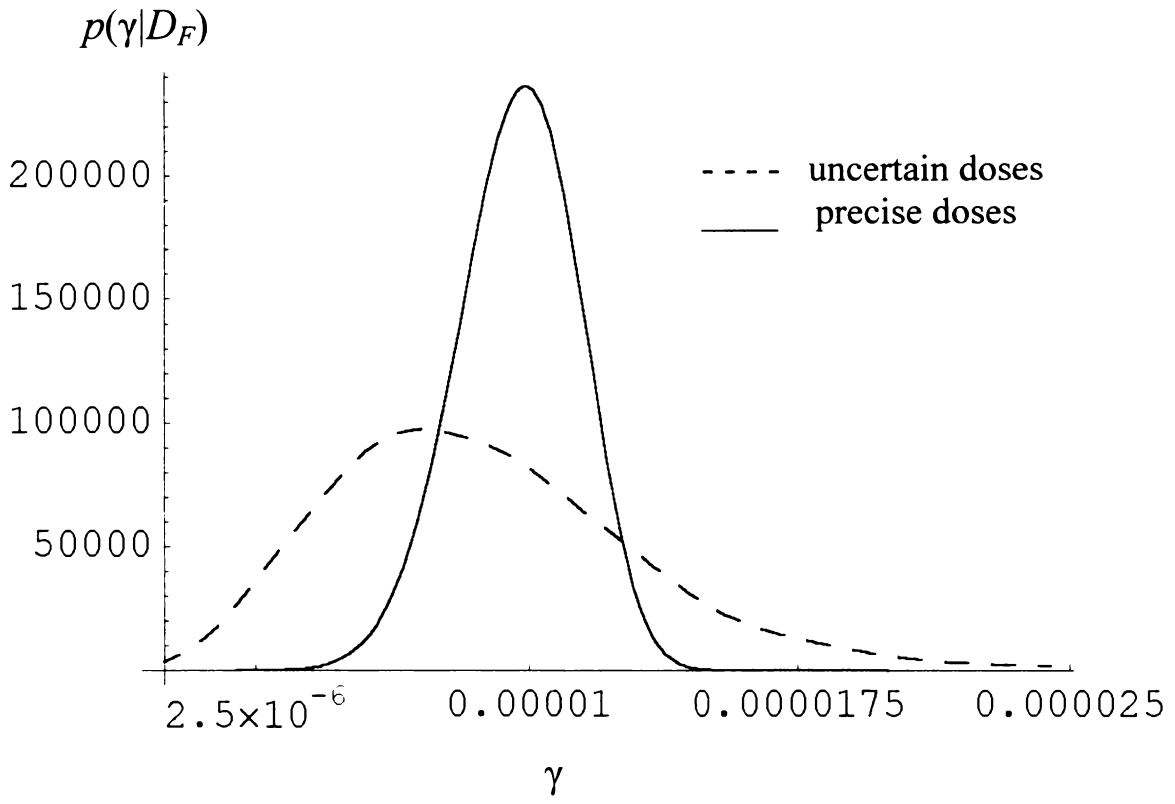

Figure 4.11: Marginal densities of γ for the FISH data

There was little difference in the marginal densities of α, but distinct differences between the marginals for β and γ. In the dose estimation example for D_F it was assumed that y_f= 35 dicentrics were observed in n_f=330 GE. The calibrative density conditional on the available data, $D_A = D_F + \{y_f | n_f\}$, with a constant prior $p(\xi_f)$ is given by

$$p(\xi_f | D_A) \propto \int_{\Gamma}\int_{B}\int_{A} (\alpha + \beta\xi_f + \gamma\xi_f^2)^{y_f} \exp\{-n_f(\alpha + \beta\xi_f + \gamma\xi_f^2)\} p(\alpha, \beta, \gamma | \boldsymbol{\lambda}, \boldsymbol{\rho}, D_F) d\alpha d\beta d\gamma$$

$p(\alpha, \beta, \gamma | \boldsymbol{\lambda}, \boldsymbol{\rho}, D_F)$ is given by Equation 4.10 and all integrations were again performed numerically with quasi-Monte Carlo integration. Figure 4.12 compares the calibrative densities for precise and uncertain doses. In this case the calibration dose uncertainty significantly increased the uncertainty of the dose estimate.

4.4. Discussion

The approach presented above provides a framework for evaluating the influence of imprecise calibration doses on parameter and dose estimates. As is the case with any hierarchical approach, different distributional assumptions about the $p(\xi_i)$ can be made. The analytical expressions obtained for posterior distributions of the parameters based on the assumption of gamma distributions for the $p(\xi_i)$ were a convenient starting point for such an analysis.

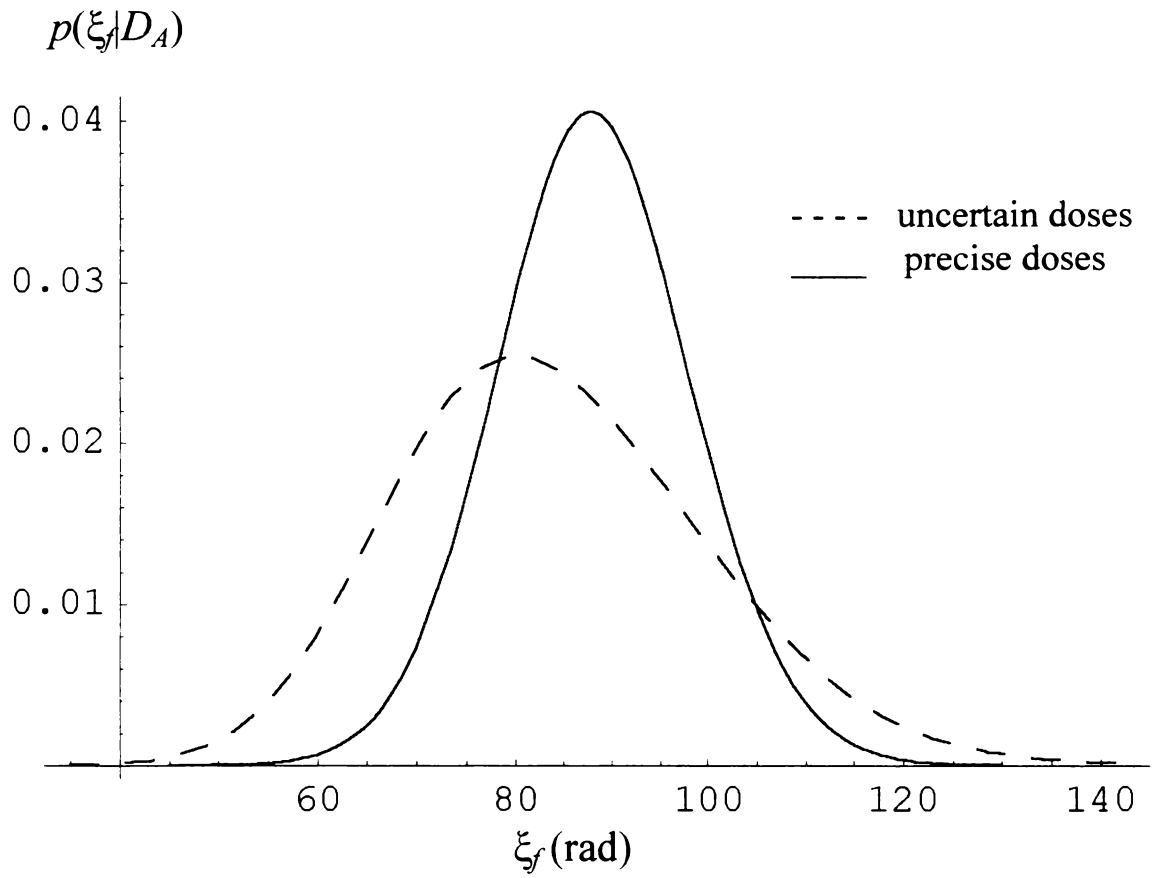

Figure 4.12: Calibrative densities for the FISH data with $y_f = 35$ and $n_f = 330$

CHAPTER 5: MODEL COMPARISON USING BAYES FACTORS AND PARTIAL BAYES FACTORS

5.1 Introduction

The selection of an appropriate model is critical for good inference. This portion of the research focuses on model comparison and selection from a Bayesian standpoint. The Bayesian approach to model comparison is well known (O'Hagan 1994; Kass 1983): given two competing models, m_1 and m_2, the probabilities of the models conditional on the same data D are compared. This idea is expressed mathematically as follows

$$\frac{p(m_1 \mid D)}{p(m_2 \mid D)} = \frac{p(D \mid m_1)}{p(D \mid m_2)} \frac{p(m_1)}{p(m_2)} \tag{5.1}$$

The term on the left is the posterior odds ratio, the first right-hand term is the Bayes Factor (BF), and the second right-hand term is the prior odds ratio. If no preexisting preference for either model exists, the prior odds ratio is set to 1 and the posterior odds ratio is then equal to the BF. This factor updates the probability that either model is valid. The BF for models 1 and 2 is given by

$$\frac{p(D|m_1)}{p(D|m_2)} = \frac{\int_{\Theta_1} L(\boldsymbol{\theta}_1|D)p(\boldsymbol{\theta}_1)d\boldsymbol{\theta}_1}{\int_{\Theta_2} L(\boldsymbol{\theta}_2|D)p(\boldsymbol{\theta}_2)d\boldsymbol{\theta}_2} \tag{5.2}$$

where $L(\boldsymbol{\theta}_1|D) \equiv$ Likelihood for parameter vector $\boldsymbol{\theta}_1$ given data D

$L(\boldsymbol{\theta}_2|D) \equiv$ Likelihood for parameter vector $\boldsymbol{\theta}_2$ given data D

$p(\boldsymbol{\theta}_i) \equiv$ joint prior distribution for parameter vector $\boldsymbol{\theta}_i$ (i=1,2)

Note that the $p(\boldsymbol{\theta}_i)$ are needed to calculate the BF. O'Hagan (1994) describes in detail the potential difficulty associated with use of the BF when there is weak prior information available regarding the $p(\boldsymbol{\theta}_i)$. In particular, improper priors may lead to infinite values for the BF, and the BF may be sensitive to the ranges of proper uniform priors. One method for dealing with weak prior information is known as Partial Bayes Factor (PBF) (Lempers 1971; O'Hagan 1994). Assuming that the data are divided into two groups y and z, where y is the training data, the PBF is given as

$$\text{Partial Bayes Factor} = \frac{p(z \mid m_1, y)}{p(z \mid m_2, y)} \qquad \textbf{(5.3)}$$

which is the ratio of the marginal densities of the data z for models 1 and 2 based on posterior densities $p(\boldsymbol{\theta}_i| y)$. The marginal densities are given by

$$p(z|\ m_i, y) = \int_{\Theta_i} L(\boldsymbol{\theta}_i|z)\, p(\boldsymbol{\theta}_i|\ y)\, d\boldsymbol{\theta}_i \qquad \textbf{(5.4)}$$

where

$L(\boldsymbol{\theta}_i| z) \equiv$ likelihood for parameter vector $\boldsymbol{\theta}_i$ given data z

$p(\boldsymbol{\theta}_i| y) \equiv$ joint posterior density for parameter vector $\boldsymbol{\theta}_i$ given training data y

The result of the integrations required by Equations 5.2 and 5.3 will be a numerical value representing the ratio of two probabilities. The logarithm of this value is referred to as the "weight of evidence" (Good 1983). Some authors, including Jeffreys (1998) and Turing as quoted in Good (1983), choose to interpret the weight of evidence on the $\log_{10}$ scale. For example, Jeffreys (1998) considers $\log_{10}(BF)>0.5$ as "substantial" evidence, $\log_{10}(BF)>1$ as "strong" evidence, and $\log_{10}(BF)>2$ as "decisive" evidence. Note that when discussing the interpretation of numerical values, the results apply to both the BF and the PBF.

The coin-tossing analogy of Good (1959) serves as a convenient device to calibrate one's interpretation of the BF (or PBF) and the corresponding weight of evidence. Suppose a coin is thought to be either fair or double-headed, designated by M_1 and M_2 respectively. If both models are assumed to be equally probable, i.e.- $p(M_1)$ and $p(M_2) = 1/2$, the prior odds ratio is 1 and the posterior odds ratio equals the BF. Suppose now that the coin is tossed ten times, each toss resulting in heads. The BF is then given by

$$\frac{p(D|M_1)}{p(D|M_2)} = \frac{\frac{1}{2}\times\frac{1}{2}\times\frac{1}{2}\times\frac{1}{2}\times\frac{1}{2}\times\frac{1}{2}\times\frac{1}{2}\times\frac{1}{2}\times\frac{1}{2}\times\frac{1}{2}}{1\times1\times1\times1\times1\times1\times1\times1\times1\times1} = \frac{\frac{1}{1024}}{1} = \frac{1}{1024}$$

Thus, the probability that the coin is double-headed, given ten heads in a row, is 1024 times greater than the probability that the coin is fair, meaning that the probability – given the data - of the coin being double-headed is 1024/1025. Note that neither this example nor the practices of Jeffreys and Turing are intended to create rigid standards for

interpreting the BF, but instead to provide "a rough descriptive statement about standards of evidence in scientific investigation" (Kass, 1993). The unique requirements and circumstances of the particular analysis must be considered when interpreting the value of BF.

As noted in Chapter 1, the BF and PBF were applied to two problems in chromosome dosimetry. In the next section, the BF is used to analyze the occurrence of so-called overdispersed data from calibration experiments involving high LET radiations. Comparisons are made between parameter and dose estimates calculated under the assumption of two competing models. In the final section, the PBF is used to compare two different Poisson models as descriptors of calibration data for experiments involving low doses of neutrons. A Poisson model with a linear mean, the accepted model, is compared to a Poisson model with a linear quadratic mean.

5.2 The Polya Model for Overdispersed Calibration Data

5.2.1 Introduction

To review, a controlled calibration experiment consists of three steps: exposing a sample of blood to known fixed doses of radiation, d_i, scoring the number of dicentrics, y_i, observed in a sample of n_i peripheral lymphocytes, and then repeating the first two steps for i=(1, 2,..., k) dose levels. The parameters of the model assumed to describe the underlying statistical relationship between y, n, and d are then estimated conditional on

the calibration data $D_c = \{d_i, y_i, n_i\}$. The usual assumption is that y is Poisson distributed with a mean that is either a linear or linear-quadratic function of d (e.g. $y_i \sim \text{Po}[n_i(\alpha+\theta d_i)]$ or $y_i \sim \text{Po}[n_i(\alpha+\theta d_i+\gamma d_i^2)]$. It is however known that data from calibration experiments involving high LET radiations can be "overdispersed" (Lloyd et al. 1979). In the present context, overdispersed refers to discrete random variables that have a variance greater than their mean. Frequentist statistical methods are routinely used to identify and account for overdispersion in data from calibration experiments (Rao et al. 1956; Lloyd et al. 1979; Jin et al. 1998). Here a Bayesian approach is taken to parameter and dose estimation when overdispersion is suspected. The Bayesian treatment introduces a new model, the Polya (Arley 1943) or negative binomial (Johnson 1969) model. This model is characterized by an additional parameter, labeled ψ below, which measures the degree of overdispersion. The BF will be used to weigh the evidence in support of the Polya model as compared to the alternative Poisson model. Bayesian methods will also be employed to derive dose estimates for hypothetical radiation accidents under both Poisson and Polya model assumptions, allowing the impact of different model choices to be evaluated.

5.2.2 Method and Data

Two different calibration data sets will be used. Both are from Lloyd et al. (1979) and consist of the number of dicentric chromosome aberrations, y_i, observed in a number of peripheral lymphocytes, n_i, after exposure to a known dose, d_i (rad). The first data set contains the results of exposure to 0.7 MeV fission neutrons from the British

Experimental Pile Zero reactor (BEPO). This data set will be referred to as the BEPO data set and is given by the vectors

$$\underline{d}=\{50, 75, 100, 150, 200, 250, 300\}$$

$$\underline{n}=\{269, 78, 115, 90, 84, 59, 37\}$$

$$\underline{y}=\{109, 47, 94, 114, 138, 125, 97\}$$

The notation for these vectors follows the naming convention for the subscripted variables introduced in the previous paragraph. The second data set describes the results of exposure to 14.7 MeV neutrons from D-T reactions. This data set will be referred to as the D-T data set and is given by the vectors

$$\underline{d}=\{5, 10, 25, 50, 101, 152, 202, 303\}$$

$$\underline{n}=\{2000, 763, 723, 568, 472, 303, 243, 67\}$$

$$\underline{y}=\{34, 25, 50, 65, 202, 202, 206, 100\}$$

Assuming the number of dicentrics y to be Polya distributed with mean $n\theta d$ results in a probability density function (Arley 1943) given by

$$f(y|n,d,\theta,\psi)=\binom{-\frac{1}{\psi}}{y}(-\psi)^{y}\left(\frac{n\theta d}{1+\psi n\theta d}\right)^{y}(1+\psi n\theta d)^{-\frac{1}{\psi}} \qquad \textbf{(5.5)}$$

where $\psi \geq 0$, $\theta \geq 0$, and the variance of y is $n\theta d(1+\psi n\theta d)$. It can be seen that in the limit $\psi \rightarrow 0$ the Polya model collapses into the Poisson model (Arley 1943). Alternatively, for $\psi > 0$ the ratio of the variance to the mean will be greater than one, indicating a Polya model. The implications of the Polya model for the mechanism of induction of dicentric aberrations are not discussed here. It is noted that violation of one or more of the independence assumptions required for Poisson behavior is often cited as the source of overdispersion (Johnson 1969; Jeffreys 1998)

In Section 2.2.1, calibrative densities were used to demonstrate the Bayesian approach to dose estimation after neutron exposures based on the assumption of a Poisson model. The salient features of the analysis are briefly repeated below as they pertain to the Polya model. The joint posterior density of the parameters in proportional ($\propto$) form with constant priors for θ and ψ is:

$$p(\theta, \psi | D_c) \propto \prod_{i=1}^{k} \binom{-\frac{1}{\psi}}{y} (-\psi)^{y} \left(\frac{n\theta d}{1+\psi n\theta d} \right)^{y} (1+\psi n\theta d)^{-\frac{1}{\psi}} \qquad \textbf{(5.6)}$$

k being the number of dose levels. Numerical integration of $p(\theta,\psi \mid D_c)$ over one of the parameters yields the marginal density for the other parameter.

For dose estimation the calibrative density, discussed by Aitchison et al. (1975), was employed again. The calibrative density for the Polya model and a controlled calibration experiment is given by Equation 5.7:

$$p(d_f|D_A) \propto p(d_f)\int_0^\infty\int_0^\infty \binom{-\frac{1}{\psi}}{y_f}(-\psi)^{y_f}\left(\frac{n_f\theta d_f}{1+\psi n_f\theta d_f}\right)^{y_f}\left(1+\psi n_f\theta d_f\right)^{-\frac{1}{\psi}} p(\theta,\psi|D_c)d\theta d\psi$$

$p(d_f)$ is the prior density of the unknown dose d_f, $p(\theta, \psi \mid D_c)$ is the joint posterior density of the parameters (Equation 5.6), and the remaining terms inside the integrand comprise the likelihood of a "future" observation based on Equation 5.5. For the BEPO data, dose estimates were made assuming $y_f = 120$ and $n_f = 55$. The dose estimates for the D-T data were based on $y_f = 400$ and $n_f = 500$.

The posterior odds for model comparison, discussed in the previous section, adapted to current circumstances is

$$\frac{p(Polya|D_c)}{p(Poisson|D_c)} = \frac{p(D_c|Polya)}{p(D_c|Poisson)}\frac{p(Polya)}{p(Poisson)} \qquad \textbf{(5.8)}$$

Again, the term on the left is the posterior odds ratio, the first right-hand term is the Bayes Factor (BF), and the second right-hand term is the prior odds ratio. No preexisting preference is assumed for either model, i.e. the prior odds ratio is set to 1, and the posterior odds ratio is then equal to the BF, given here by

$$\frac{p(D_c|Polya)}{p(D_c|Poisson)} = \frac{\int_0^\infty \int_0^\infty L(\theta,\psi|D_c)p(\theta,\psi)d\theta d\psi}{\int_0^\infty L(\theta|D_c)p(\theta)d\theta} \quad \textbf{(5.9)}$$

where

$L(\theta,\psi|D_c)$ is the Polya likelihood

$L(\theta|D_c)$ is the Poisson likelihood given calibration data D_c.

The proper prior distributions for the parameters are denoted by $p(\theta,\psi)$ and $p(\theta)$. A priori, the parameters θ and ψ are assumed to be independent i.e. $p(\theta,\psi) = p(\theta)\,p(\psi)$. Note that $p(\theta)$ stands for different distributions in the numerator and denominator of Equation 5.9 since, as always, distributions are labeled by their arguments. $p(\theta)$ and $p(\psi)$were constructed using published information regarding dose-response parameters for dicentric chromosome aberrations. The sensitivity of the BF were assessed by using several different combinations of prior distributions. Differences in experimental conditions, particle energy, etc. were accounted for by increasing the standard deviations of the prior distributions.

For the analysis of the BEPO data set, one proper uniform (U) and three normal (N) priors for the slope parameter were derived using published estimates of θ and its standard error ($\theta = 0.0087 \pm 0.0003$) for exposure to 0.85 MeV neutrons (Lloyd et al. 1975). The priors used are $p(\theta) \sim U[0.0087 \pm 5\times 0.0003]$ and $p(\theta) \sim N[\mu,\sigma^2]$ with $\mu =$ 0.0087 and $\sigma = \{2\times 0.0003, 3\times 0.0003, 5\times 0.0003\}$, respectively

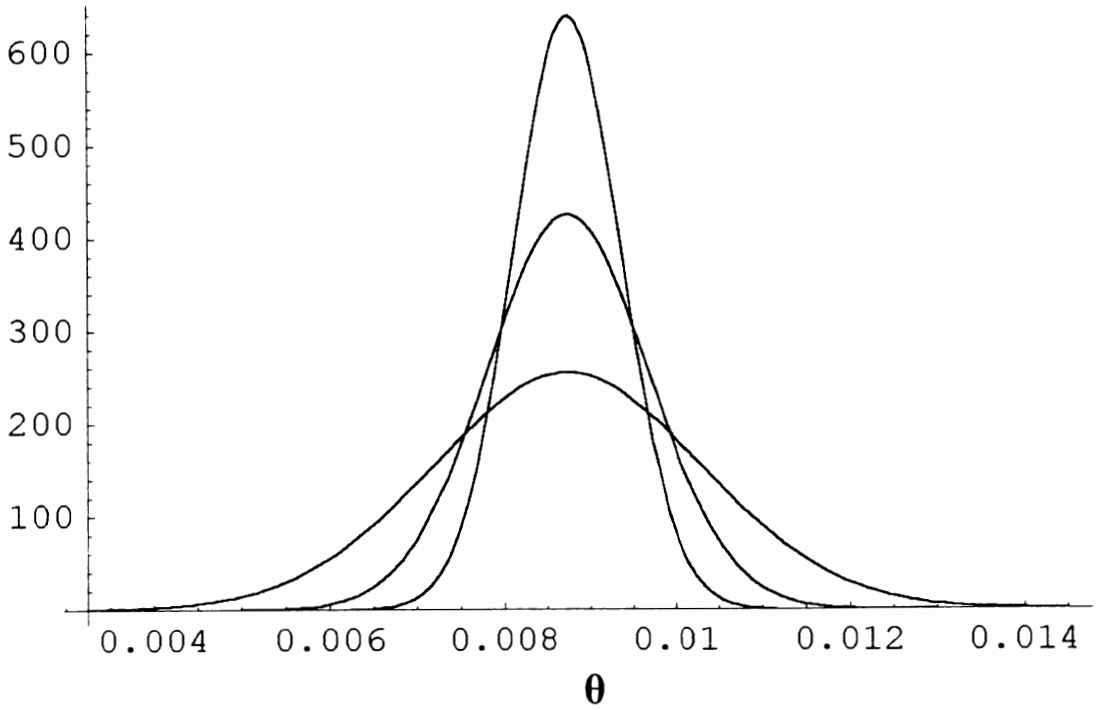

Figure 5.1: Normal priors for the slope parameter θ for the BEPO data

Likewise, three gamma priors for ψ were derived using published expert opinion that values of 1.1 or 1.2 are appropriate as the ratio of the variance to the mean for calibration experiments involving neutrons (Lloyd et al. 1983). The priors used were $p(\psi) \sim Ga[\alpha, \beta]$ with $\alpha = \{1, 2, 5\}$ and $\beta = \{10, 10, 50\}$, respectively. The gamma distributions, parameterized so that $E(\psi) = \alpha / \beta$ and $Var(\psi) = \alpha / \beta^2$, are shown on Figure 5.2:

The prior distributions used in the analysis of the D-T data set are obtained from posterior distributions derived from Poisson and Polya likelihoods with the data of Sasaki et al. (1971) for a calibration experiment involving 14.0 MeV neutrons.

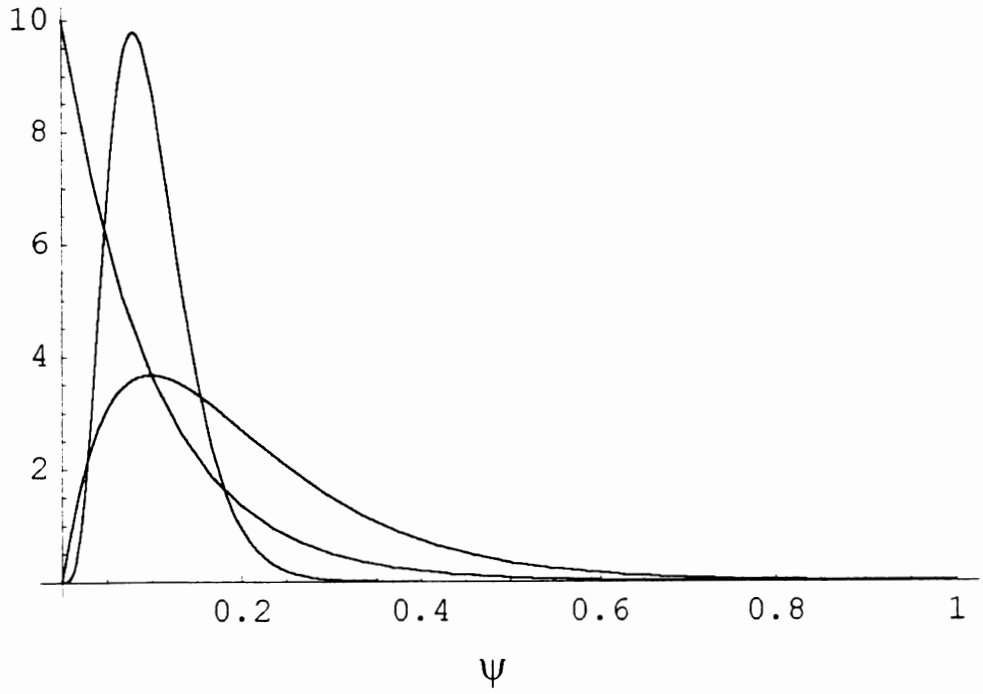

Figure 5.2: Gamma priors of ψ for the BEPO data

This data set will be referred to as the Sasaki data set, denoted by D_s, and is given by the vectors

$$\underline{d}=\{15, 21, 42, 82, 124, 165, 248, 329, 428, 660\}$$

$$\underline{n}=\{1511, 1198, 500, 305, 500, 500, 277, 308, 200, 30\}$$

$$\underline{y}=\{15, 46, 44, 88, 208, 293, 239, 315, 330, 84\}$$

The data for the zero dose level were not considered since the aberration rates at all dose levels are large enough to make the background rate negligible. The posterior densities obtained from the Sasaki data set were used to calculate expectations and standard

deviations for the parameters, from which prior distributions were determined as described below. The posterior expectations and standard deviations are:

$$E(\theta|D_s)_{Po} = 0.0032;\ SD(\theta|D_s)_{Po} = 7.928\times10^{-5}$$

$$E(\theta|D_s)_{Pl} = 0.0032;\ SD(\theta|D_s)_{Pl} = 6.042\times10^{-4}$$

$$E(\psi|D_s) = 0.3187;\ SD(\psi|D_s) = 0.1882$$

The subscripts indicate the model used for the likelihood. Two proper uniform and four normal priors were used for the slope parameter θ. They are $p(\theta) \sim U[0.0032 \pm 5\times 7.928\times10^{-5}]$, $p(\theta) \sim U[0.0032 \pm 5\times 6.042\times10^{-4}]$, and $p(\theta) \sim N[\mu_i, \sigma_i^2]$ with $\mu_i = 0.0032$ and $\sigma_i = \{2\times 7.928\times10^{-5}, 4\times 7.928\times10^{-5}, 2\times 6.042\times10^{-4}, 4\times 6.042\times10^{-4}\}$ for $i=(1, 2, 3, 4)$. The normal priors are shown in Figure 5.3:

Three gamma priors were used for ψ, given by $p(\psi) \sim Ga[\alpha, \beta]$ with $\alpha = \{1.0, 1.6, 2.9\}$ and $\beta = \{3.125, 5, 9\}$, respectively. The priors are shown in Figure 5.4.

The ranges of values for the BF and the weight of evidence, resulting from different combinations of the above priors, are given in the Results section below.

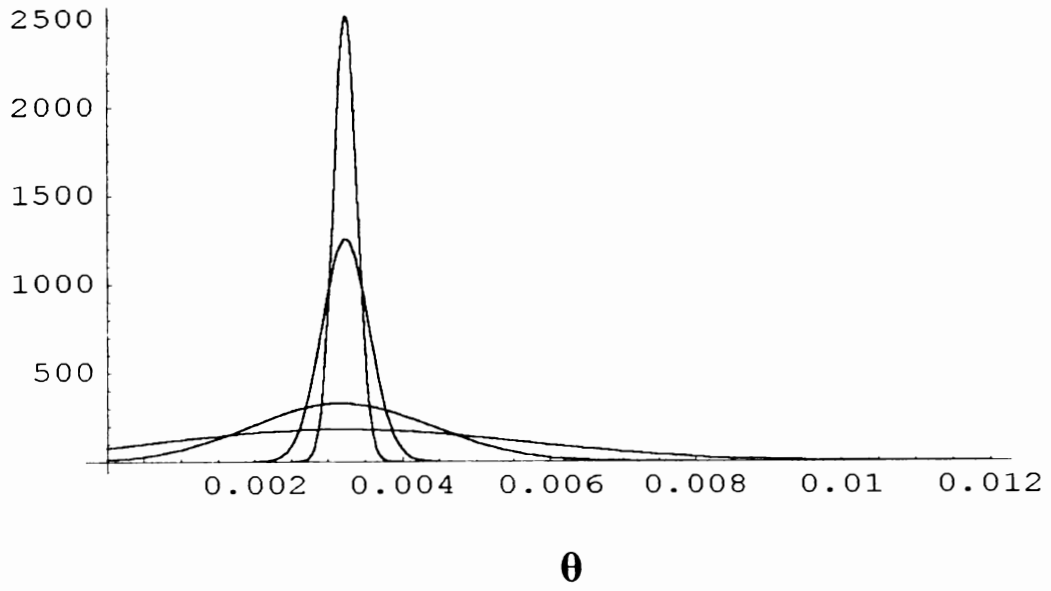

Figure 5.3: Normal priors for the slope parameter θ for the D-T data

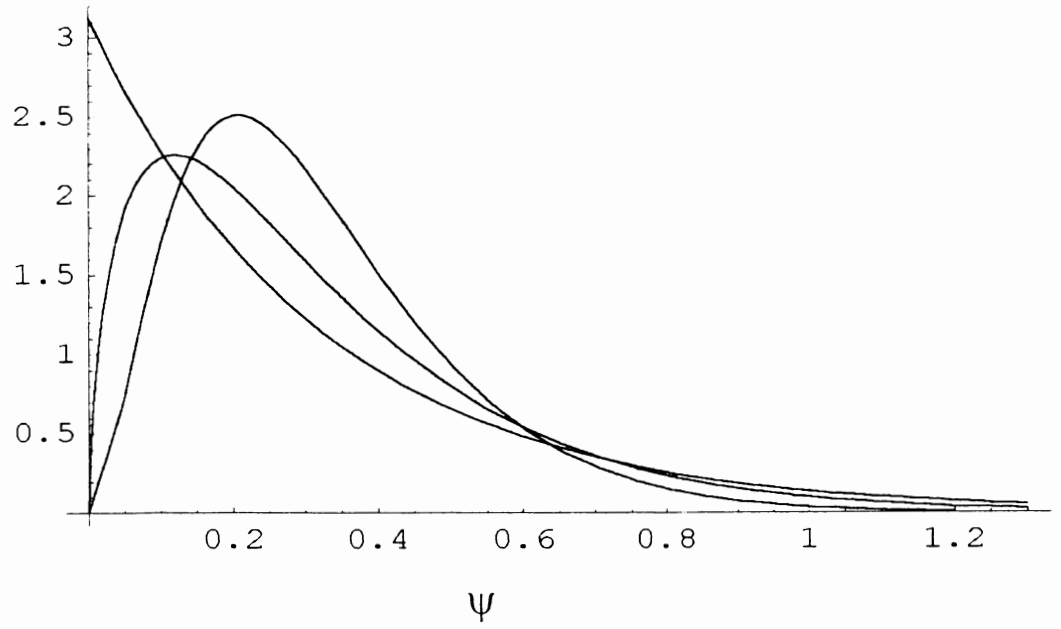

Figure 5.4: Gamma priors of ψ for the D-T data

5.2.3 Results

BEPO data

The values of the BF for different combinations of the prior distributions listed in Section 5.2.2 range from 0.0022 to 0.0037, indicating support for the Poisson model. The corresponding range for weight of evidence is –2.66 to –2.43. Referring to the coin-tossing example of Good, the BF of 0.0022 (representing the least support for the Polya model) equates the probability of the Polya model being the best descriptor of the BEPO data to the probability of a fair coin producing between 8 and 9 heads in a row in as many tosses. Figures 5.5, 5.6, and 5.7 reveal only slight differences between Poisson and Polya parameter and dose estimates. This is expected given the marginal density of ψ seen in Figure 5.6 and the fact that the Polya model collapses into the Poisson model as $\psi \rightarrow 0$.

D-T data

The values of the BF for several different combinations of the prior distributions listed in Section 5.2.2 range from 8221.5 to 12802.9, indicating support for the Polya model. The corresponding range for weight of evidence is 3.91 to 4.11. The smallest value of the BF, 8221.5, again representing the least support for the Polya model, equates the probability of the Poisson model being the best descriptor of the D-T data to the probability of a fair coin producing 13 heads in a row in as many tosses. The results of parameter and dose estimation shown in Figures 5.8, 5.9, and 5.10 reveal significant differences between the

two models. Especially striking is the increased dispersion of the calibrative density seen in Figure 5.10, which indicates greater uncertainty about d_f.

From the results it is clear that the Polya model is a better descriptor of the D-T data, and provides results differing little from those obtained with the Poisson model for the BEPO data. The additional computational burden incurred by considering the parameter ψ is small. Considering this computational feasibility, the fact that the Polya model collapses into the Poisson model as ψ goes to zero and the potential discrepancy between the Polya and Poisson based dose estimates (see Figure 5.10 for example), it is clear that an initial assumption of a Polya model is the preferred and conservative approach to chromosome dosimetry for high LET radiations.

5.3 Partial Bayes Factor for Comparing Linear and Linear Quadratic Poisson Means

5.3.1 Introduction

In Section 2.2.2 Bayesian methods were used to provide parameter and dose estimates for exposure to low doses of neutrons under the assumption that the mean of y is linear in dose, i.e. $y \sim \text{Po}[n\,(\alpha+\theta d)\,]$. While this assumption is consistent with the current practice in chromosome dosimetry, plots using approximate 99% probability intervals for the linear, shown in Figure 5.11, and linear quadratic fits (i.e. $y \sim \text{Po}[n(\alpha+\beta d+\gamma d^2)]$), shown in Figure 5.12, seem to suggest that the latter may the better choice.

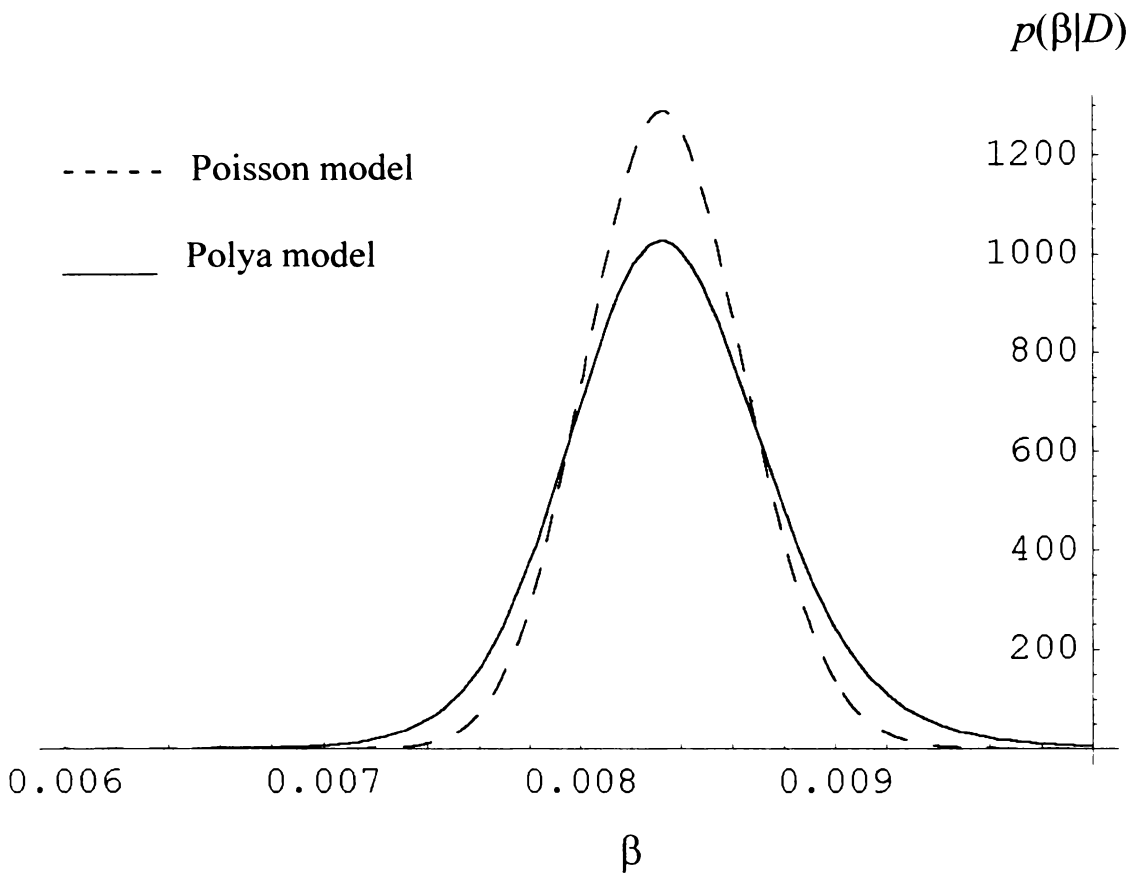

Figure 5.5: Estimates of the slope parameter β for the BEPO data set

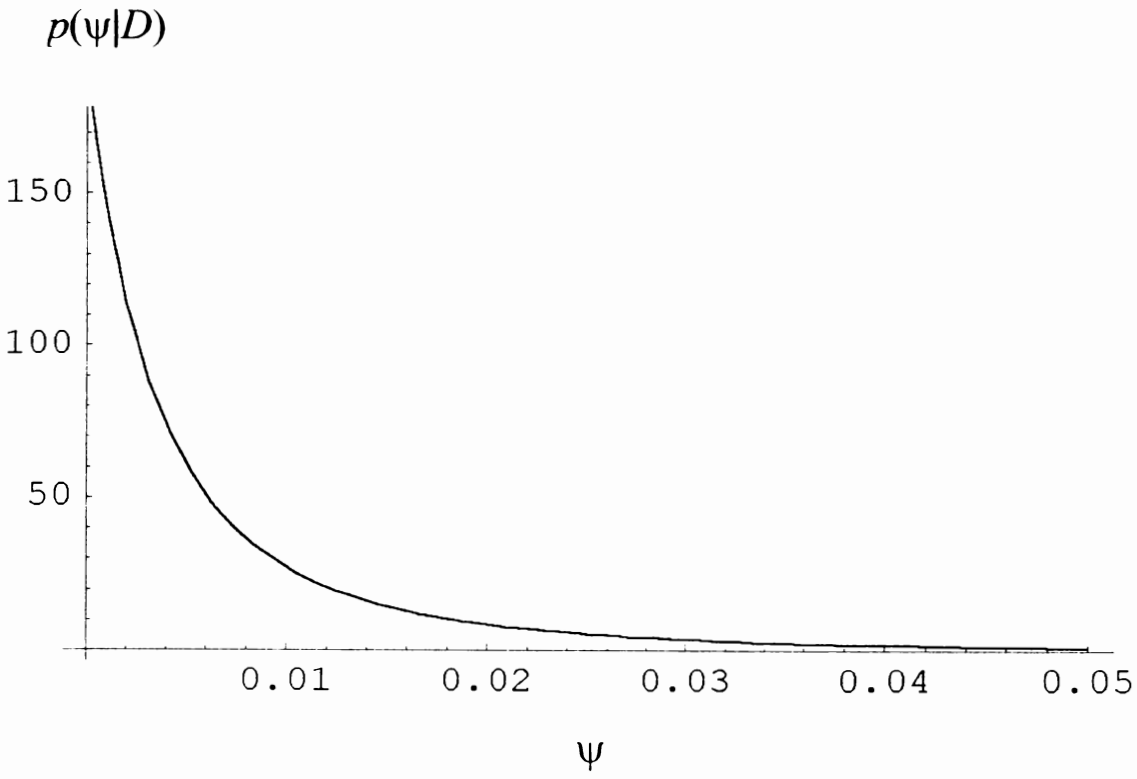

Figure 5.6: Estimate of ψ for the BEPO data set

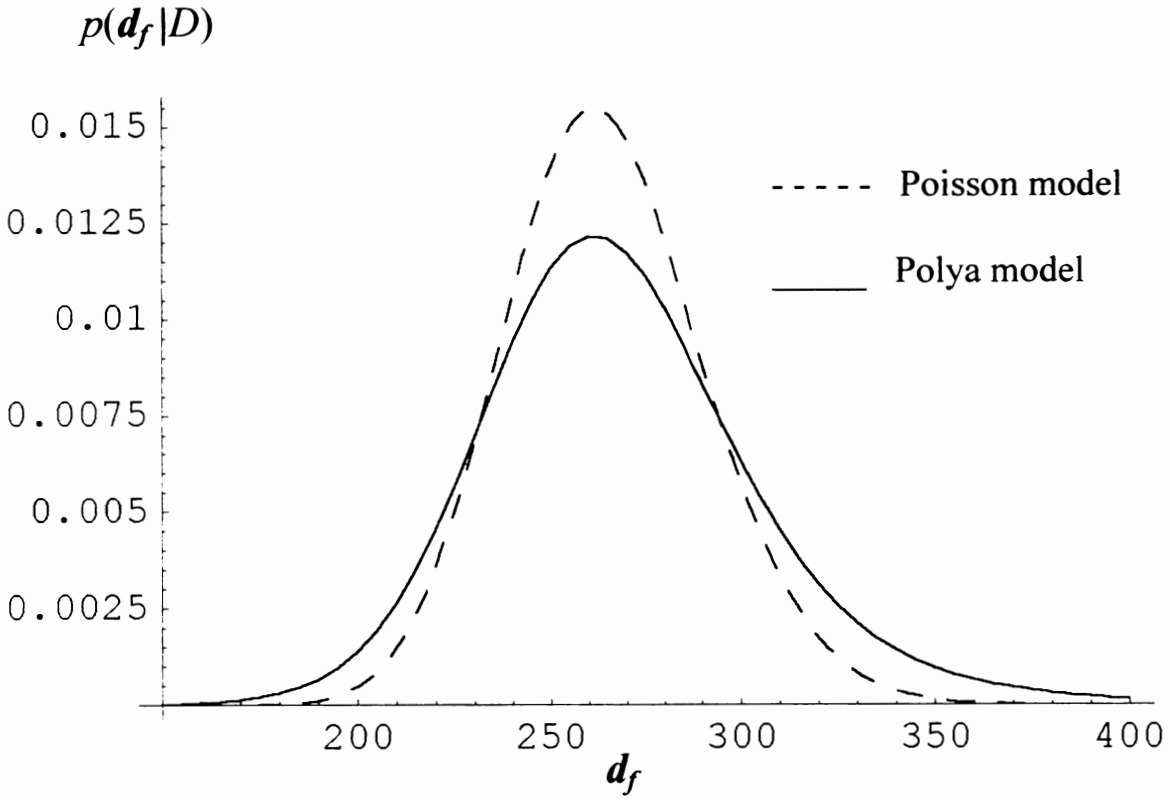

Figure 5.7: Calibrative densities of d_f for the BEPO data set with y_f=120 and n_f=55

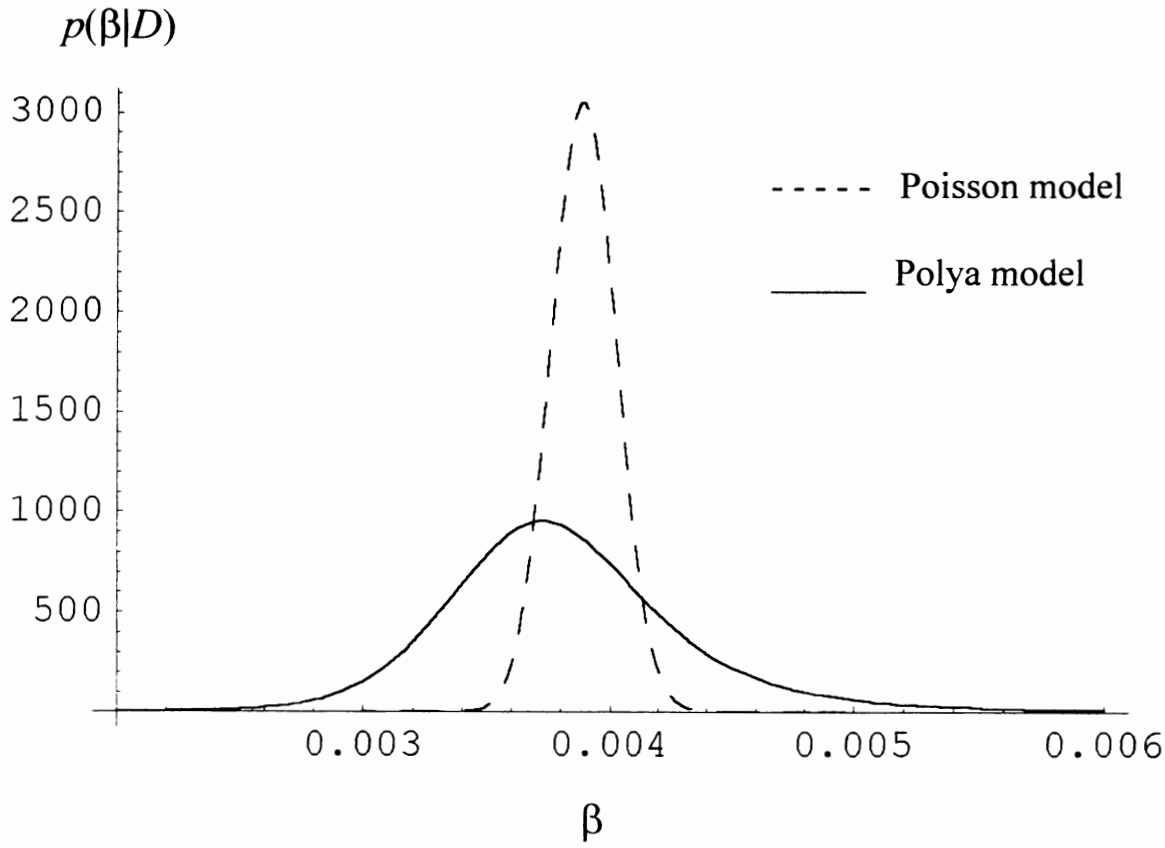

Figure 5.8: Estimates of the slope parameter β for the D-T data set

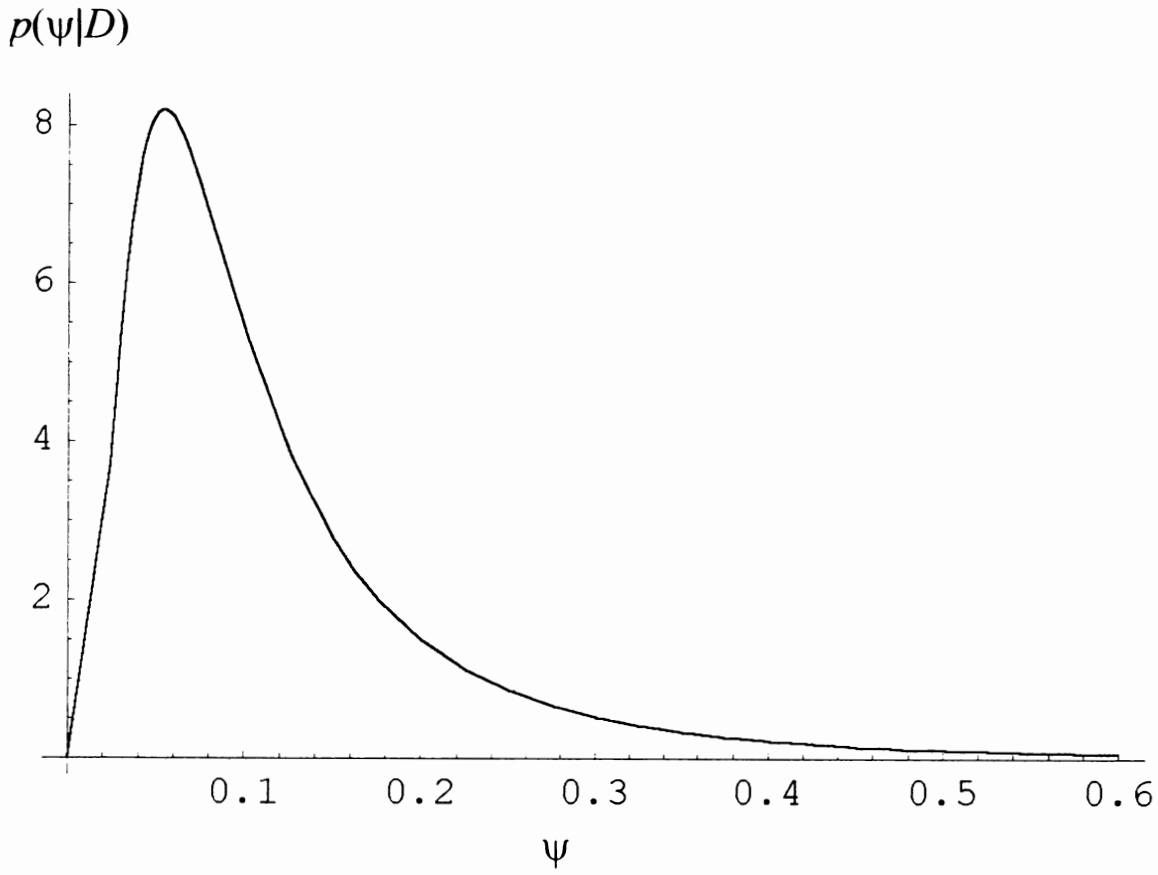

Figure 5.9: Estimate of ψ for the D-T data set

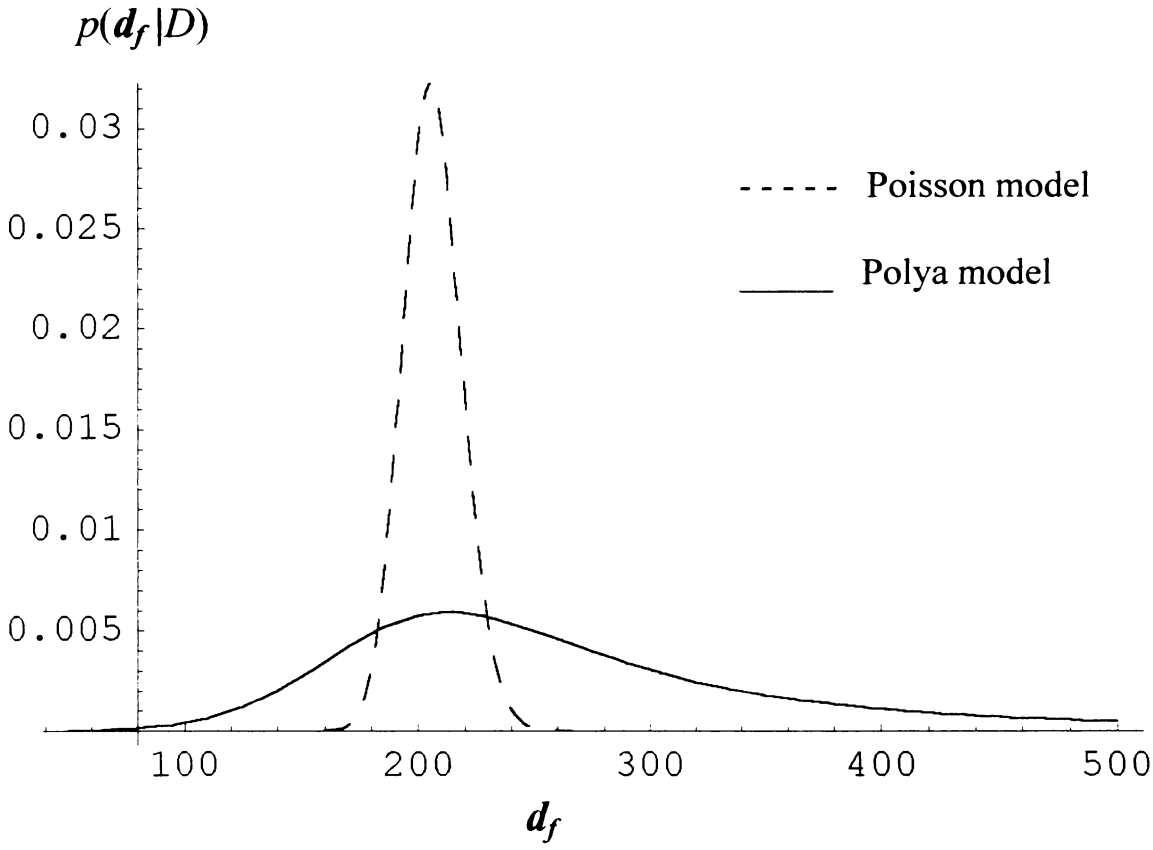

Figure 5.10: Calibrative densities of d_f for the D-T data set with y_f=400 and n_f=500

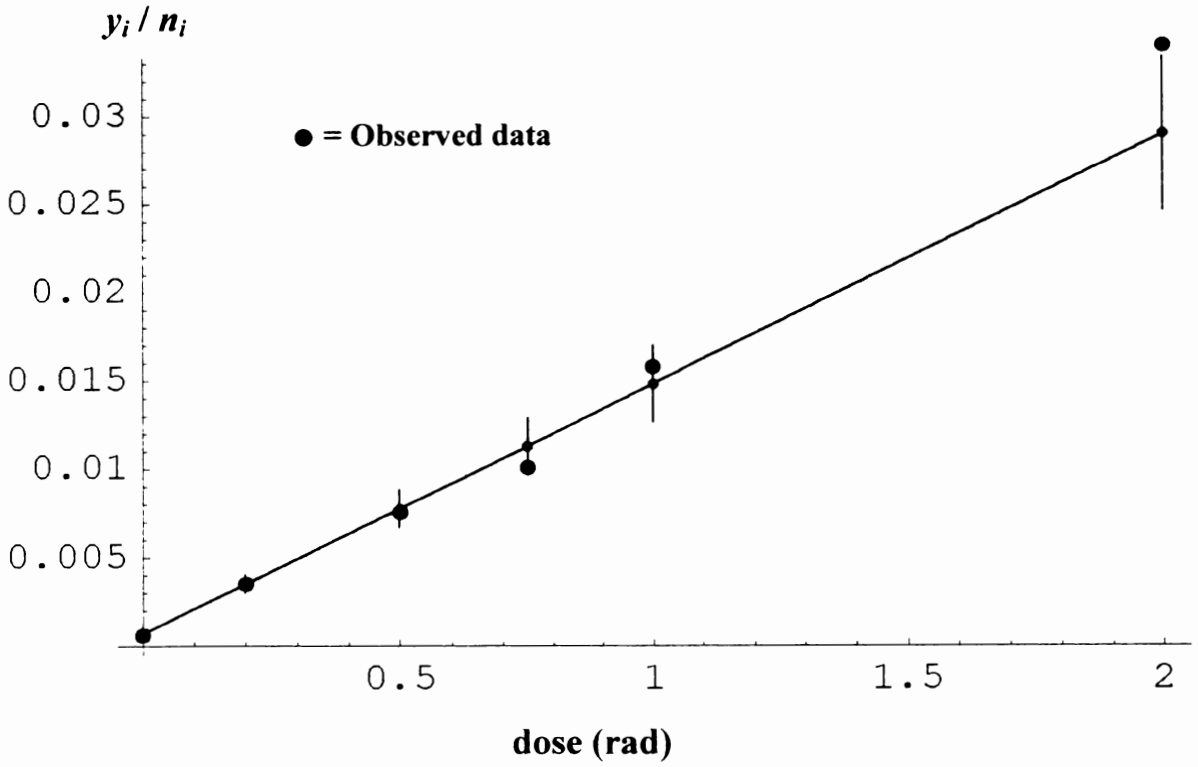

Figure 5.11: Linear Fit to the ^{252}Cf data

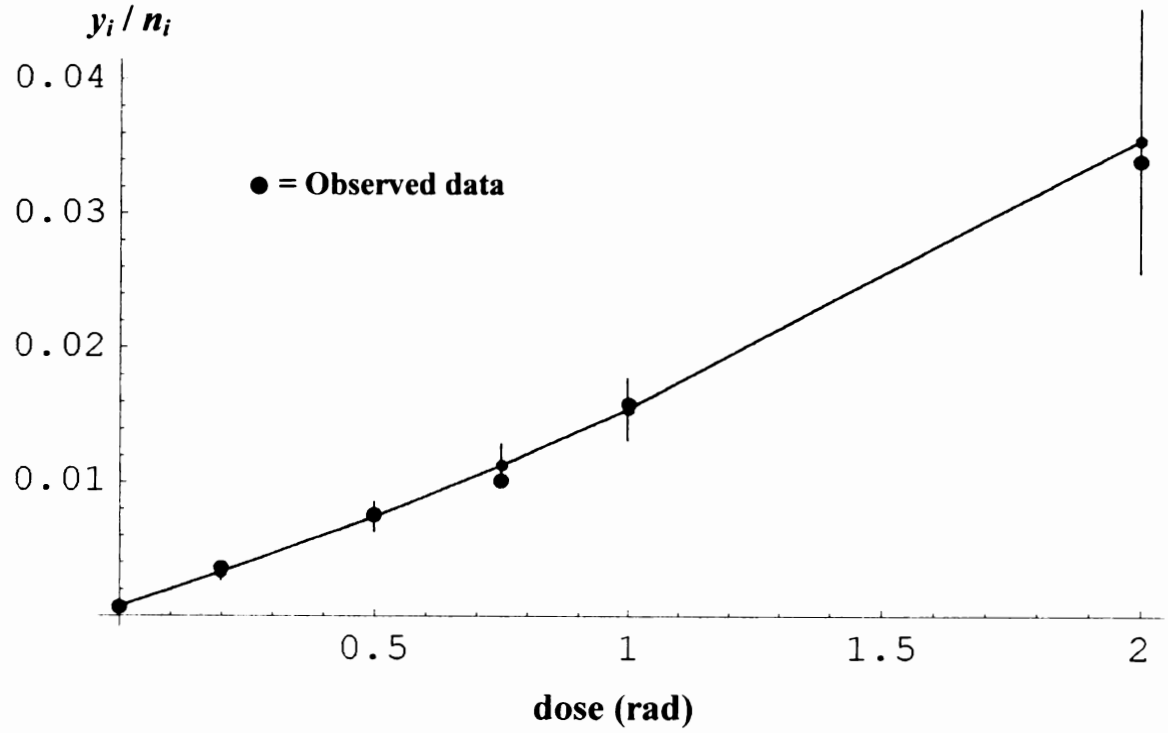

Figure 5.12: Linear-Quadratic Fit to the ^{252}Cf data

5.3.2 Method

Assuming no prior preference for either model, the posterior odds ratio is equal to the BF:

$$\frac{p(linear|D_c)}{p(lin.quad.|D_c)} = \frac{p(D_c|linear)}{p(D_c|lin.quad.)}$$

$$= \frac{\int_0^\infty \int_0^\infty L(\alpha,\beta|D_c)\,p(\alpha,\beta)\,d\alpha\,d\beta}{\int_0^\infty \int_0^\infty \int_0^\infty L(\alpha,\beta,\gamma|D_c)\,p(\alpha,\beta,\gamma)\,d\alpha\,d\beta\,d\gamma} \qquad \textbf{(5.10)}$$

where $L(\alpha,\beta|D_c) \equiv$ likelihood for the linear model

$L(\alpha, \beta, \gamma | D_c) \equiv$ likelihood for the linear quadratic model

In this case, none of the usual sources of prior information such as similar data from other calibration experiments involving low doses of neutrons are available. Therefore, the PBF will be used to circumvent the lack of prior knowledge. Assuming the calibration data are divided into two groups r and s, where s is the training data, the PBF is given by

$$\text{PBF} = \frac{p(r|linear, s)}{p(r|lin.quad., s)}$$

$$= \frac{\int_0^\infty \int_0^\infty L(\alpha, \beta | r) p(\alpha, \beta | s) d\alpha d\beta}{\int_0^\infty \int_0^\infty \int_0^\infty L(\alpha, \beta, \gamma | r) p(\alpha, \beta, \gamma | s) d\alpha d\beta d\gamma} \qquad \textbf{(5.11)}$$

Two different divisions are used below. In the first, s is comprised of the first two dose levels, and r consists of the last four. The second division takes the first three doses levels for s, leaving the last three for r.

5.3.3 Results

For the first division of the calibration data, PBF = 12.13. The corresponding value for the weight of evidence is 1.08. Referring to the coin-tossing example of Good, the PBF of 12.13 equates the probability of the linear-quadratic mean being the best descriptor of

the data to the probability of a fair coin producing between 3 and 4 heads in a row in as many tosses. For the second division of the calibration data, PBF = 2.07. The corresponding value for the weight of evidence is 0.32. Referring again to the coin-tossing example of Good, the PBF of 2.07 equates the probability of the linear-quadratic mean being the best descriptor of the data to the probability of a fair coin producing 1 head in as many tosses. The conclusion is that there is no compelling evidence to abandon the standard assumption of a mean linear in dose in favor of a mean linear quadratic in dose for describing the induction of dicentric chromosome aberrations by low doses of neutrons.

CHAPTER 6: COMPARTMENTAL MODELING OF ^{45}Ca BIOKINETICS

6.1 Introduction

The objective of this chapter is to continue the work of Lo (2000) on the 2-compartment 3-parameter model describing the exchange of ^{45}Ca between plasma and bone surface in beagles. The compartmental model, data, and distributional assumptions are presented in Section 6.2. In Section 6.3, numerical integration is used to calculate the expected value and standard deviation of compartmental activities at different times. In Section 6.3, a method is demonstrated for compartmental modeling with missing observations. The chapter concludes with a discussion in Section 6.4

6.2 Model and Data

The 2-compartment model representing the exchange of ^{45}Ca between the bone surface and the plasma is shown in Figure 6.1.

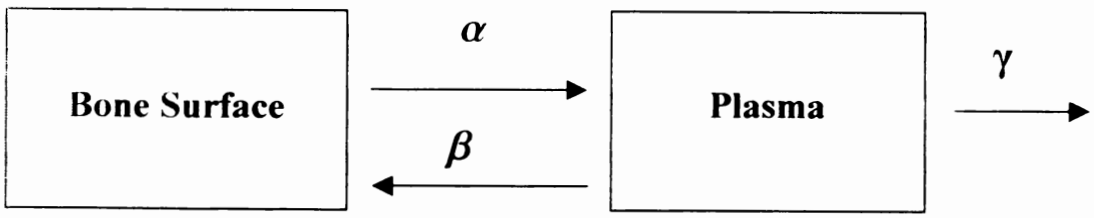

Figure 6.1: ^{45}Ca compartmental model

The activities at the bone surface and in the plasma at time t_u are denoted $a_1(t_u, \boldsymbol{\theta})$ and $a_2(t_u, \boldsymbol{\theta})$ respectively where $\boldsymbol{\theta} = \{\alpha, \beta, \gamma\}$. The parameters α, β, and γ are the transfer coefficients for the compartmental model and represent the rate at which activity enters or exits the two compartments. The average movement of the ^{45}Ca activity is described by the following set of differential equations:

$$\frac{da_1(t,\boldsymbol{\theta})}{dt} = -\alpha a_1(t,\boldsymbol{\theta}) + \beta a_2(t,\boldsymbol{\theta}) \qquad \textbf{(6.1)}$$

$$\frac{da_2(t,\boldsymbol{\theta})}{dt} = \alpha a_1(t,\boldsymbol{\theta}) - \beta a_2(t,\boldsymbol{\theta}) - \gamma a_2(t,\boldsymbol{\theta}) \qquad \textbf{(6.2)}$$

Subject to initial conditions of $a_1(0, \boldsymbol{\theta})=0$ and $a_2(0, \boldsymbol{\theta})= a_0$, the following solutions for Equations 6.1 and 6.2 were obtained using the method of eigenvalues (Jacquez 1985):

$$a_1(t,\boldsymbol{\theta}) = \frac{a_0\beta}{\sqrt{((\alpha+\beta+\gamma)^2 - 4\alpha\gamma)}}\left(\exp\{\lambda_2 t\} - \exp\{\lambda_1 t\}\right) \qquad \textbf{(6.3)}$$

$$a_2(t,\boldsymbol{\theta}) = \frac{a_0}{\sqrt{((\alpha+\beta+\gamma)^2 - 4\alpha\gamma)}}\left((\lambda_2+\alpha)\exp\{\lambda_2 t\} - (\lambda_1+\alpha)\exp\{\lambda_1 t\}\right) \qquad \textbf{(6.4)}$$

where

$$\lambda_1 = -\frac{1}{2}\left((\alpha+\beta+\gamma) + \sqrt{(\alpha+\beta+\gamma)^2 - 4\alpha\gamma}\right)$$

$$\lambda_2 = -\frac{1}{2}\left((\alpha+\beta+\gamma) - \sqrt{(\alpha+\beta+\gamma)^2 - 4\alpha\gamma}\right)$$

The solutions are the expectation functions for the time-dependent compartmental activities.

The data are from Rowland et al. (1966) and consist of ten timed and paired observations of ^{45}Ca specific activity at the bone surface, denoted y_1, and in the plasma, denoted y_2. The data are listed in Table 6.1.

Table 6.1: ^{45}Ca biokinetic data from Rowland et al (1966)

Time (hours)	Compartment Activity (μCi/mg ^{45}Ca)	
(t_u, u=0:10)	Bone Surface (y_1)	Plasma (y_2)
0.0	0.00	27.1
0.2	1.10	22.0
0.52	2.81	17.0
1.0	3.39	15.0
2.0	3.53	14.0
4.0	4.37	9.5
6.0	4.89	8.0
24.0	5.79	5.0
48.0	4.16	2.3
120.0	1.97	1.3
408.0	0.21	0.1

The observed activities at time t_u are denoted $\mathbf{y}_u = \{y_{1u}, y_{2u}\}$ and assumed to be normally distributed with means $a_1(t_u, \boldsymbol{\theta})$ and $a_2(t_u, \boldsymbol{\theta})$ respectively. The error associated with an observation y_{iu} is denoted ε_{iu}, and given by

$$\varepsilon_{iu} = y_{iu} - a_i(t_u, \boldsymbol{\theta}) \tag{6.5}$$

The errors are assumed to come from independent multivariate normal distributions with $E(\varepsilon_{iu})=0$, $E(\varepsilon_{iu}\,\varepsilon_{jv})=0$ for $u \neq v$, and $E(\varepsilon_{iu}\,\varepsilon_{ju})=\sigma_{ij}$. The variance covariance matrix is denoted Σ, and it's inverse by $\mathbf{A}$:

$$\boldsymbol{\Sigma} = \begin{bmatrix} \sigma_{11} & \sigma_{12} \\ \sigma_{21} & \sigma_{22} \end{bmatrix} = \{\sigma_{ij}\}$$

and

$$\mathbf{A} = \Sigma^{-1} = \frac{1}{\sigma_{11}\sigma_{22} - \sigma_{12}\sigma_{21}} \begin{bmatrix} \sigma_{22} & -\sigma_{12} \\ -\sigma_{21} & \sigma_{11} \end{bmatrix} = \{\sigma^{ij}\}$$

6.3 Calculation of the Expected Value and Standard Deviation of the Compartmental Activity

6.3.1 Introduction

Previous work by Lo (2000) used point estimates of the transfer coefficients to estimate the time-dependent compartmental activity. This use of point estimates, while

computationally more convenient, neglects the uncertainty about the estimates of the transfer coefficients when calculating the activities. In this portion of the research, a more rigorous approach was used to estimate the compartmental activity at fixed times. Specifically, the expected value and standard deviation of compartmental activities were calculated numerically with quasi-Monte Carlo integration (Wolfram 1996).

6.3.2 Method

The method employed here is based on Box et al. (1965, 1992). Much of their original notation is used to facilitate reference to the original work. Assuming that observations of the activity, $\mathbf{y}_u$, are independent, the joint posterior density of the parameters in proportional form is derived as

$$p(\boldsymbol{\theta}, \mathbf{A}|D) \propto \prod_{u=1}^{n} p(D|\boldsymbol{\theta}, \mathbf{A}) p(\boldsymbol{\theta}, \mathbf{A})$$

$$\propto |\mathbf{A}|^{\frac{n}{2}} \exp\{-\frac{1}{2}\sum_{i=1}^{2}\sum_{j=1}^{2}\sigma^{ij}S(\boldsymbol{\theta})\} p(\boldsymbol{\theta}, \mathbf{A}) \qquad \textbf{(6.6)}$$

D represents the observation pairs $\{\mathbf{y}_u, t_u\}$ for u = (1, 2,…, 10), and S (θ) is a 2×2 matrix containing the sum of squares and sum of products of the deviations between the observed y_{iu}'s and the expected values $a_i(t_u, \boldsymbol{\theta})$:

$$S(\boldsymbol{\theta}) = \begin{bmatrix} S_{11}(\boldsymbol{\theta}) & S_{12}(\boldsymbol{\theta}) \\ S_{21}(\boldsymbol{\theta}) & S_{22}(\boldsymbol{\theta}) \end{bmatrix} \tag{6.7}$$

where

$$S_{ij}(\boldsymbol{\theta}) = \sum_{u=1}^{n} [y_{iu} - a_i(t_u, \boldsymbol{\theta})][y_{ju} - a_j(t_u, \boldsymbol{\theta})] \tag{6.8}$$

The prior distributions for the parameters are assumed to be independent (i.e. $p(\theta,\mathbf{A}) = p(\theta)p(\mathbf{A})$). Prior distributions for the elements of θ are assumed to be proportional to a constant, and non-informative Jeffrey's priors are used for the elements of **A**:

$$p(\theta) \propto \text{constant}$$

$$p(\mathbf{A}) = |\mathbf{A}|^{-\frac{3}{2}}$$

The joint posterior density of the parameters in proportional form may then be written as

$$p(\boldsymbol{\theta}, \mathbf{A}|D) \propto |\mathbf{A}|^{\frac{n-3}{2}} \exp\{-\frac{1}{2}\sum_{i=1}^{2}\sum_{j=1}^{2}\sigma^{ij}S(\boldsymbol{\theta})\}$$

$$\propto |\mathbf{A}|^{\frac{n-3}{2}} \exp\{-\frac{1}{2}\text{tr}(\mathbf{A}S(\boldsymbol{\theta}))\} \tag{6.9}$$

tr(**A** S(θ)) is the trace of the 2×2 matrix formed by multiplying **A** and S(θ). Next, the dependence on **A** is eliminated using results for the Wishart distribution (Box et al. 1992):

$$p(\boldsymbol{\theta}|D) \propto \int_{\mathbf{A}>0} |\mathbf{A}|^{\frac{n-3}{2}} \exp\{-\frac{1}{2}\mathrm{tr}(\mathbf{AS}(\boldsymbol{\theta}))\} d\mathbf{A}$$

$$\propto |\mathbf{S}(\boldsymbol{\theta})|^{-\frac{n}{2}} \qquad \textbf{(6.10)}$$

$|S(\theta)|$ is the determinant of the "S-matrix" given by Equations 6.6 and 6.7. Marginal densities for individual parameters were calculated by numerical integration over the other parameters.

Fits for the compartmental activities were obtained by computing the expected values of the compartmental activities at different times. The expected value of the activity and the standard deviation of the expected value in compartment i at time t_u are calculated in the usual manner

$$E(\mathrm{a}_i(t_u, \boldsymbol{\theta})) = \int_{\Gamma}\int_{B}\int_{A} \mathrm{a}_i(t_u, \boldsymbol{\theta}) p(\boldsymbol{\theta}|D) d\alpha d\beta d\gamma \qquad \textbf{(6.11)}$$

$$SD(\mathrm{a}_i(t_u, \boldsymbol{\theta})) = \left(\int_{\Gamma}\int_{B}\int_{A} (\mathrm{a}_i(t_u, \boldsymbol{\theta}))^2 p(\boldsymbol{\theta}|D) d\alpha d\beta d\gamma - (E(\mathrm{a}_i(t_u, \boldsymbol{\theta})))^2 \right)^{\frac{1}{2}} \qquad \textbf{(6.12)}$$

6.3.3 Results

Figures 6.2, 6.3, and 6.4 show the marginal densities for the transfer coefficients. The fits for the compartmental activities were obtained by calculating the expectation and

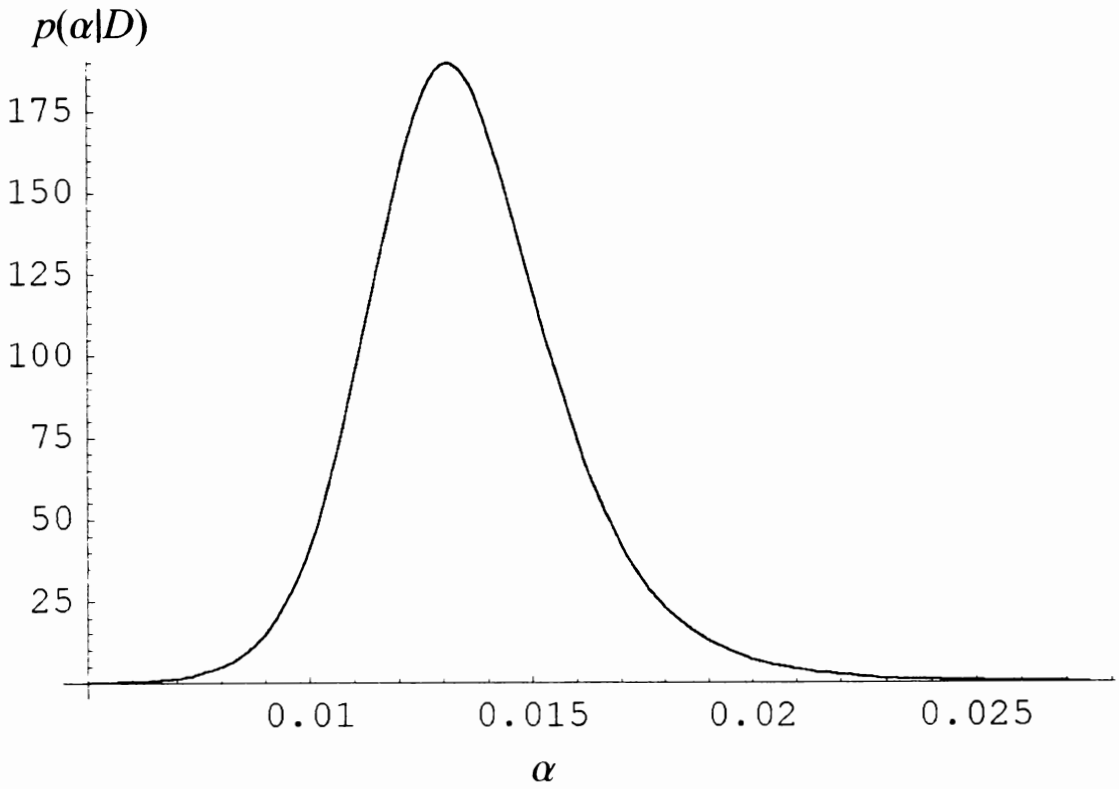

Figure 6.2: Marginal density of α for the ^{45}Ca biokinetic data

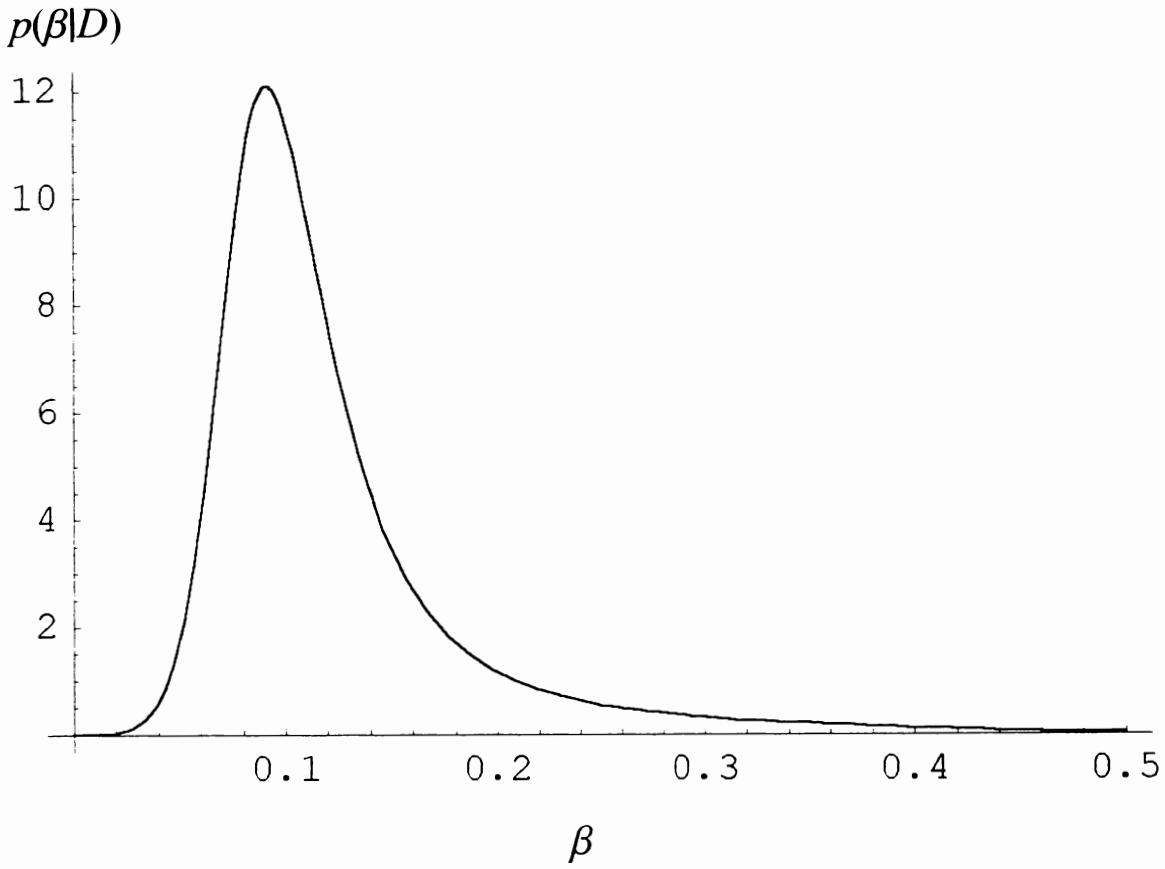

Figure 6.3: Marginal density of β for the ^{45}Ca biokinetic data

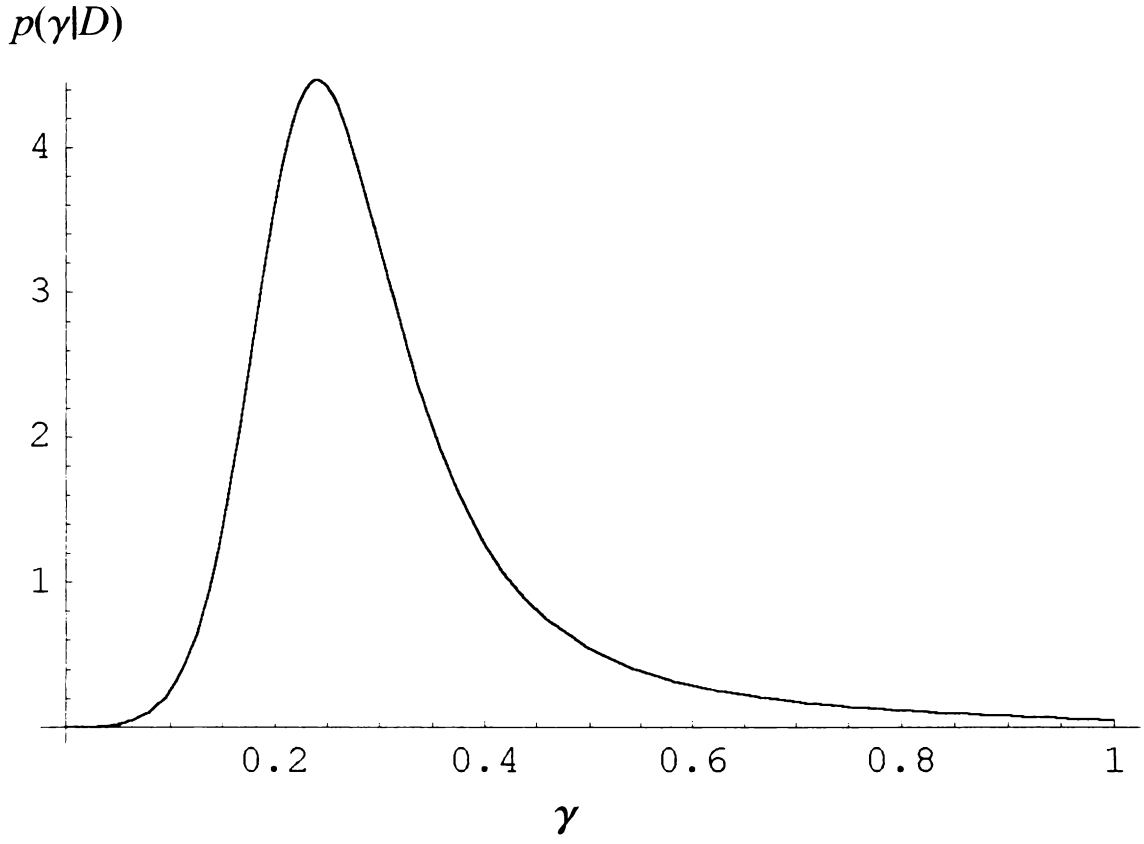

Figure 6.4: Marginal density of γ for the ^{45}Ca biokinetic data

standard deviation of the activities from t=1 until t=500 (hours). Figure 6.5 show the fit for the bone surface activity data, where the expected values are represented by the solid line, the expected values ± one standard deviation by the dashed lines, and the original data by the dots.

Figure 6.6 show the fit for the plasma activity data, where the expected values are again represented by the solid line, the expected values + one standard deviation by the dashed lines, and the original observations by the dots.

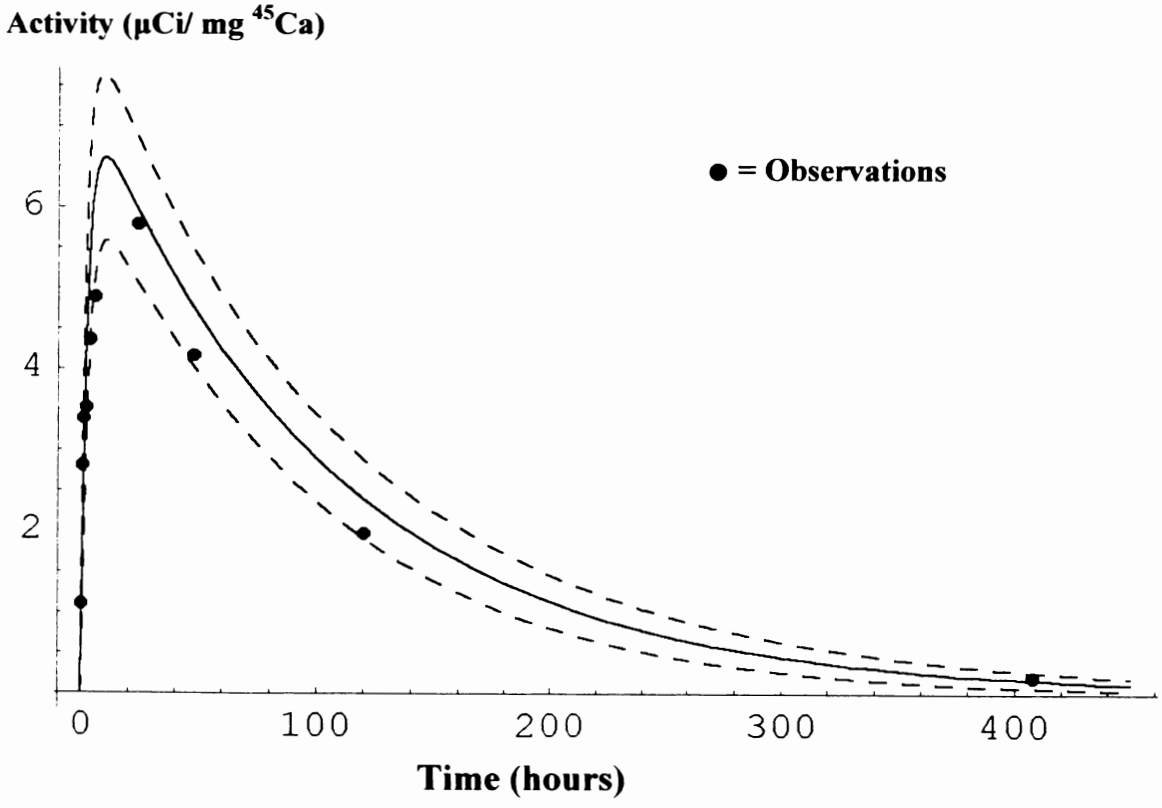

Figure 6.5: Fit of the Bone Surface Specific Activity

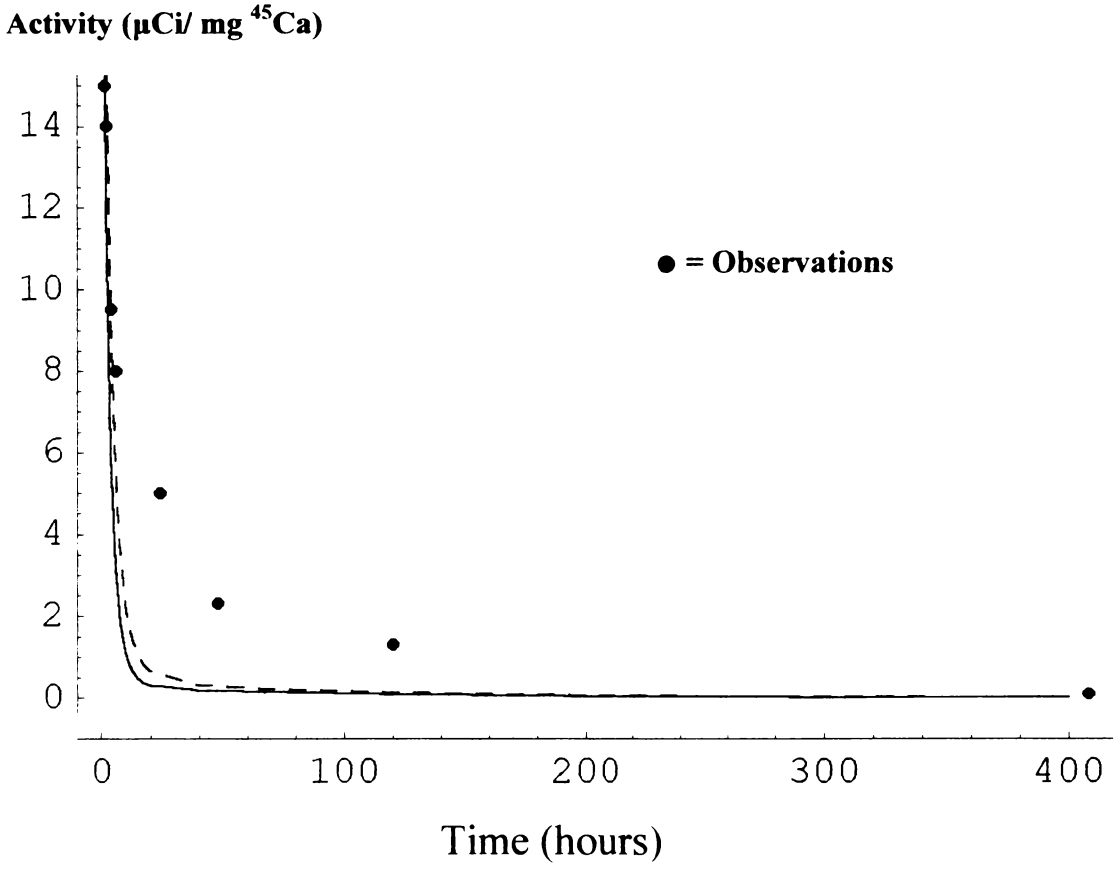

Figure 6.6: Fit of the Plasma Specific Activity

Figures 6.3 and 6.4 reveal mixed results. The fit of the bone surface activity data is excellent, all of the original data points lie within one standard deviation of the expected value. However, the fit of the plasma data is rather poor. Something is wrong with either the model or with the data. The results provide an opportunity to point out one of the reasons why compartmental modeling should be conducted with solutions to differential equations rather than with sums of exponentials. Were the latter approach to be used, there is no doubt that a "better" fit from a sum of squared errors perspective would result. The resulting model would be overfit; subsequent inference would be based on a model that fit noise rather than one based on the actual dynamics of the system. Using solutions to the differential equations avoids the problem of overfitting.

6.4 Compartmental Modeling with Missing Observations

6.4.1 Introduction

The data used in the last section are complete, meaning that there are observations of both compartmental activities for each observation time. In practice it is not uncommon for one or more of the observations to be missed during the course of an experiment or during occupational monitoring. In this section a modification of the general approach of Box et al. (1970) for estimation of missing values in multiresponse nonlinear modeling was applied to the specific topic of compartmental modeling with missing observations. The method allows posterior distributions to be derived for not only the transfer coefficients, but for the missed observations as well.

6.4.2 Method

This approach below is identical to that used in the last section with the exception that the missed observations are treated as additional parameters. All of the response data are represented by $\mathbf{y}'=(\mathbf{y_1}', \mathbf{y_2}')$, where y_i' is a 1×n column vector containing all of the observations for compartment i. The vector y′ is rearranged and partitioned into two parts $\mathbf{y_0}'$ and $\mathbf{y_m}'$, where $\mathbf{y_0}'$ represents the observations actually obtained and $\mathbf{y_m}'$ stands for the parameters representing the missed observations. Again assuming that the observations are independent, the joint posterior density of the parameters is proportional form is:

$$p(\boldsymbol{\theta}, \mathbf{A}, \mathbf{y}_m | D) \propto \prod_{u=1}^{n} p(D|\boldsymbol{\theta}, \mathbf{A}, \mathbf{y}_m) p(\boldsymbol{\theta}, \mathbf{A}, \mathbf{y}_m)$$

$$\propto |\mathbf{A}|^{\frac{n}{2}} \exp\{-\frac{1}{2}\sum_{i=1}^{2}\sum_{j=1}^{2}\sigma^{ij}S(\boldsymbol{\theta}, \mathbf{y}_m)\} p(\boldsymbol{\theta}, \mathbf{A}, \mathbf{y}_m) \quad \textbf{(7.4)}$$

$S(\theta,\mathbf{y_m})$ is again a 2x2 matrix with elements $S_{ij}(\theta,\mathbf{y_m})$ corresponding to the sum of squares and sum of products of the deviations between the $\mathbf{y_i}$'s and the expected values $a_i(t_u, \boldsymbol{\theta})$.

The prior distributions for the parameters are assumed to be independent (i.e. $p(\theta,\mathbf{A},\mathbf{y_m}) = p(\theta)p(\mathrm{A})p(\mathbf{y_m})$). Prior distributions for the elements of θ and $\mathbf{y_m}$ are assumed to be proportional to a constant, and non-informative Jeffrey's priors are again used for the elements of **A**. Proceeding as in the last section, the dependence on **A** is eliminated using

properties of Wishart distributions. The resulting joint posterior density of the parameters is given by

$$p(\boldsymbol{\theta}, \mathbf{y}_m | D) \propto |\mathbf{S}(\boldsymbol{\theta}, \mathbf{y}_m)|^{-\frac{n}{2}} \quad \textbf{(7.5)}$$

Marginal densities for individual parameters were obtained with quasi-Monte Carlo numerical integration over the other parameters. For the purposes of demonstration, two examples were considered. In the first, the 7th observation of the bone surface activity, $y_{1,7}$, was omitted from the ^{45}Ca biokinetic data. For the second example, $y_{1,7}$ and the 8th observation of plasma activity, $y_{2,8}$, were omitted. In each case the observations omitted were chosen arbitrarily.

6.4.3 Results

Figures 6.7, 6.8, and 6.9 compare the marginal densities for the transfer coefficients with 1 and 2 observations missing. Figures 6.10 and 6.11, respectively, show the posterior densities for $y_{1,7}$ with 1 and 2 missing observations, and for $y_{2,8}$ with 2 missing observations.

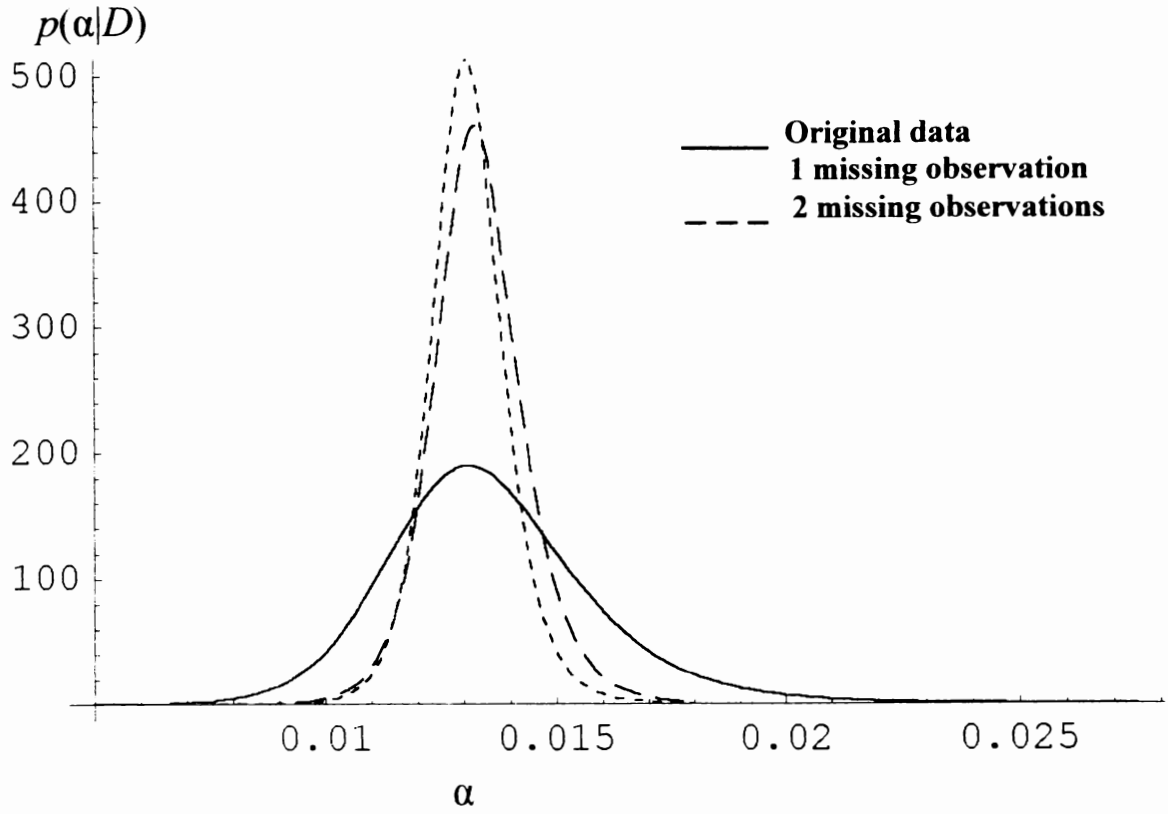

Figure 6.7: Marginal densities for α with 0, 1, and 2 observations missing

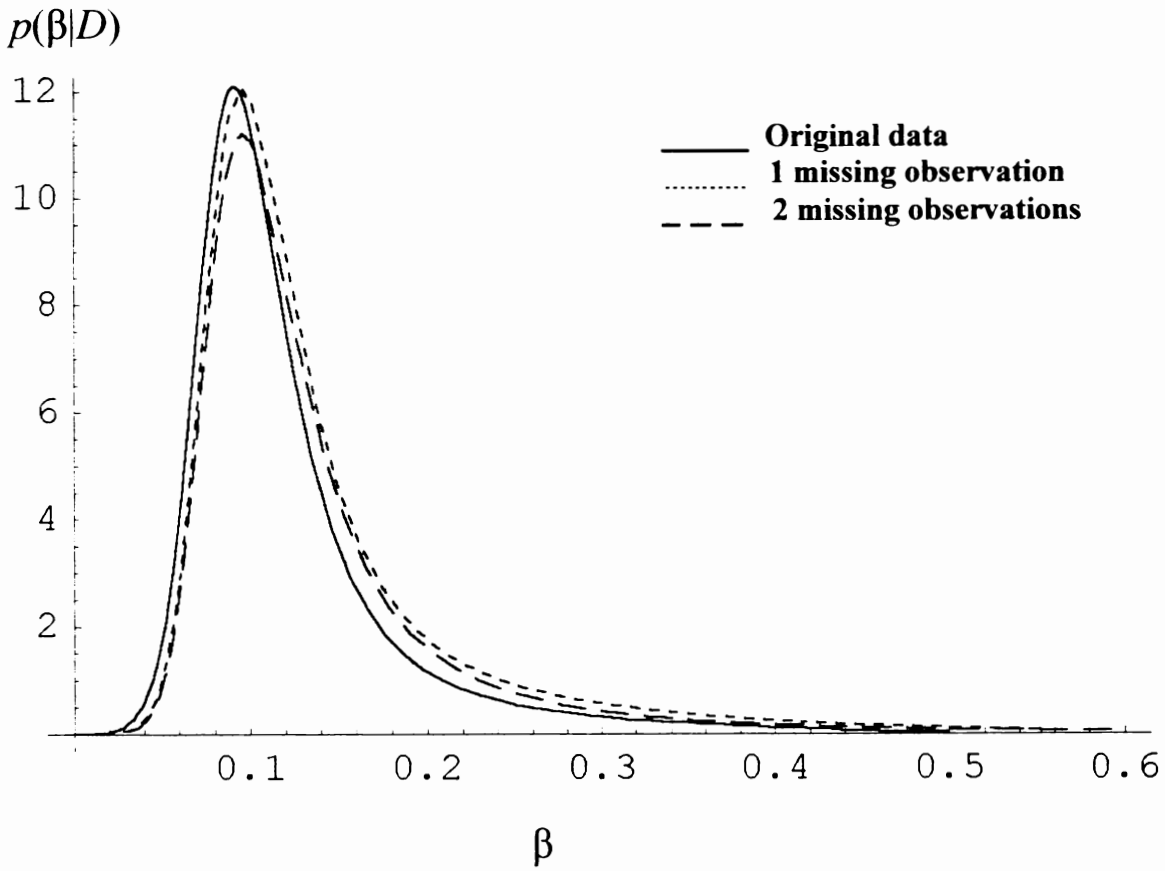

Figure 6.8: Marginal densities for α with 0, 1, and 2 observations missing

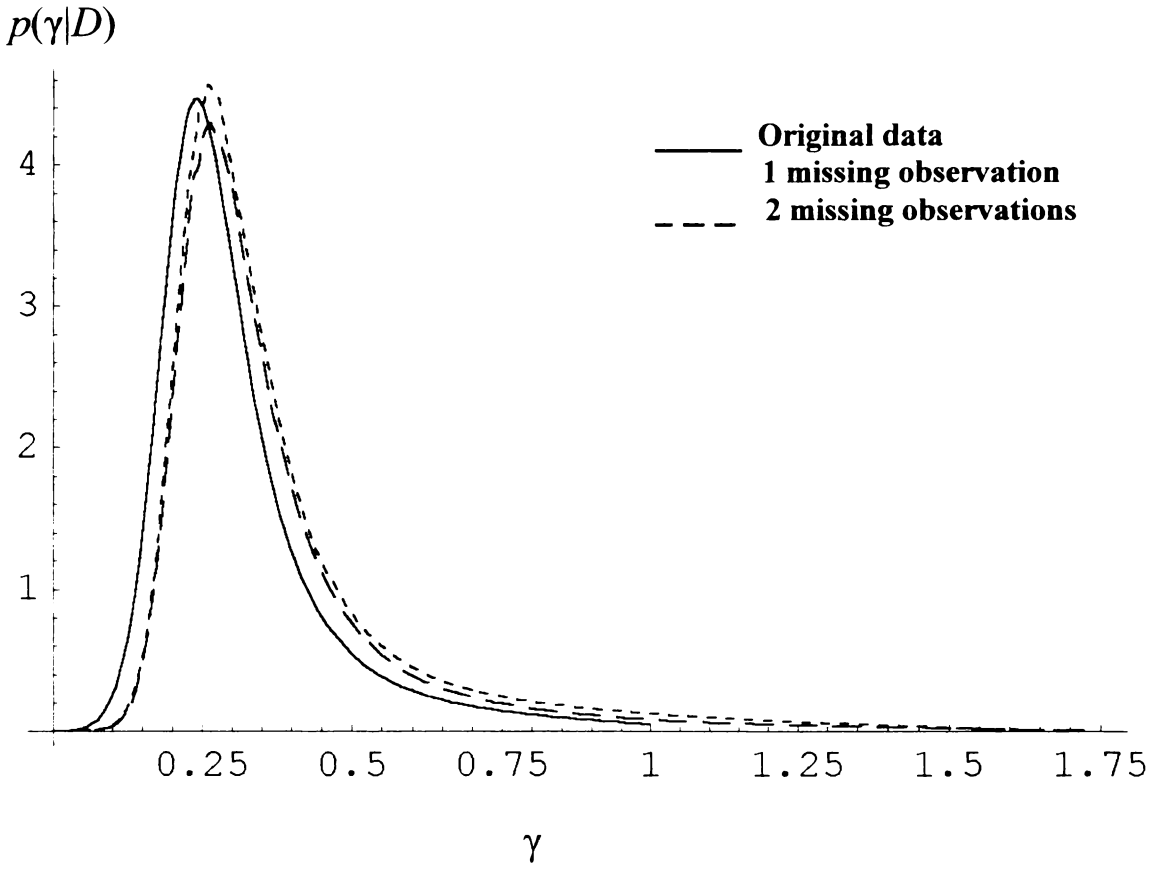

Figure 6.9: Marginal densities for γ with 0, 1, and 2 observations missing

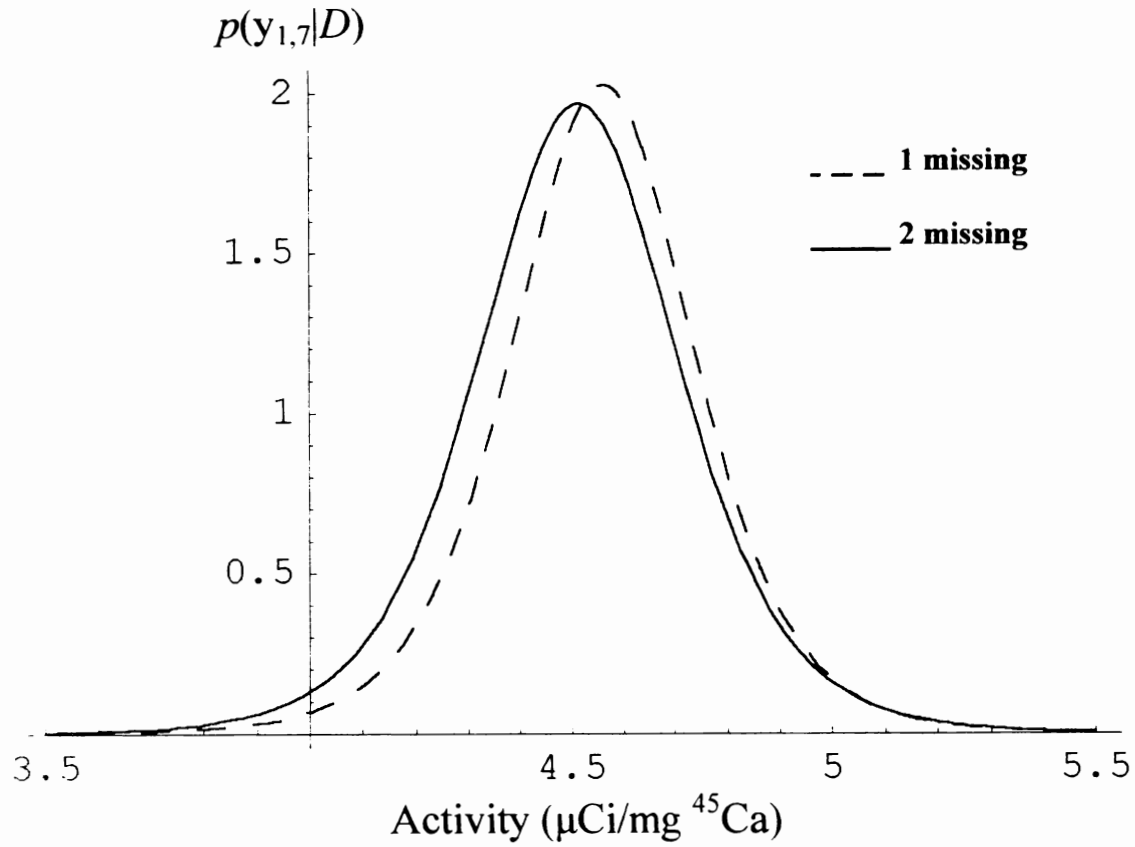

Figure 6.10: Marginal densities for the 7th observation of bone surface activity, $y_{1,7}$, with 1, and 2 observations missing

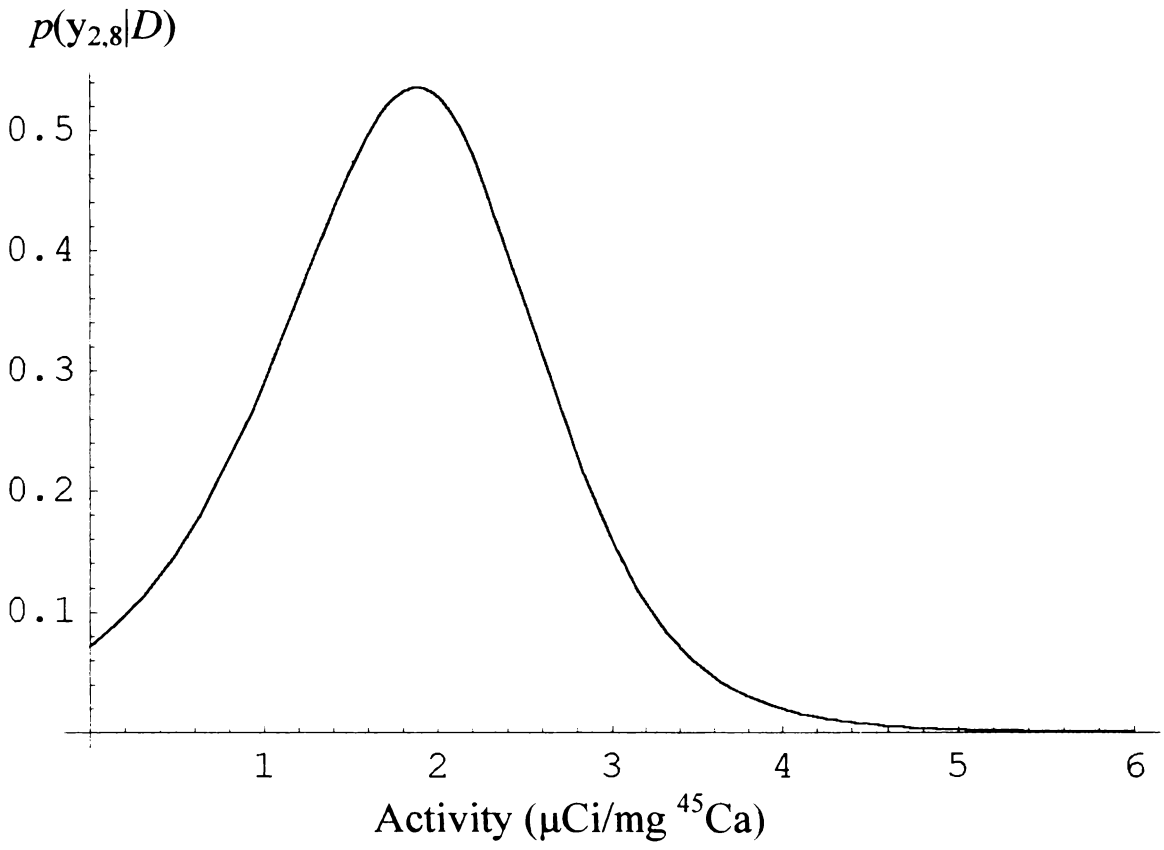

Figure 6.11: Marginal density for the 8th observation of plasma activity, $y_{2,8}$, with 2 observations missing

The only figure that shows a significant discrepancy between marginal densities is Figure 6.7, which reveals that the uncertainty of the posterior density of α actually decreases when estimated with 1 and 2 missing observations. This may be attributable to the arbitrarily omitted observations containing a disproportionate amount of measurement error.

6.5 Discussion

The fit obtained for the plasma specific activity shown in Figure 6.6 and the marginal densities of α with shown in Figure 6.7 are indicative of problems with the ^{45}Ca biokinetic data. In the first case, a better fit is expected. Even if the expected values do not agree with the actual data, the uncertainty of the expected values should be more reflective of the actual data. With respect to Figure 6.7, it was anticipated that considering less data would result in greater parameter uncertainty; the exact opposite occurred.

In both sections, more general methods for multiresponse nonlinear fitting were adapted to compartmental modeling. In Section 6.3, the uncertainty of parameter estimates was considered when estimating compartmental activities for fixed times, an improvement over the usual practice of using point estimates. The latter approach ignores all information about the uncertainty of the parameter estimates. As noted in Section 6.4.1, there are many reasons why observations may be missed in practice. In Section 6.4 a tool was developed for estimating the transfer coefficients as well as the missed observations.

CHAPTER 7: POSTERIOR DENSITIES FOR COMPARTMENTAL ACTIVITIES

7.1 Introduction

In Chapter 6 expected values and variances were calculated for the time-dependent compartmental activities of the ^{45}Ca biokinetic model. This represents an improvement over the use of point estimates of the activities, but even those results remain unsatisfactory based on the premise that uncertainty should be described with probability distributions. This point is made forcefully clear by Lindley (1983) :

"The probability distribution is a *complete* statement and point or interval estimates, or significance tests are not necessary. "No estimation problem *per se* is acknowledged to exist (de Finetti, 1961)". Estimates may be calculated – for example, $E(\theta \mid D)$ is a possible point estimate - but they are derived from the full specification and information is necessarily lost in using them".

With this in mind, attempts were made to derive posterior probability distributions for the compartmental activities at a fixed time t_f. Two different approaches were considered. The first is a reinterpretation of the method used in the Chapter 6 for compartmental modeling with missing observations, which yields the predictive density for an observation of the compartmental activity at time t_f. The second involves a transformation of variables using the joint posterior density of the parameters derived as

in Chapter 6, resulting in a posterior density for the expected value of the compartmental activity at time t_f. The former is always attainable relatively easily, while the latter is not except for very simple compartmental models. The methods are discussed in the Section 7.2 and demonstrated in Section 7.3. The chapter concludes with a discussion of the results and a comparison of the two methods in Section 7.4.

7.2 Method

7.2.1 Predictive Density for a Future Observation of Activity

Consider a generic *m*-compartment model with *k* common parameters denoted by $\boldsymbol{\theta}=\{\theta_1, \theta_2, \theta_3, \ldots, \theta_k\}$. Let $\mathbf{y_u}=\{y_{1u}, y_{2u}, y_{3u}, \ldots, y_{mu}\}$ represent observations of the activity contained in each of the *m* compartments at time $t=t_u$ for u=(1, 2, …, n-1). It is desired to obtain posterior densities for observations of the compartmental activities at time $t=t_f$, denoted by $p(\mathbf{y_f} | t_f, D)$ where $\mathbf{y_f}=\{y_{1f}, y_{2f}, y_{3f}, \ldots, y_{mf}\}$ and *D* represents the totality of the experimental data ($\mathbf{y_u}$ and the associated t_u for u=(1, 2, …, n-1)). One means of obtaining $p(\mathbf{y_f} | t_f, D)$ is the predictive density, given in general form by

$$p(\mathbf{y}_f | t_f, D) \propto \int_{\Psi} L(\mathbf{y}_f | \boldsymbol{\psi}, t_f, D) p(\boldsymbol{\psi} | D) d\boldsymbol{\psi} \qquad \textbf{(7.1)}$$

$L(\mathbf{y_f} \mid \psi, t_f, D)$ is the likelihood of the observation vector of interest and $p(\psi \mid D)$ is the joint posterior density of the parameters. This predictive density will now be derived for a generic compartmental model.

The following response model is assumed for the observed activity in each compartment at time t_u:

$$y_{iu} = a_i(t_u, \boldsymbol{\theta}) + \varepsilon_{iu}$$

$a_i(t_u,\theta)$ is the expectation function for the i^{th} compartment obtained by solving the system of differential equations that describe the movement of activity inside the compartmental model. It is assumed that the ε_{iu} come from independent multivariate normal distributions with $E(\varepsilon_{iu})=0$, $E(\varepsilon_{iu}\,\varepsilon_{jv})=0$ for $u \neq v$, and $E(\varepsilon_{iu}\,\varepsilon_{ju})=\sigma_{ij}$. The variance covariance matrix is again denoted Σ, and its inverse by $\mathbf{A}$:

$$\boldsymbol{\Sigma} = \{\sigma_{ij}\}$$

and

$$\mathbf{A} = \Sigma^{-1} = \{\sigma^{ij}\}$$

Letting $\mathbf{a_u}=\{a_1(t_u,\theta), a_2(t_u,\theta), a_3(t_u,\theta), \ldots, a_m(t_u,\theta)\}$ represent the expectation functions associated with the m compartments time t_u, the likelihood of $\mathbf{y_u}$ is given by the multivariate normal distribution

$$L(\mathbf{y}_u|\boldsymbol{\theta}, \mathbf{A}) = |\mathbf{A}|^{\frac{1}{2}} \exp\{-\frac{1}{2}(\mathbf{y}_u - \mathbf{a}_u)'\mathbf{A}(\mathbf{y}_u - \mathbf{a}_u)\} \quad \textbf{(7.2)}$$

The predictive density is derived as follows

$$p(\mathbf{y}_f|t_f, D) \propto \int_{\Theta}\int_{\mathbf{A}} L(\mathbf{y}_f|\boldsymbol{\theta}, \mathbf{A}, t_f, D)p(\boldsymbol{\theta}, \mathbf{A}|D)d\mathbf{A}d\boldsymbol{\theta} \quad \textbf{(7.3)}$$

$$\propto \int_{\Theta}\int_{\mathbf{A}} |\mathbf{A}|^{\frac{1}{2}} \exp\{-\frac{1}{2}(\mathbf{y}_f - \mathbf{a}_f)'\mathbf{A}(\mathbf{y}_f - \mathbf{a}_f)\}\prod_{i=1}^{n-1}|\mathbf{A}|^{\frac{1}{2}} \exp\{-\frac{1}{2}(\mathbf{y}_i - \mathbf{a}_i)'\mathbf{A}(\mathbf{y}_i - \mathbf{a}_i)\}p(\boldsymbol{\theta}, \mathbf{A})d\mathbf{A}d\boldsymbol{\theta}$$

$$\propto \int_{\Theta}\int_{\mathbf{A}} \prod_{i=1}^{n}|\mathbf{A}|^{\frac{1}{2}} \exp\{-\frac{1}{2}(\mathbf{y}_i - \mathbf{a}_i)'\mathbf{A}(\mathbf{y}_i - \mathbf{a}_i)\}p(\boldsymbol{\theta}, \mathbf{A})d\mathbf{A}d\boldsymbol{\theta} \quad \textbf{(7.4)}$$

where the contribution for i=n corresponds to the likelihood of $\mathbf{y}_f$. Proceeding as in Chapters 6, independent uniform priors are chosen for the θ_i, Jeffreys priors for **A**, and the dependence on **A** is eliminated using properties of the Wishart distribution. The following expression for the predictive density results:

$$p(\mathbf{y}_f|t_f, D) \propto \int_{\Theta}|\mathbf{S}(\boldsymbol{\theta}, \mathbf{y}_f)|^{-\frac{n}{2}}d\boldsymbol{\theta} \quad \textbf{(7.5)}$$

$|\mathbf{S}(\boldsymbol{\theta}, \mathbf{y}_f)|$ is the determinant of the m×m matrix containing the sum of squares and sum of products of the deviations between the observed y_{iu}'s and the expected values $a_i(t_u, \boldsymbol{\theta})$:

$$S_{ij}(\mathbf{y}_f, \boldsymbol{\theta}) = \sum_{u=1}^{n} [y_{iu} - a_i(t_u, \boldsymbol{\theta})][y_{ju} - a_j(t_u, \boldsymbol{\theta})], \qquad i,j = (1, 2, \ldots, m)$$

Marginal posterior densities for the future obsservation of an individual compartment's activity at time t_f, say y_{1f} for example, may be obtained by numerical integration over the other y_{if} and θ.

7.2.2 Posterior Density for the Expected Value of Activity

The generic *m*-compartment model discussed in the previous section will be used again. Proceeding as in Chapter 6, the following form is obtained for the joint posterior density of the parameters conditional on the (n-1) timed pairs of observations

$$p(\boldsymbol{\theta}|D) \propto \int_{\mathbf{A}} \prod_{u=1}^{n-1} p(D|\boldsymbol{\theta}, \mathbf{A}) p(\boldsymbol{\theta}, \mathbf{A}) d\mathbf{A}$$

$$\propto |\mathbf{S}(\boldsymbol{\theta})|^{-\frac{n-1}{2}} \qquad \textbf{(7.6)}$$

The desired quantity is the posterior density for the expected value of the activity in compartment *i* at time t_f, denoted $p(a_i(t_f) \mid D)$. Using the truncated notation of $a_i = a_i(t_f)$, a transformation of variables may performed using the standard result from probability calculus given in Equation 7.7:

$$p(a_i, \xi_1, \xi_2, ..., \xi_{k-1} | D) = p(\theta_1(a_i, \xi_1, \xi_2, ..., \xi_{k-1}), \theta_2(\xi_1), ..., \theta_k(\xi_{k-1}) | D) \left| \frac{\partial(\theta_1, \theta_2, ..., \theta_k)}{\partial(a_i, \xi_1, \xi_2, ..., \xi_{k-1})} \right|$$

where

$\theta_1(a_i, \xi_1, \xi_2, ..., \xi_{k-1}) =$ inverse of a_i

$\xi_j = \theta_{j+1}$

$\left| \frac{\partial(\theta_1, \theta_2, ..., \theta_k)}{\partial(a_i, \xi_1, \xi_2, ..., \xi_{k-1})} \right|$ = Jacobian of the transformation

The desired quantity, $p(a_i(t_f) | D)$, is subsequently obtained by numerically integrating out the ξ_j. While a nonzero Jacobian confirms the existence of an inverse function, in the case of compartmental models the explicit form of the inverse function cannot be obtained except for a few simple models. Consequently, the marginal posterior density for the expected value will rarely be attainable. Below a simple 2-compartment caternary model is considered for which the explicit form of the inverse function can be obtained for the expected value of the activity in compartment 1.

7.3 Examples

7.3.1 2-Compartment Caternary Model

The method will be demonstrated first with simulated data for the 2-compartment caternary model shown in Figure 7.1

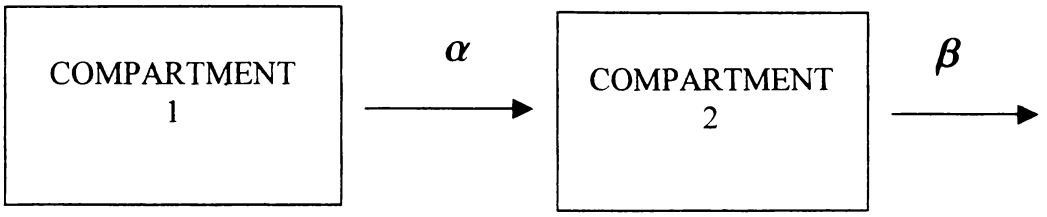

Figure 7.1: 2-compartment caternary model

The activities in compartment 1 and compartment 2 at time t_u are denoted $a_1(t_u, \alpha)$ and $a_2(t_u, \alpha, \beta)$ respectively. The differential equations describing the movement of activity through the model are given by

$$\frac{da_1(t,\alpha)}{dt} = -\alpha a_1(t,\alpha) \qquad \textbf{(7.8)}$$

$$\frac{da_2(t,\alpha,\beta)}{dt} = \alpha a_1(t,\alpha) - \beta a_2(t,\alpha,\beta) \qquad \textbf{(7.9)}$$

Subject to the initial conditions of $a_1(0, \alpha)=1$ and $a_2(0, \alpha, \beta)= 0$, the following solutions were obtained to the system of differential equations

$$a_1(t,\alpha) = \exp\{-\alpha t\} \tag{7.10}$$

$$a_2(t,\alpha,\beta) = \frac{\alpha(\exp\{-\alpha t\} - \exp\{-\beta t\})}{\beta - \alpha} \tag{7.11}$$

Data were simulated by setting α=0.6 and β=0.2 in Equations 7.10 and 7.11 and evaluating for t=0.5:5 in increments of 0.5. Normal noise obtained by random sampling from a normal distribution with mean zero and standard deviation of 0.05 was then added to the precise values. The data are plotted in Figure 7.2.

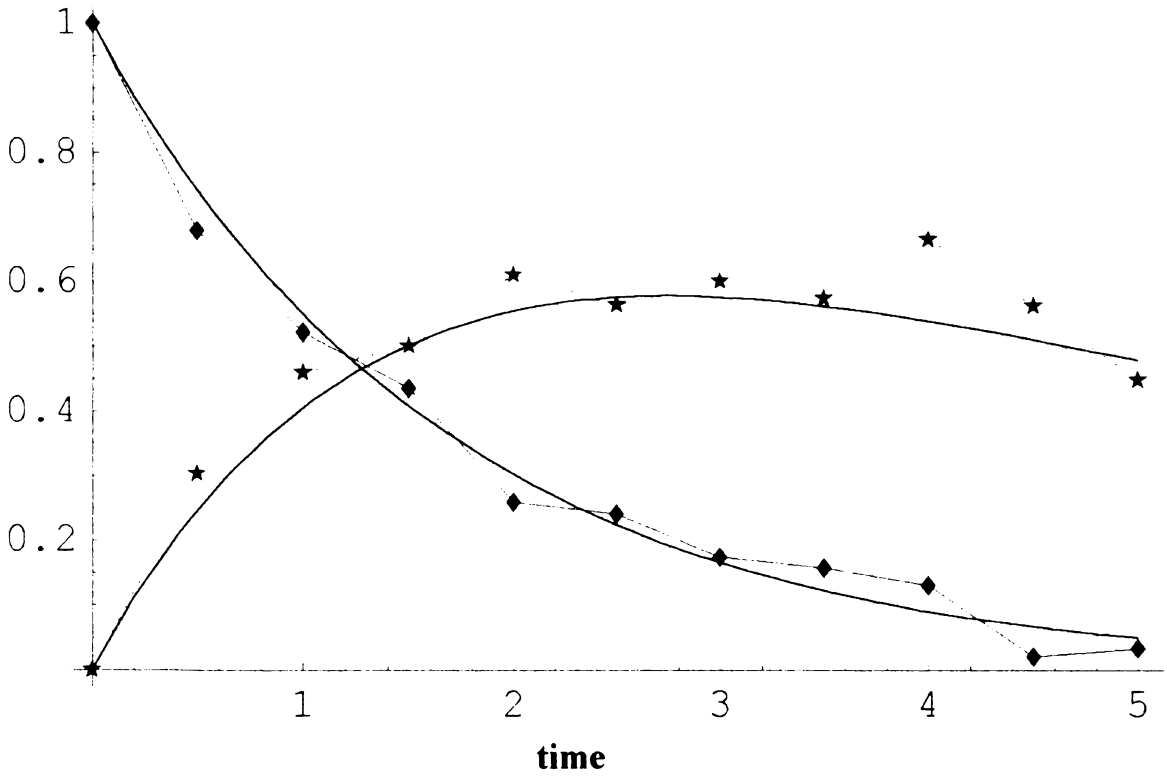

Figure 7.2: Simulated data for 2-compartment caternary model

A convenient feature of this model is that the expectation function for the activity in compartment 1 is dependent only on α, permitting derivation of the explicit form of the inverse of $a_1(t_u, \alpha)$. The posterior density for the expected value of the activity in compartment 1 for a fixed time t_f is calculated as follows

$$p(a_1(t_f)|D) = \int_B p(\alpha(a_1), \beta) \left| \frac{d\alpha(a_1(t_f))}{da_1(t_f)} \right| d\beta \qquad \textbf{(7.12)}$$

where the integration over β is performed numerically and $\alpha(a_1(t_f))$ is the inverse of a_1 given by

$$\alpha(a_1) = -\frac{\ln(a_1)}{t_f} \qquad \textbf{(7.13)}$$

Figure 7.3 shows the resulting posterior density for the expected value of the activity in compartment 1 along with the predictive density for the observed value of the activity, both calculated for t_f=3.25.

It is clear from Figure 7.3 that the predictive density for the observed value shows more uncertainty, a reflection of the potential measurement error associated with observation. Clearly, the posterior density of the expected value is a more attractive estimate from the standpoint of precision. Unfortunately, explicit inverse functions cannot be obtained for

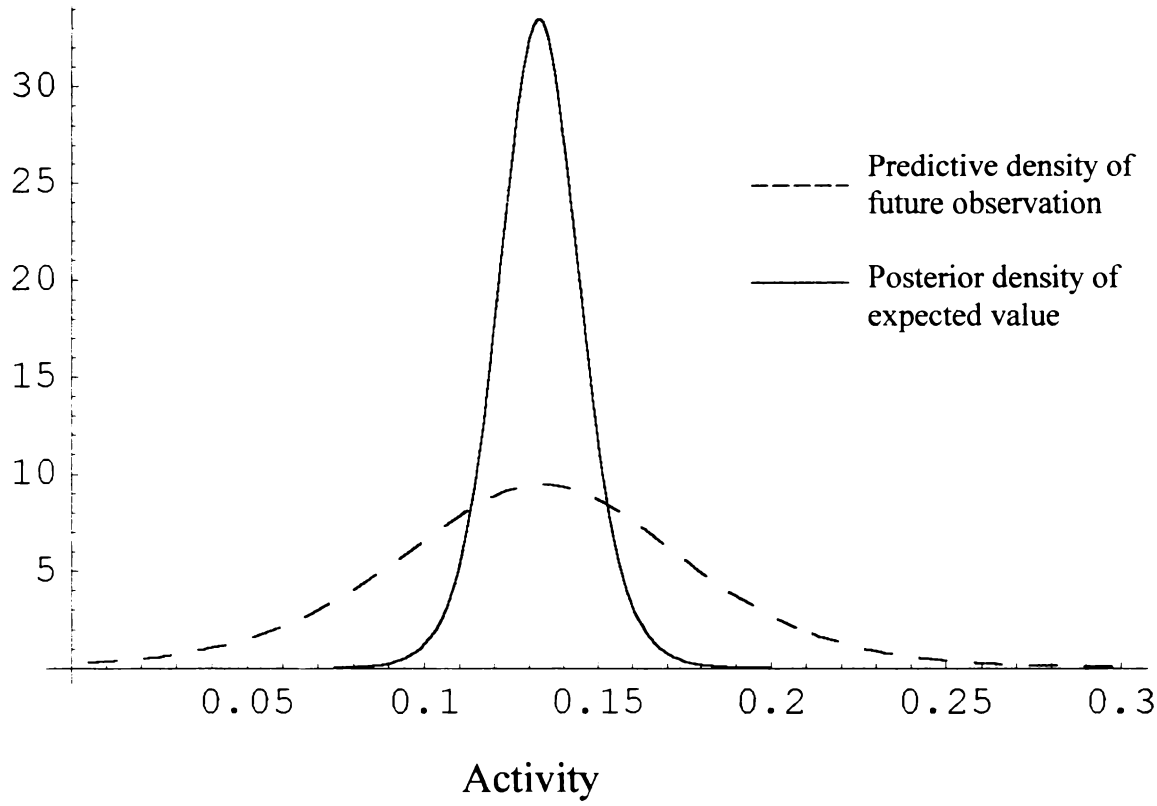

Figure 7.3: Marginal densities of the activity in compartment 1 for the 2-compartment caternary model at t_f =3.25

more complex models. In such cases, an approximation to the posterior density for the expected value is best obtained using point estimates of the expectation and variance, obtained as in Section 6.3, and assuming normality. This approach will be used for the remainder of this chapter.

The posterior density for the activity in compartment 2 at time $t_f = 3.25$ is examined next. Figure 7.4 shows a comparison of the predictive density for the observed activity in compartment 2 a time t=3.25 and the associated posterior density for the expected value calculated with an assumption of normality.

The results again show a pronounced difference between the uncertainties of the densities. It is also notable that the predictive densities in Figures 7.3 and 7.4 appear to have a normal shape with the same mode as the posterior density for the expected value, and a greater variance.

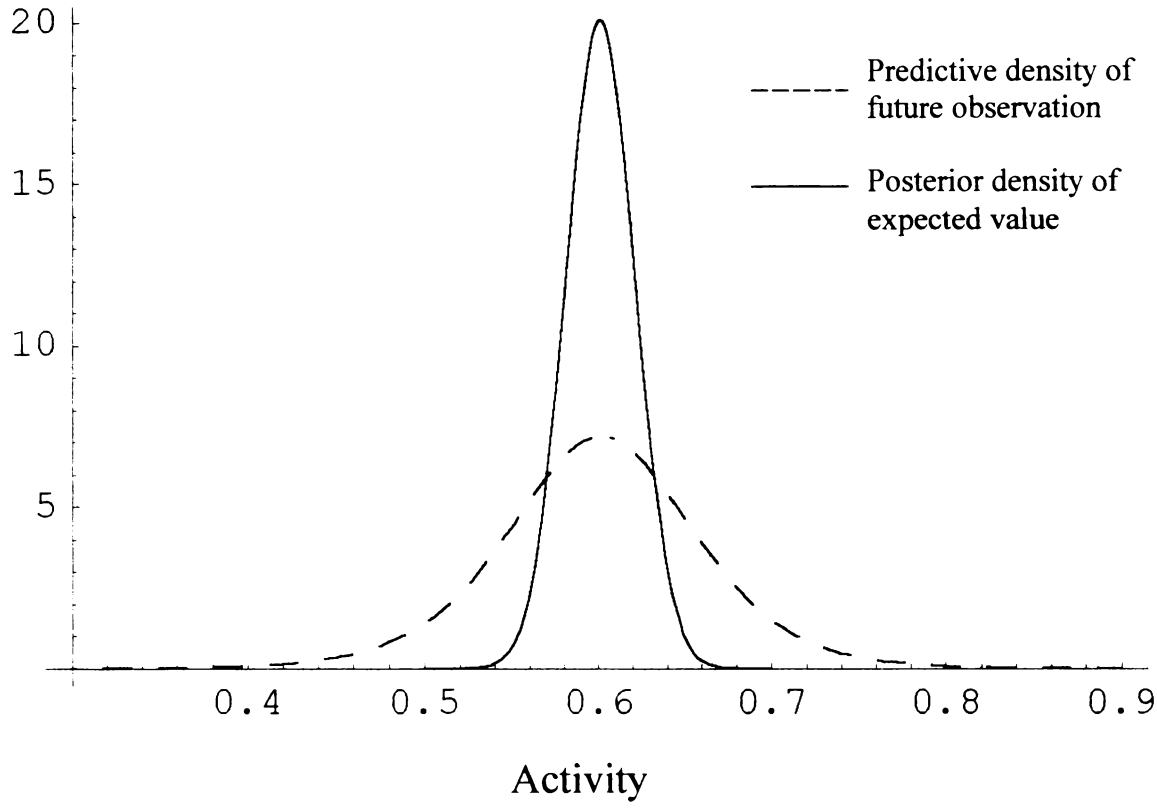

Figure 7.4: Marginal densities of the activity in compartment 2 for the 2-compartment caternary model at t_f =3.25

7.3.2 2-compartment ^{45}Ca model

To avoid unnecessary repetition the reader is referred to Section 6.2 for the specifics of the ^{45}Ca biokinetic model and the associated data. Predictive densities were derived for the observed activity at the bone surface and in the plasmas for t_f=100 (hours). Figure 7.5 shows the predictive density of the observed value and the posterior density of the expected value for bone surface activity. The latter was calculated under the assumption of normality.

In Figure 7.5 the discrepancy between the two probability densities is less pronounced than for the caternary model considered earlier. It is thought that this is a reflection of the excellent fit of the bone surface activity (Chapter 6, Figure 6.5). Figure 7.6 shows the predictive density of the observed value and the posterior density of the expected value for plasma activity at t_f=100 (hours). The latter was again calculated under the assumption of normality.

In this case there is a large discrepancy between the two probability densities. The degree of the discrepancy is such that the predictive density is truncated to make the posterior density for the expected value visible. The complete predictive density is shown in Figure 7.7.

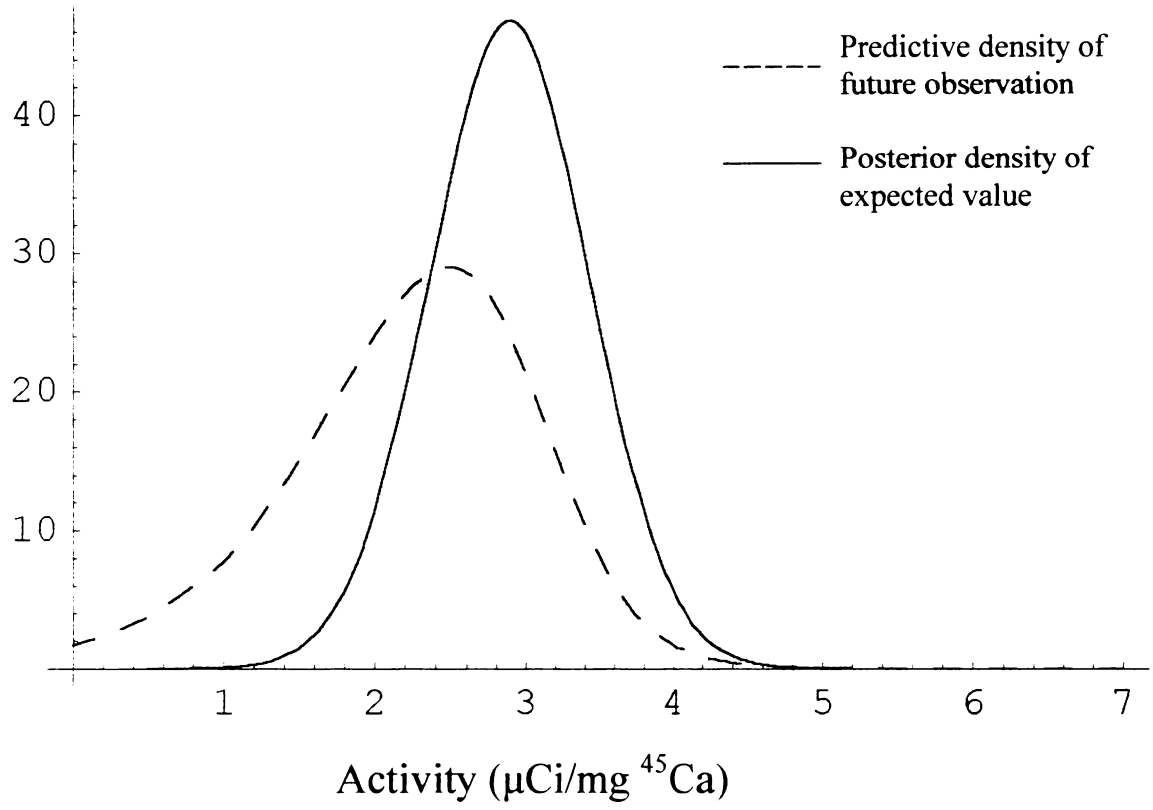

Figure 7.5: Marginal densities for the bone surface activity at t_f=100 (hours)

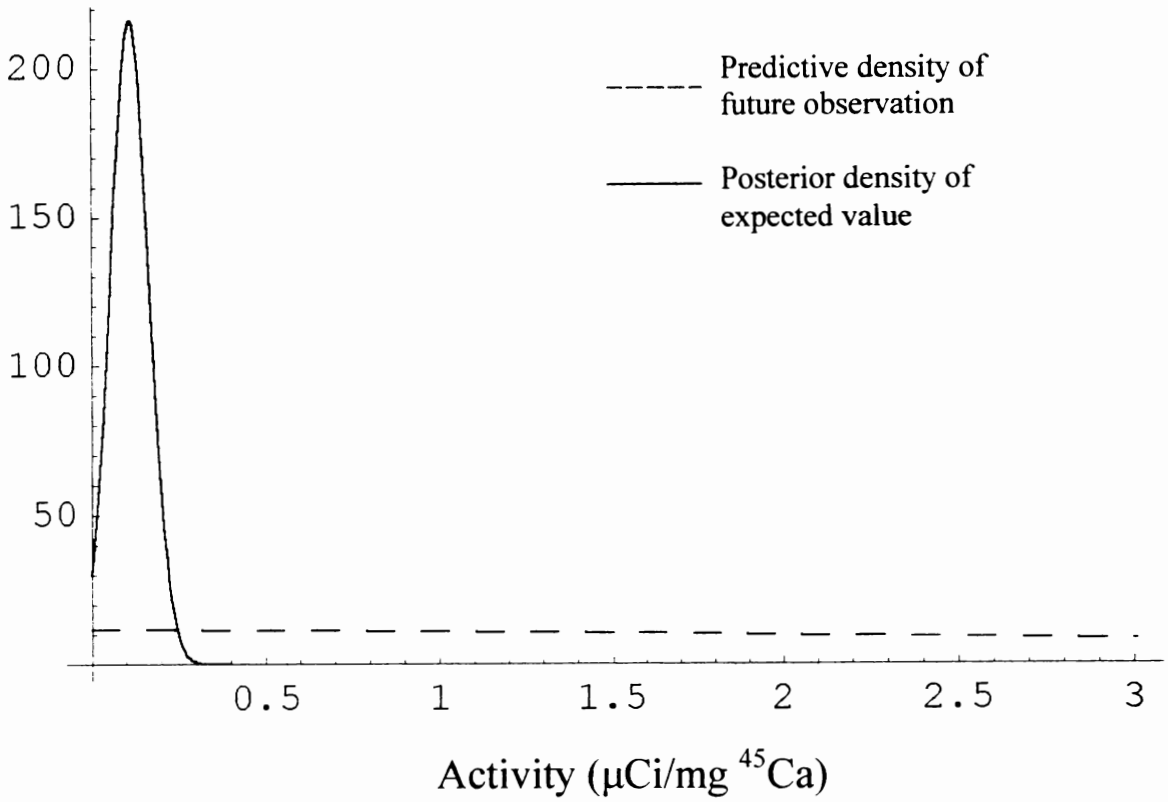

Figure 7.6: Marginal densities for the plasma activity at t_f=100 (hours)

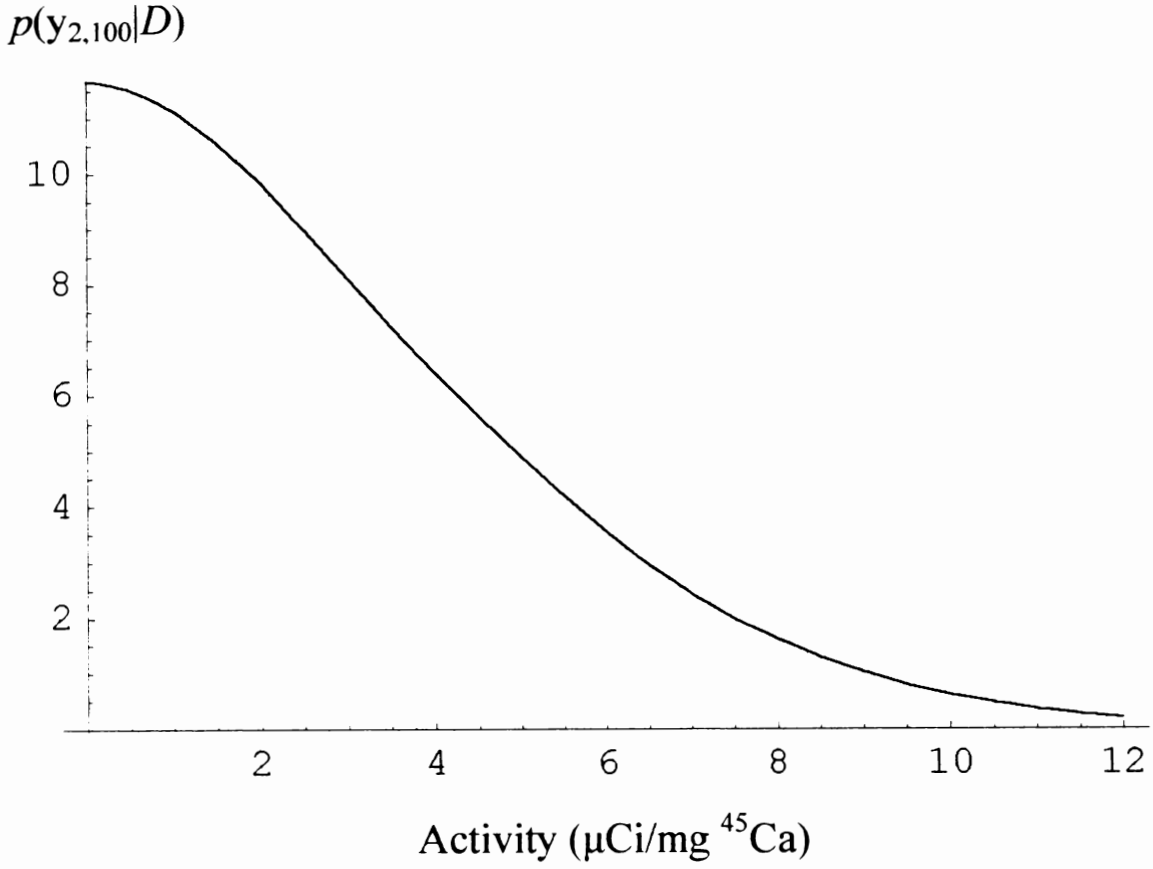

Figure 7.7: Predictive density for future observation of the plasma activity at t_f=100 (hours)

The disagreement between the two densities is understandable when one considers the poor fit obtained for the plasma data (Chapter 6, Figure 6.6).

7.4 Discussion

In this chapter the calculation of probability densities for compartmental activities was considered. It was shown that while the posterior density for the expected value is typically a more desirable description of compartmental activity at a fixed time, it is directly attainable only in simple cases when the inverse of the expectation function can be explicitly obtained. Otherwise, the suggestion is to use an assumption of normality and the point estimates for the expected value and variance of the compartmental activity or the more diffuse predictive density for the observed value of the activity.

CHAPTER 8: CONCLUSIONS, ORIGINAL CONTRIBUTIONS, AND RECOMMENDATIONS FOR FUTURE WORK

8.1 Conclusions and Original Contributions

The objective of this research was to provide original solutions to several problems in external and internal radiation dosimetry from a Bayesian standpoint. The rationale for a Bayesian standpoint was discussed in Chapter 1. The discussion considered not only the advantages of a Bayesian approach as compared to frequentist alternatives, but also the potential computational difficulties. The point was made that current steady increase in the availability of computing power is mitigating the computational burden. The specific original accomplishments in radiation dosimetry include the following:

1. The work of Groer et al. (1987) for dose estimation with chromosome dosimetry was expanded to different models and radiation types. Several new calibration data sets and dose response models were considered: response to gamma rays and low doses of neutrons. In each case posterior densities were derived for the parameters of dose response models and the calibrative density was used to quantify the uncertainty of dose estimates made following hypothetical radiation exposures. The parameter and dose estimates were found with reasonable computational effort, reinforcing the practicality of Bayesian methods for chromosome dosimetry.

2. A new method was derived and demonstrated for dose estimation with chromosome aberrations following a criticality event. Because the doses received during a criticality event are from a combination of fission spectrum neutrons and gamma rays, the dose estimation process is more complex than for doses deposited by a single type of radiation. The method permits estimation of the total dose, as well as the contributions from neutrons and gamma rays. The method is an improvement over the frequentist methods currently in use as it permits an uncertain neutron to gamma dose ratio. Analytical results were provided for intermediate expressions, minimizing the computational burden of subsequent analyses.

3. An original method was developed and demonstrated for chromosome dosimetry that considers the inherent uncertainty of the doses in controlled calibration experiments. The fact that all doses in calibration experiments are to some degree imprecise estimates is obvious. The approach was demonstrated for three different dose response models: linear dependence on dose with no background term, linear dependence on dose with a background term, and linear-quadratic dependence on dose with a background term. This approach and the simplified intermediate expressions provide a coherent means of accounting for uncertain calibration doses with minimal computational effort.

4. A new model, the Polya or negative binomial model, was considered for chromosome dosimetry with high LET radiations. The occurrence of overdispersion for high LET radiations violates the standard assumption of a Poisson model. The Bayes Factor was used to show that the Polya or negative binomial model is a better choice for high LET

radiations. In addition to model comparison, posterior densities for the parameters and calibrative densities were calculated for two calibration data sets under the assumption of a Polya model. The use of the Polya model and the calibrative density is an original and clear improvement over the current practice of retaining the Poisson model and ad-hoc adjustments based on estimates for the variance/mean ratio.

5. The expected values and associated standard deviations of the specific activity at the bone surface and in the plasma were calculated for the ^{45}Ca biokinetic compartmental model using the data of Rowland et al. (1960). This was a continuation of the work of Lo (2000) but with increased computing power. Calculation of expected values and standard deviations with numerical integration is an improvement on the use of point estimates of the transfer coefficients to estimate time-dependent compartmental activities.

6. The general method of Box et al. (1970) for dealing with missing observations in nonlinear multiresponse modeling was adopted for compartmental modeling. There are many reasons why observations may be missed in practice; the method demonstrated in Chapter 6 is a coherent means of imputing the missed observations using all available data. The method was demonstrated for one and two missed observations with the ^{45}Ca data of Rowland et al. (1960).

7. In recognition of the Bayesian notion that the probability distribution is the best descriptor of an unknown quantity, two new and different approaches were taken to deriving posterior densities for the compartmental activity at a fixed time. The first

approach is a reinterpretation of the method of Box et al. (1970) for dealing with missing observations in nonlinear multiresponse modeling, and yields the predictive density for an observation of the activity. The second method considered is based on a transformation of random variables approach, and yields the posterior density for the expected value of the activity. The predictive density was found to be computable in all cases, but is less desirable since it always shows greater uncertainty. The posterior density for the expected value was found to be computable only for extremely simple compartmental models.

In summary, eight new applications of Bayesian methods were developed and applied to problems in internal and external radiation dosimetry. Each application addressed a specific deficiency in current practices. The totality of this effort shows that a Bayesian approach is a practical alternative to the frequentist approaches used in radiation dosimetry.

8.2 Recommendations for Future Work

With respect to external radiation dosimetry, more work can be done on the topic of chromosome dosimetry following criticality accidents. The examples considered in this research were based on limited data. More analyses should be conducted with more expansive calibration data sets. On the larger front, future work should focus on fostering wider acceptance and use of the calibrative density for dose estimation. The calibrative density has several novel and desirable features that represent an improvement over the

methods currently being used for dose estimation. Specifically, the calibrative density permits information from diverse sources to be incorporated in the dose estimation process in a formal and coherent manner, and yields results that describes uncertainty probabilistically

For internal radiation dosimetry, future work should continue on two fronts, one computational and the other experimental. On the computational front, more complex models will require increased computing power and the use of novel numerical routines for combining solutions of systems of differential equations and multi-dimensional numerical integration. A specific area of focus should be numerical methods for performing the transformation of variables discussed in Chapter 7. On the experimental front, there is a pronounced lack of data on individual compartmental activities. The reason for this is twofold: difficulty in collecting data for individual compartments and the widespread acceptance of regression techniques that do not require data on each compartment. Progress on this front will come in response to perceived need; the case must be made in practical situations, like nuclear medicine, for estimation of transfer coefficients and time-dependent compartmental activities with solutions to the system of differential equations instead of regression techniques.

REFERENCES

REFERENCES

Aitchison, J. and Dunsmore. I.R. 1975. *Statistical Prediction Analysis*, Cambridge University Press, (Cambridge).

Anderson, D.H. 1983. *Compartmental Modeling and Tracer Kinetics*, Springer-Verlag, (Heidelberg).

Arley, N. 1943. *On the Theory of Stochastic Processes and Their Application to the Theory of Cosmic Radiation*, John Wiley and Sons, Inc. (New York).

Bender, M.A., Awa, A.A., Brooks, A.L., Evans, H.J., Groer, P.G., Littlefield, L.G., Pereira, C., and Preston, R.J. 1988. Current status of cytogenic procedures to detect and quantify previous exposures to radiation, *Mutation Research*. **196**, 103-159

Bothwell, A.M., Whitehouse, C.A., and Tawn, E.J. 2000. The Application of FISH for Chromosome Aberration Analysis in Relation to Radiation Exposure, *Radiation Protection Dosimetry*. **88(1)**, 7-14

Box, G.E.P. and Draper, N.R. 1965. The Bayesian estimation of common parameters from several responses, *Biometrika*. **54**, 355-365

Box, G.E.P., Draper, N.R., and Hunter, W.G. 1970. Missing Values in Multiresponse Nonlinear Model Fitting, *Technometrics*. **12(3)**, 613-620

Box, G.E.P. and Tiao, G.C. 1992. *Bayesian Inference In Statistical Analysis*, John Wiley and Sons, Inc. (NewYork)

De Finetti, B. 1961. The Bayesian Approach to the Rejection of Outliers, *Proceedings of the Fourth Berkeley Symposium on Mathematics, Statistics, and Probability*. **1**, 199-210

De Finetti, B. 1974. *Theory of Probability (vols 1 and 2)*, John Wiley and Sons, Inc. (NewYork)

Gavalas, G.R. 1968. *Nonlinear Differential Equations of Chemically Reacting Systems*, Springer

Godfrey, K. 1983. *Compartmental Models and Their Applications*, Academic Press, Inc. (London)

Good, I.J. 1959. Kinds of Probability, *Science*. **129,** 443-447

Good, I.J. 1983. *Good Thinking: The Foundations of Probability and Its Applications*, University of Minnesota Press (Minneapolis).

Groer, P.G. and Perrira, C.A. 1987. Calibration of a Radiation Detector: Chromosome Dosimetry for Neutrons, *Probability and Bayesian Statistics*, Plenum Publishing, 225-232

Groer, P.G. 1998. Chromosome Dosimetry for Neutrons from a ^{252}Cf Source, *Transactions of the American Nuclear Society*, Annual Meeting

Howson, C. and Urbach, P. 1989. *Scientific Reasoning: The Bayesian Approach (Second Edition)*, Open Court (Chicago)

Inoue, Y. 1995*a*. *Dicentric Yields Induced in Rabbit Blood Lymphocytes by Low Doses of ^{252}Cf Neutrons*, JAERI 95-073, Japan Atomic Energy Research Institute

Inoue, Y. 1995*b*. *Dicentric Yields Induced in Rabbit Blood Lymphocytes after Exposure In Vitro to X-rays,* JAERI 95-039, Japan Atomic Energy Research Institute

Jacquez, J.A. 1972. *Compartmental Analysis in Biology and Medicine*, Elsevier

Jeffreys, H. 1998. *Theory of Probability (Third Edition)*, Clarendon Press (Oxford).

Jin, C.Z., Liu, X.L., Zhang, Z.Y., and Luo, Y.S. 1998. Present Status and Prospects for Biological Dosimetry Using Chromosome Aberration Analysis, *Radiation Protection Dosimetry*. **77(1),** 29-32

Johnson, N.L. and Kotz, S. 1969. *Discrete Distributions*, Houghton Mifflin Co. (Boston)

Kass, R.E. 1993. Bayes factor in practice, *The Statistician*. **42,** 551-560

Lempers, F.B. 1971. *Posterior Probabilities of Alternative Linear Models*, Rotterdam University Press

Lindley, D.V. 1966. Discussion portion of P. Sprent's paper entitled "A Generalized Least-squares Approach to Linear Functional Relationships", *Journal of the Royal Statistical Society, Series B*. **28**, 375-389

Lindley, D.V. and El-Sayyad, G.M. 1967. The Bayesian Estimation of a Linear Functional Relationship, *Journal of the Royal Statistical Society, Series B*. **30**, 190-202

Lindley, D.V. 1971. *Making Decisions*, Wiley-Interscience Press

Lindley, D.V. 1983. Theory and Practice of Bayesian Statistics, *The Statistician*. **32(1)**, 1-11

Lindley, D.V. 1987. The Probability Approach to the Treatment of Uncertainty in Artificial Intelligence and Expert Systems, *Statistical Science*. **2(1)**, 3-44

Lloyd, D.C., Edwards, A.A., and Purrot, R.J. 1979. Radiation Induced Chromosome Aberrations and the Poisson Distribution, *Radiation and Environmental Biophysics*. **16**, 89-100

Lloyd, D.C. and Edwards, A.A. 1983. Chromosome Aberrations in Human Lymphocytes: Effect of Radiation Quality, Dose, and Dose Rate, *Radiation-Induced Chromosome Damage in Man*. Alan R. Liss, Inc. (New York).

Lo, Y. 2000. *Bayesian Parameter Estimation for Compartmental Models in Biology and Physics*, Dissertation, University of Tennessee-Knoxville

Moquet, J.E., Edwards, A.A., Lloyd, D.C., and Hone, P. 2000. The Use of FISH Chromosome Painting for Assessment of Old Doses of Ionising Radiation, *Radiation Protection Dosimetry*. **88(1)**, 27-33

O'Hagan, A. 1994. *Kendall's Advanced Theory of Statistics Volume 2B-Bayesian Inference*, John Wiley and Sons, Inc. (London).

Rao, C.R. and Chakravarti, I.M. 1956. Some small sample tests of significance for a Poisson distribution, *Biometrics*. **12**, 264-282

Rowland, R.E. 1966. Exchangeable Bone Calcium, *Clinical Orthopedics and Related Research*. **49**, 233-248

Sasaki, M.S. 1971. Radiation-induced chromosome aberrations in lymphocytes: Possible biological dosimeter in man, *Biological Aspects of Radiation Protection*, Springer (Berlin).

Savage, L.J. 1972. *The Foundations of Statistics (2nd edition)*, Dover Publishing

Voison, P., Lloyd, D., and Edwards, A. 1997. Chromosome aberrations Scoring for Biological Dosimetry in a Criticality Accident, *Radiation Protection Dosimetry*. **70**, 467-470

Welch, T.J.C., Potchen, E.J., and Welch, M.J. 1972. *Fundamentals of the Tracer Method*, W.B. Saunders Company

Welling, P.G. 1986. *Pharmacokinetics-Processes and Mathematics*, American Chemical Society

Wolfram, S. 1996. *The Mathematica Book*, Cambridge University Press

APPENDIX

See attached CD ROM (plate 1) for Appendix material

The CD contains Mathematica code (version 4.0, Student Edition) used in this dissertation. The code is contained in a Mathematica notebook named "appendix.nb". The contents of the notebook are arranged according to chapter and topic in the dissertation.

VITA

Ryan Scott Brame was born in Mayfield, Kentucky on July 28, 1969. He attended Mayfield City Schools, graduating from Mayfield High School in 1987. He spent three years at Murray State University before enrolling at the University of Tennessee, Knoxville in 1994. He received his Bachelor of Science in Nuclear Engineering in May of 1998 and Master of Science in Nuclear Engineering in August of 1999. He remained at the University of Tennessee and received his Doctor of Philosophy in May of 2002.